ABSTRACT

TYAGI, PREETI. Nanocellulose-based Sustainable Barrier and Antimicrobial Coatings (Under the direction of Dr. Lokendra Pal and Dr. Martin Hubbe).

The use of biomaterials, especially nanocellulose, has been limited due to their constraints for water barrier properties. The other main constraint with biomaterials used for large scale application is the cost of raw materials and limited supply. The aim of this study is to explore sustainable ways to modify nanocellulose materials including cellulose nanofibers (CNF) and cellulose nano crystals (CNC) for obtaining less hydrophilic nanocellulose-based coatings. Along with obtaining gas, oil and water barrier properties from CNF and CNC, the antimicrobial aspect was also integrated into nanocellulose coatings to improve the scope of application.

The first part of the research was focused on obtaining a less hydrophilic and oleophobic sustainable modified CNC coating using a composite forming approach. For this task, CNC were preferred over CNF because the crystalline structure of CNC don't allow penetration any liquid through their crystalline packed structure. To prepare functionalized CNC-composite, additives such as high aspect ratio montmorillonite (MMT) clay, soy protein and alkyne-ketene-dimer (AKD) were employed to improve the packing density of the films. The Fourier-Transform Infrared Spectroscopy (FTIR) confirmed that fewer hydroxyl groups, which are the principal means of hydrophilicity of CNC, were exposed on the surface in CNC-composite coated paper compared to CNC. The CNC-composite coatings were confirmed to have improved water barrier properties and superior oil resistance.

The second part of the research includes studying the potential of CNC-composites and CNF in a multilayer coating system. Employing CNF as bottom layer and CNC-composite as top layer was hypothesized to be the best way to minimize the surface energy of coatings along with obtaining highest oxygen and gas barrier properties. The results were validated by measuring

surface energy and water contact angle hysteresis. The more hydrophobic protein moieties were confirmed over the top surface of multilayer coated paper surface using Time-of-Flight Secondary Ion Mass Spectrometry (ToF-SIMS). A substantial increment in gas and oil barrier properties compared to commercial plastic materials and a significant improvement in water barrier properties were observed.

In the third part of the research, potential of CNC along with chitosan was explored for their antimicrobial properties. There were two motives of using CNC in chitosan matrix: one, it would help in overcoming the water absorption and softness issues arising with chitosan. The second hypothesis was based upon the rod-like, rigid, stiff and narrow morphology of CNC particles; that would synergistically help chitosan as bactericidal agent by causing significant damage to the cell membrane due to its specified morphology. The morphology of rigid CNC particles protruding out of the chitosan surface was confirmed using scanning electron microscopy, auger microscopy and ToF-SIMS. The chitosan and CNC composite in a specified ratio showed a significant reduction in bacterial growth along with improving hydrophilicity of chitosan.

The last part of the research (Chapter 5) was aimed at combining barrier and antimicrobial properties in one all-rounder coating recipe by changing the feedstock for preparing nanocellulose. In this work, the hemp hurds cellulose fibers were obtained using four different treatments ranging from mild (water) to a chemically intensive pulping process, namely water-autohydrolysis, mild alkaline/carbonate (4% Na_2CO_3), unbleached kraft, and bleached kraft. To see the impact of feedstock, hardwood (Eucalyptus) chips were also treated using similar pulping methods, except autohydrolysis. The obtained cellulose fibers were given mechanical treatment to obtain lignin containing and bleached CNF. The objective of using lignin containing hemp hurd cellulose fibers was to obtain a low-cost CNF, which are less hydrophilic and have the potential to show

antimicrobial activity due to the presence of active compounds in them. The hemp hurd powder was confirmed to have the cannabidiol (CBD) using gas chromatography and mass spectrometry (GC-MS). The CBD peak in GC-MS was confirmed by comparing it with standard CBD. The antimicrobial activity of extractives from hemp hurd powder and auto hydrolyzed defibrillated cellulose fibers were confirmed against *E. coli*. The lignin containing CNF showed less hydrophilicity from both the feedstock hemp and *Eucalyptus*. The antimicrobial and barrier properties result of hemp hurd CNF gives a huge motivation to explore them deeply for qualitative and quantitative chemical characterization.

Nanocellulose-based sustainable barrier and antimicrobial coatings

by
Preeti Tyagi

A dissertation submitted to the Graduate Faculty of
North Carolina State University
in partial fulfillment of the
requirements for the degree of
Doctor of Philosophy

Forest Biomaterials

Raleigh, North Carolina
2019

APPROVED BY:

_____	_____
Dr. Lokendra Pal Committee Co-Chair	Dr. Martin A. Hubbe Committee Co-Chair
_____	_____
Dr. Lucian A. Lucia	Dr. Hasan Jameel
_____	_____
Dr. Ronalds Gonzalez	Dr. Orlando J. Rojas External Member

DEDICATION

To my parents (Mr. Vinesh Kumar Tyagi and Mrs. Rakhi Tyagi) for their endless support and sacrifices.

BIOGRAPHY

Preeti Tyagi was born in a small village town of Roorkee in Uttarakhand, India to her parents in 1991. She stayed with her parents until 2001 and moved to a public boarding school in Haridwar, Uttarakhand, India with her younger brother. After completing her high school at boarding school in Haridwar in 2008, she went to G. B. Pant University of Agriculture and Technology, Pantnagar, India to study Bachelor of Technology in Biotechnology. During her bachelor she was interested in sports such as table-tennis, volleyball and basketball and played many inter-college tournaments for basketball. After completing her undergraduate with distinction, she joined Indian Institute of Technology, Roorkee for her masters in Pulp and Paper Technology in 2012. During her masters she received a merit based DAAD (Deutscher Akademischer Austauschdienst) scholarship for completing her master's research dissertation under the direction of Dr. Harald Grossmann at the University of Technology, Dresden, Germany. After receiving her degree, Preeti went on to work for VOITH Paper as a Product Application Engineer for two years, during which time she helped support paper mills by providing technical assistance for the development of forming fabric applications. She Joined North Carolina State University in 2016 to pursue her Ph.D. degree under the direction of Dr. Lokendra Pal and Dr. Martin Hubbe in the Department of Forest Biomaterials.

Outside of research, she likes travelling to new destinations, doing adventurous events such as sky diving, river rafting and bungee jumping etc. She also enjoys spending time outdoors with her friends.

ACKNOWLEDGMENTS

First, I am immensely grateful to my mentors Dr. Lokendra Pal and Dr. Martin Hubbe for providing me with the wonderful opportunity to carry out this doctoral work and grow under their able guidance. Dr. Pal's encouragement, support, trust, and patience throughout my doctoral studies have been commendable. The freedom of thinking and sense of responsibility, Dr. Pal instill in his students are unparalleled. Dr. Pal have contributed so much to my professional and personal development that I will appreciate forever. Whenever, I found myself in trouble during writing or explaining the concepts of detailed mechanisms, Dr. Hubbe was always there for me. I am thankful to Dr. Hubbe for sharing his enormous amount of knowledge and inspiring me to constantly think about the new research ideas. I acknowledge, Dr. Lucia for sharing his enormous knowledge in chemistry and ideas during my all research projects. I sincerely thank to Dr. Jameel for being part of my committee and encouraging me all the times by challenging me with his new ideas even outside of the work. I thank to Dr. Gonzalez for bringing the idea of Tissue Pack Innovation lab to the department, which was a big part of my research. I could not get much time with Dr. Rojas but he always motivated me through his immense contribution in the field of nanocellulose, through his talks at NCSU, ACS conferences and research articles.

I thank to all the graduate students at Forest Biomaterials without whom, this journey would have been much harder. I would like to thank especially Sachin, Carolina, Camilla, Tiago, Joseph, Marielis, Salonika, Salem, Juliana, Darlene, Mike, Shelly, Matt, Joshua, Heather, Eliezer, Maria, Grace, Franklin, Adam for their unconditional support. I like to thank all the staff members at Forest biomaterials: Barbara, Beverly, Ambre, Melissa, Leena. I thank to Reny, Lisa and Dr. Charlie Opperman at the Department of Plant pathology for allowing me to work in their lab and helping me throughout the process and answering my persistent questions calmly. I thank to all

the AIF lab managers and research associates specially Chuck, Elaine, Phillips, Roberto and BB who helped me doing all the characterization part and teaching me the techniques. I would also like to acknowledge my roommate (Faeza) and friends like family (Sweta, Ritesh, Pikaso, Salonika, Leena and Sonali) in USA without whom the stay in USA would not be as wonderful. I thank to my overseas friends, Khushbu, Shalinee, Shilpi, Parul and Radha who always supported me even from miles.

Finally, I am grateful to my parents for their immense sacrifices, support and trust in me. I am so grateful to my parents sacrifice that they send me away from home to have a better education which was not possible in my hometown when I was 10. Their constant commitment and sacrifices for our education has been inspiring and never can be repaid. I have been lucky to have a younger brother like Parag, who always believed in me and encouraged me to aim for achieving my goals and dreams. I have been so fortunate to have Rajnish as my boyfriend for understanding and being patient with me for all three years of my PhD. My PhD journey would have been much more stressful without your unconditional care, love and support.

TABLE OF CONTENTS

LIST OF TABLES

LIST OF FIGURES

CHAPTER 1. Introduction and Background

Breakthrough research on bio-based materials is not only focusing on reducing dependence on fossil feedstock and the environmental impact of petroleum-based waste, but also on taking advantage of the large functional diversity of biomass-derived building blocks for the synthesis of unique materials, which are not achievable by employing conventional resources [1]. The forest products industry needs to be reformed to create high value and a wide range of products due to new digitization era and lost demand of printing papers [2,3]. However, packaging and tissue paper have potential growth numbers, provided by a number of reports [4,5] For the future economical sustainability of forest industry, either it needs to improve the current product lines with better and unique properties, or must create new product lines based on new technologies [3,6,7].

The development of nanocellulose, particularly cellulose nanofibrils (CNF) [8] and cellulose nanocrystals (CNC) [9] using wood pulp has opened enormous opportunities for the forest industry due to its multitude of applications studied academically [10]. Nanocellulose has been studied for its potential applications such as rheology modifier, biomedical [11–14], polymer composites [15–18], paper additives and coatings [19–24], and others [14,25–27]. Though numerous studies show the potential applications of nanocellulose, very few studies suggest potential scalable, feasible and viable applications [20]. For instance, either the earlier studied applications require intensive chemical modifications of nanocellulose that are limited to the lab scale, or are limited in some aspects of scaling-up viable applications [28–30]. This progress related to cellulose nanomaterials is still very much on the research and development level, and larger scale utilization is yet to emerge.

1.1 Motivation

There are many demands from the market that require a growing number of substantial advances in technology, leading to greater innovation at numerous levels. The packaging and

hygiene industry is one of the leading potential market for the forest based paper industry [6]. Market demands for more sustainable packaging and hygiene products are increasing, as are regulatory requirements that are forcing companies to consider new alternatives [31]. For instance, FDA limited the use of fluorinated compounds in U.S fast food packaging, which is a principle compound family representing oil and grease barrier coatings for paper based food packaging [32].

1.2 Ojectives

In light of the current needs, the objective of this research was to develop sustainable and industrially viable nanocellulose based multifunctional coatings for gas, water, oil, and grease resistance. Considering the multifunctionality of nanocellulose, the antimicrobial properties of CNC were also studied in a CNC-Chitosan system that exhibited synergistic behavior, which will be elucidated shortly. The antimicrobial activity of CNF obtained from hemp hurd fibers will also be studied, considering the fact that hemp contains five major cannabinoids responsible for its antimicrobial property [33].

A major part of the work was devoted to obtaining a sustainable barrier coating against gases, oil and grease, and water using CNC and CNF. In '**Paper I' (Chapter 2)** a sustainable functionalized CNC-composite (CNC*) barrier coating was developed using high aspect ratio nanoclay, natural amphililic binders, and hydrophobisizing agents showing excellent resistance against gases and substantially good resistance properties against oil and grease. '**Paper II' (Chapter 3)** describes how the unmodified CNF and CNC* coating helped in attaining an excellent oil and grease resistant coating. To obtain an excellent barrier coating for gases and grease, a CNF layer was first coated on a substrate followed by a CNC* layer. This provided more gas and grease barrier properties with less sensitivity to moisture. **'Paper III' (Chapter 4)** describes the use of CNC to make antimicrobial coating for tissue and hygiene products. CNC was

shown to perform synergy along with chitosan to improve its antimicrobial property and improve its water absorption capacity to be used in tissue paper and hygiene products.

Chapter 5 describes the way to obtain sustainable antimicrobial and barrier coating using hemp (*Cannabis sativa L.*) nanofibrils. The work included the preparation of fibrillated nanocellulose from hemp, surface modification using cannabinoids, and its application as barrier paper coating and films. Further, chapter 5 includes a complete description of antimicrobial activity testing of these products against Gram negative bacteria.

The work in Papers I, II and III presents the use of CNC and CNF for developing multifunctional barrier and antimicrobial barrier coatings. By using CNF and CNC in one integral multilayer system, excellent barrier properties against gases, oil, and grease were achieved. The unique needle-shaped geometry of CNC along with chitosan can be a sustainable and forest-based solution for developing antimicrobial hygiene products. These observations provide an interesting starting point, considering the development of future forest-based products combining low-cost with high functionality.

1.3 Background

In the past decade, cellulosic nanomaterials such as microfibrillated cellulose (MFC), CNF, and CNC have shown enormous potential in the forest products industry. The discovery of microfibrillated cellulose in 1977 by an American scientist Ablin F. Turbak in the ITT Rayonier Eastern Research Division (ERD) Lab in Whippany, N.J., opened new opportunities for the forest industry. Following that discovery, other nano-scale variations of cellulose such as CNF [8,34–37], CNC [9,28], TEMPO (2,2,6,6-tetramethylpiperidine-1-oxyl)-CNF [38] were prepared using different processes. CNFs are the nano-fibers with diameters in the nanoscale range of 20-50 nm and lengths of several micrometers, with amorphous as well as crystalline regions, chemical composition, and

degrees of polymerization of 300 to several thousand, depending on the sources and methods of preparation (Tables 1-1 and 1-2) [23,36,39]. The terms "MFC" and "CNF" are both used in the literature, depending on the relative widths of the fibrils. However, no strict dimensions have been defined to differentiate between these two highly fibrillated celluloses (MFC and CNF) [23]. Separation of cellulose nanofibers from the native plant fiber involve several steps of chemical/enzymatic pretreatment and a final mechanical separation process. Several mechanical methods have been developed to produce CNFs, such as microfluidization, ultrafine grinding, refining, high intensity ultrasonication, steam explosion, cryo-crushing, etc.[40] Among these, ultrafine grinding and homogenization techniques are the most studied and used methods for CNF preparation [41,42].

Table 1-1. Chemical composition of nanofibers from different sources after selective chemical treatments

Raw material/Feedstock	Cellulose	Hemicellulose	Lignin	Extractives	References
Unbleached wood pulp	40 ±2	23 ± 2	21 ± 1	2 ± 0.2	[43]
Bleached wood pulp	91 ± 1	4 ± 1	1 ± 0.5	0.5 ± 0.1	
Kenaf bleached pulp	92 ± 0.5	4.7 ± 0.7	0.5 ± 0.3	0.4 ± 0.1	[44]
Kenaf unbleached pulp	82.6 ± 0.9	11.8 ± 0.4	1.8 ±0.4	0.8 ± 0.2	
Hemp untreated pulp	75.56 ± 4.0	11 ± 1	7.0 ± 2		[45]
Hemp bleached pulp	94.53	1.59	2.71		
Untreated Flax fibers	75.4 ± 0.2	13.4 ±2.8	3.4 ± 0.9		[46]
Chemically purified fibers	88.8 ± 1.5	9.1 ± 1.0	0.4 ± 0.1		

Table 1-2. Diameter of cellulose nanofibers and nanocrystals from various sources

	Source	Diameter	References
Cellulose nanofibers	Bacterial cellulose	40-70	[47]
	Bagasse	5-15	[48]
	Banana rachis	3-5	[49]
	Hemp	30-200	[45]
	Kenaf	10-70	[50]
	Rubber wood	10-90	[44]
Cellulose nanocrystals	Jute	3-10	[51]
	Cotton linter	10-13	[52]
	Rice straw	30.7	[53]
	Eucalyptus wood	11-15	[54]
	Kenaf bast	2-5	[55]

CNCs are the sole crystalline derivatives of cellulose that are prepared by acid hydrolysis of various forms of cellulose, resulting in diameters in the range of 2 to 30 nm with lengths of several hundred nm. CNCs can be prepared upon acid hydrolysis of cellulose by hydrolyzing the amorphous regions of cellulose, leaving behind only the domains having crystalline structures [56]. There are many options for acids such as sulfuric acid, hydrochloric acid, bromic acid and phosphoric acid, which can be used to hydrolyze cellulose to give rise to nanocellulose crystals [56,57]. The surface structure and functionality of cellulose crystals depends on the type of acid used for degradation of amorphous regions (Table 1-3). Thus, one can obtain surface charged or neutral nanocrystals depending on the requirements. Sulfuric acid is most commonly used to prepare a negatively charged and stabilized suspension of rod-like nanocellulose crystals [57]. Dong et. al. optimized the production of CNC from wood pulp cellulose by hydrolyzing it with 64 wt% sulFuric acid at 45°C for 45 minutes and then quenching the suspension with deionized water followed by a centrifugation step to obtain concentrated CNCs. During hydrolysis, sulfuric acid diffuses through the most accessible part of cellulose, i.e. the amorphous region, and as the reaction continues, it hydrolyzes the crystalline surface as well. Thus, it results in the conversion of primary

hydroxyl ($^{-}$OH) groups to sulfate groups (-OSO^{3-}) on CNC surfaces. The charge density of the crystalline surface depends on the concentration of the acid, the reaction time, and the temperature [56,57]. Figure 1-1 gives the morphological differences between CNF and CNC [58].

Table 1-3. Different acids used to prepare CNC and their attributes

Acid	Special attribute	References
Sulfuric acid (H_2SO_4)	Charged surface due sulfate groups on CNC surface (C_6-O-SO^{-}_3) (Stable colloidal dispersion)	[56]
Hydrochloric acid (HCl)	No surface charge on CNC (unstable colloidal dispersion)	[59]
hydrobromic acid (HBr)	No surface charge on CNC (unstable colloidal dispersion)	[60]
phosphoric acid (H_3PO_3)	Charged surface due phosphate groups on CNC surface (C_6-O-PO^{-}_3H) (Stable colloidal dispersion)	[61]

These nano-scale variants of cellulose (MFC, CNF and CNC) have been suggested suitable for many applications such as strength promoters and barrier materials [62–67], as well as for advanced applications, such as in preparing transparent flexible films [68–70], magnetic or superabsorbent aerogels [71,72], and films with tunable optical properties [73]. Using nanocellulose as an additive or applying it as a coating for packaging material is a potentially big area for research [23,74–76]. One important function of a package can be to inhibit the passage of gases or liquids into or out of the contained products. Nanocellulose has been studied intensely for gas and oxygen barrier properties related to their use as coatings for potential applications in packaging [22,23,77]. A few studies are focused on liquid (polar and non-polar both) barrier properties of nanocellulose. Most of these studies are carried out with physical or chemical modifications of nanocellulose coatings over substrates such as glass [78–80]. Another study focusing on nanocellulose is antimicrobial activity in

conjugation with other materials such as sodium alginate [81], allicin [82], polyrhodamine [83], nitric oxide and chitosan [84].

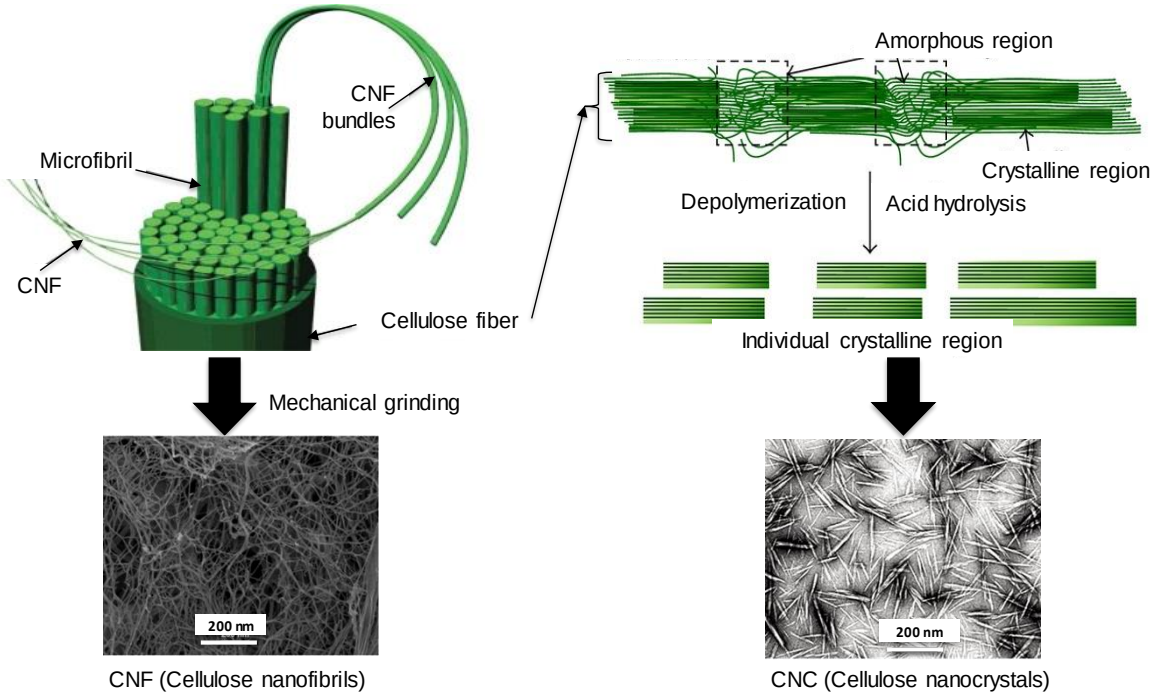

Figure 1-1. Morphological difference between cellulose nanofibers (CNF) and cellulose nanocrystals (CNC) (Source: [42])

Another recently developed variant of nanocellulose is lignin containing nanocellulose [85]. Few studies have been done to produce lignin containing nanocellulose fibers (LCNF) [86–90] and lignin containing nanocellulose crystals from wood as raw material [91–93]. LCNF and LCNC have been shown to be different compared to CNF and CNC respectively in terms of morphology, dewatering, flocculation rheology and mechanical properties [88,94]. Also, LCNF and LCNC have been found to be more hydrophobic compared to CNF and CNC [86,87,90,94], which can be an advantage for many packaging applications. Although, lignin content is considered to interfere with hydrogen bonding between fibrils during coating or film formation [95,96], the mechanical strength of LCNF films has shown improved results when compared to CNF films [87,90,94]. This has been explained based on uniform distribution of lignin seemingly aiding stress-transfer between

fibrils and thus preserving mechanical properties [94]. Compared to bleached nanocellulose, LCNF and LCNC have also been shown to be thermally stable material [88,91]. Lignin containing nanocellulose can be another low-cost sustainable solution for feasible applications. A detailed description of applications of different variants of nanocellulose as a barrier coating and its antimicrobial activity is provided in the following sections.

1.4 Nanocellulose based functional coatings

Nanocellulose has potential use as a functional coating for barrier and mechanical strength properties. The mechanisms and limitations of functional nanocellulose based coatings is described later.

1.4.1 Gas Barrier

A gas barrier packaging coating or film should prevent the penetration of specific gases, aroma/odor which could compromise the integrity of the packed product. Typically, gas barrier coatings and packaging are available for resistance to oxygen, moisture, CO_2 and aroma. Several materials are being used for providing such barrier properties such as glass, tin, aluminum, ceramics, uncoated/coated/laminated plastic films and paper. All these materials possess one or two advantages over the other. For example, glass and tins are excellent barriers, and are strong and heavy. On the other hand plastics and coated papers are comparatively poor barriers but light weight. Printability is another principal requirement for todays' barrier packaging materials [97].

The permeability of gases through a substrate is defined as the quantification of permeate (gas and vapor) transmission through a resisting material [98,99]. In a packaging substrate without any defects such as pinholes or cracks, the primary mechanism of gas or vapor flow is diffusion. Permeate diffusion across the substrate depends upon the types of gas molecules, temperature,

differences in pressure, concentration gradient, film thickness, and area. According to Henry's law theory, gas molecules are unable to permeate a substrate if they are insoluble into the substrate material [100]. Thus, gas permeation into semicrystalline polymers is influenced by their amorphous regions, porosity, and tortuosity created by their network structure to increase flow path for gas molecules [101–103]. Figure 1-2 depicts the basic theory of permeation of gas molecules through the substrate using Henry and Fick's laws.

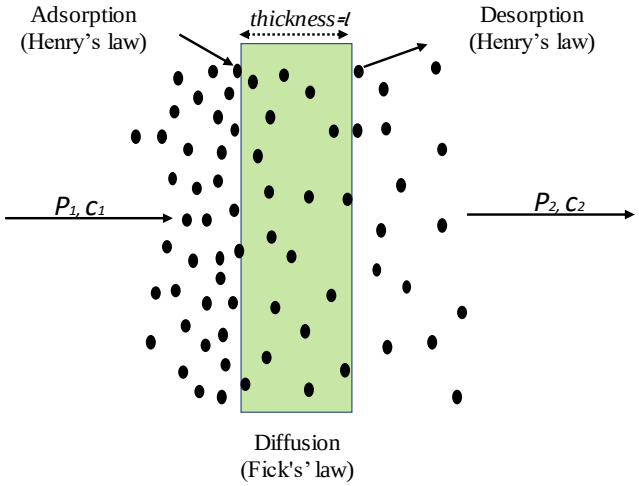

Figure 1-2. Mechanism of gas or vapor flow through a film

The permeation flux (j) of gas molecules through a film of thickness (l) in stationary conditions can be given by Fick's First Law (equation 1-1):

$$J = -D.\frac{\Delta c}{l} = -D.\frac{S\Delta P}{l} \ldots\ldots\ldots Eq.1-1$$

Where, J (mol cm^{-2} s^{-1}) is the diffusion flux, D (cm^2/s) is the diffusion coefficient or diffusivity and Δc (mol/cm3) is the concentration difference across the membrane thickness l (cm). In its steady state condition, the equilibrium of the gas concentration c at the surface and the gas partial pressure p obey Henry's law. When the permeant is a gas, it is more convenient to measure the vapor pressure P (atm), so Δc can be replaced by $S\Delta P$, where S (mol/cm3 atm) is the solubility

coefficient which reflects the amount of permeant in the polymer and ΔP is the pressure difference across the substrate. Similarly, the transmission rate (TR) of gas molecules can be expressed as the volume of gas permeant passing through the substrate per unit area and time, and can be given as equation 1-2:

$$\mathrm{TR} = \mathrm{k}[\frac{\mathrm{V}}{\mathrm{T}(29\mathrm{N} - \mathrm{t})} \ldots\ldots\ldots Eq.1-2$$

Where k = 9.89 x 10^8, TR is the permeance ($cm^3/m^2/day/atm$), V is the measured gas volume (mL) transmitted or permitted through film, N is the slope of the measured curve (sec), T is the temperature (K), and t is the time-lag value (sec).

Like other polymers, the gas barrier properties of nanocellulose films or coatings are determined by the crystallinity and the network structure formed by the constituting units. The lower oxygen permeability of nanocellulose films and coatings is due to two major reasons. One is the non-solubility of oxygen (non-polar) into nanocellulose (polar) and the second is the more tortuous path of gas molecules through the network structure formed by nanocellulose fibrils in films and coatings [67,104]. Increasing tortuosity of coatings or films increases the path length of gas molecules and lowers the permeability through film structure. High crystallinity and dense packing due to the nanoscale size of CNF and CNC results in a high oxygen barrier. Due to the structural properties discussed above, CNF forms a more entangled, dense network solid matrix to provide oxygen barrier properties. In earlier literature, CNF films and coatings have shown promising results, but only at lower relative humidity (RH) values (23%-50%). For instance, Osterberg et al. studied a rapid method of making CNF films with a high oxygen barrier property, at RH < 65%; the oxygen permeability (OP) of these films was below 0.6 cm^3 μmm^{-2} d^{-1} kPa^{-1}. However, the OP of CNF films increased with an increase in relative humidity. This is mainly due to the

plasticizing and swelling of nanofibrils through the adsorption of water molecules at high relative humidities [105]. Modified CNFs such as acetylated and carboxymethylated CNFs have demonstrated excellent oxygen barrier properties at lower relative humidities. Likewise, TEMPO-oxidized CNF films have resulted in a tremendous drop in the oxygen permeability of PVA and PET films, but acetylation affected bonding and other mechanical properties of the derivatized films [106,107].

However, CNC can be a potentially more promising base material than CNFs for the preparation of barrier films that can resist air permeation even at higher moisture contents due to its crystalline structure. Compared to CNFs, CNCs are more crystalline and have less accessibility to water absorption and swelling. However, films comprised of CNCs alone have been rarely tested for oxygen barrier ability due to their brittleness. A reduction in oxygen permeability by adding 50% sulfonated CNC in xylan and the sorbitol matrix was observed [108]. Pereira et al. performed a similar test with the polyvinyl alcohol (PVOH) matrix and used CNCs as a filler [109]. Though 100% of CNC films have not demonstrated similar results compared to CNF films for improving oxygen barriers [110], they have the potential advantage of overcoming moisture sensitivity due to their higher crystallinity. This property of CNCs has been explored in this study by making it synergetic with other suitable additives for preparing an all-around film for barrier properties.

1.4.2 Oil and grease barrier

Similar to nanocellulose films that have lower permeability due to their non-polar nature, i.e., less solubility (Henry's law), a solid CNC or CNF film should be impermeable or at least minimally permeable as per *surface diffusion theory.* This is according to which molecules with higher polarity (such as water vapor) are selectively adsorbed onto the surface of the membrane and pass through the membrane by moving from one adsorption site to another [98]. Due to the non-

polarity of oils, barrier properties of these fluid should demand similar surface characteristics as for oxygen barrier films, except that the state of fluid is different [111]. Though non-polar liquids are rare to diffuse through the packed crystalline structures of nanocellulose without defects, CNF has amorphous parts, which causes diffusion of liquids through it [75]. When we use CNC as a film or coating, good oil and grease resistance barrier properties can be obtained, considering their high crystallinity [67,74]. However, brittleness of the film and cylindrical geometry of CNC particles make it hard to form defect-free films [112,113].

Very few publications have dealt with the potential of CNF or CNC films to serve as oil and grease barriers [20,74]. For making a film or coating suitable for oil and grease containing food packaging, it must show substantial resistance to the passage of oils and grease. Studies have shown that CNF films prepared for oxygen barrier performance also tend to perform for reducing oil/grease permeability through the matrix [20,75,114]. Kisonen et. al. observed an increase in contact angle with glycerin for CNF films coated with O-acetyl-galactoglucomannan (GGM) composites and concluded it as improving oil and grease barrier properties. Several studies have shown the impact of nanocellulose on oil and grease barrier properties of plastic composite materials. when used as a reinforcing agent [115]. Very few publications show the barrier properties of individual CNF and CNC films or coatings [116,117].

1.4.3 Water and vapor barrier

Targeted water and vapor barrier properties are very important for a packaging material. Several studies on nanocellulose have focused on the evaluation of water and vapor barrier properties [114,118–122] and obtained a minimum value of 34 g/m^2/day using chemically modified CNF in PLA composite [123]. However, unmodified nanocellulose containing films and coatings have proven to be poor water vapor barriers due to the hydrophilic nature of the cellulose molecule.

Cellulose bears hydroxyl groups on the pyranol structure of its anhydroglucose (AGU) unit. These hydroxyl groups make the cellulose and its derivative hydrophilic [124]. Chemically native cellulose does not get dissolved in water, but water can pass through the porous layer made up of cellulose [125]. Films constituted of CNFs are not purely crystalline in nature and thus, contain some amorphous domains. When water passes through these amorphous regions, it leads to swelling of the amorphous part and greatly alters the local properties of the nanocellulose films as a whole. Although the crystalline regions of the film should not become swollen with water, Aulin et al demonstrated the swelling of CNC films during QCM-D tests, which could be due to the penetration of water between two crystals, causing water imbibition into the film [125]. Sacui et al studied the morphology and structural properties of CNCs from different sources and demonstrated that dispersive energy (hydrophobic interactions) makes a larger contribution to the total surface energy than acid-base surface energy (hydrophilic). This results in a larger total surface energy of nanocellulose containing films and coatings [126].

Several factors such as the chemical composition of wood sources [127], addition of plasticizers [128], crystallinity, etc., affect the water barrier function of films and coatings. To minimize the penetration of water, certain post treatments such as acetylation [107], gas phase esterification [129], and treatment with alkyl ketene dimer [130]are performed. Most of these treatments tend to reduce the wettability of nanocellulose films. The water contact angle has been measured in the hydrophobic range using the aforementioned chemical modifications [94,107,131,132]. However, mechanical strength and oxygen barrier properties were dramatically attenuated due to a reduction in hydrogen bonding between fibrils [67,128].

1.4.4 Mechanical strength enhancer

For practical and realistic applications, nanocellulose-based barrier coatings should provide enough strength to the substrate in addition to holding out gases or liquids. The level of hydrogen bonding between CNF/CNC during film formation and the coating process influences the strength properties of the coated substrate [133]. This is further influenced by fibrillation, crystallinity, chemical modification, cellulose raw material, and the production method used to obtain nanocellulose [127,130,134–141]. In addition, the techniques used for the coating application or film preparation [66,142,143] and drying conditions [144] employed affect strength properties. Furthermore, the degree of polymerization of cellulose and the porosity and moisture content of nanocellulose films and coated substrates such as paper have also been reported to influence the mechanical properties of films [145]. The tensile strength index and elastic moduli of bare CNF films are found to be 130–212 kNm/kg and 8–11 GPa, respectively [133]. For pure CNC films, the range for elastic moduli has been reported as 5-10 GPa [146]. From this, we see that there are similarities in the strength properties of CNF and CNC films; however, both types of nanocelluloses also have distinct features. For instance, CNCs are more rigid (less flexible) and have lower porosity than CNFs [147,148]. These properties of CNCs add strength, function, and value to many hybrid materials that incorporate these crystalline nanoparticles, such as emulsions, hydrogels, foams, paints, adhesives, and thin films [23,140,149].

In addition, CNC films tend to be more brittle compared to CNF films, which might create problems in coating and packaging applications. For instance, if CNC is used in coating applications for folding cartons, it may lead to failure of both strength and barrier properties due to brittleness. In such a case, Although the coated material has a higher modulus, the elongation distance before failure can be much lower [150–153]. Plasticizers such as glycerol and sorbitol can be

used to reduce the brittleness or rigidity of nanocellulose films [131,154–156]. However, this comes at the cost of the mechanical strength of the films or coated substrate [23].

1.4.5 Antimicrobial applications

Antimicrobial applications are of the areas where nanocellulose has been considered [157–159]. Nanocellulose itself does not possess any antimicrobial properties.[160,161] However, it has been studied for in an antimicrobial support function in conjunction with antimicrobial agents such as antibiotics, polycationic polymers, organic and inorganic nanoparticles, etc. [159,162–166]. Several studies have also been focused on imparting antimicrobial properties to packaging using nanocellulose along with active antimicrobial agents [167–171]. These antimicrobial agents (except antibiotics) are more useful when microbes have developed resistance to conventional antibiotics [172].

Different antimicrobial agents such as nanoparticles and cationic agents such as zinc oxide (ZnO) interacts upon microbial cells using different modes. For instance, most known metals and metal oxide nanoparticles (NPs) such as silver (Ag), gold (Au), copper oxide (CuO), and iron oxide (Fe_2O_3) interact with bacterial membranes, causing membrane disruption. This can be done either by (1) disruption of membrane potential or (2) by generation of reactive oxygen species (ROS) [173–175]. In an ROS pathway of cell disruption, free radicals are produced due to nanoparticles-cell membrane interactions. These radicals further initiate secondary membrane damage and protein and DNA malfunctioning, resulting in a more radical production. Most of these cell disruption actions are nanoparticle size dependent [176–178]. Other pathways of cell disruption are photocatalytic or photoactivation pathways [179]. In this pathway, the generation of ROS is induced by visible or UV light. For example, TiO_2 and nitric oxide (NO) in the presence of near UV- light cause lipid peroxidation that finally results in respiratory malfunction and cell death [180]. Among organic

nanoparticles, cationic polymers such as Poly-ε-lysin, quaternary ammonium compounds, quaternary phosphonium or sulfonium groups, benzoic acid, chitosan, and polycationic nanoparticles are studied for their antimicrobial activity [172]. Among these, chitosan has been considered as the most sustainable and safest antimicrobial agent against a broad spectrum of bacteria, fungi and viruses. Chitosan is obtained by N-deacetylation of N-acetylglucosamine chitin found in the exoskeleton of insects such as crab shells [181]. The antimicrobial activity of chitosan depends upon factors such as pH and solvents [182,183]. Though the antimicrobial mode of action of chitosan is not fully understood [174], it has been shown that it causes dysfunction of membrane potential, respiration, modulation cell division, and nutrition transportation [183]. The antibacterial schematic mechanisms associated with these nanomaterials are summarized in figure S 1-3 [172]. Some examples of nanocellulose films and coatings as carriers for these antimicrobial agents to enhance their antimicrobial activity are discussed below. Abdulkhani et al. evaluated the antimicrobial activity of the CNF and polylactic acid (PLA) composite coated with ethanolic extract of propolis (EEP) [184]. Barud et al. prepared bacterial cellulose and Ag-NPs composite membrane using hydrolytic decomposition of silver nitrate and antimicrobial activity for both gram positive and gram negative bacteria [163]. A multilayer system of TEMPO-oxidized nanocellulose (TOCN), polyvinyl acetate (PVA) and polypyrrole (PPy) was synthesized by Bideau et al. using the chemical polymerization method, and its antimicrobial activity was tested against *B. subtilis* (gram positive) and *E. coli* (gram negative). Certain studies have been done by conjugating nanocellulose with other antibiotics for antimicrobial applications [82,164,166]. Though it has been shown that nanocellulose fibrils have no antimicrobial properties, on the other hand, acid hydrolyzed CNC has been studied for their moderate antimicrobial properties [82]. Due to the slow release properties of antimicrobial agents through nanocellulose networks in films and coatings, it

has been studied for wound healing processes [161,165,185]. Chitosan has also been used with nanocellulose as a blend or in the form of composite for antimicrobial applications [157]. In summary, CNF and MFC have been involved extensively for controlled and slow release studies

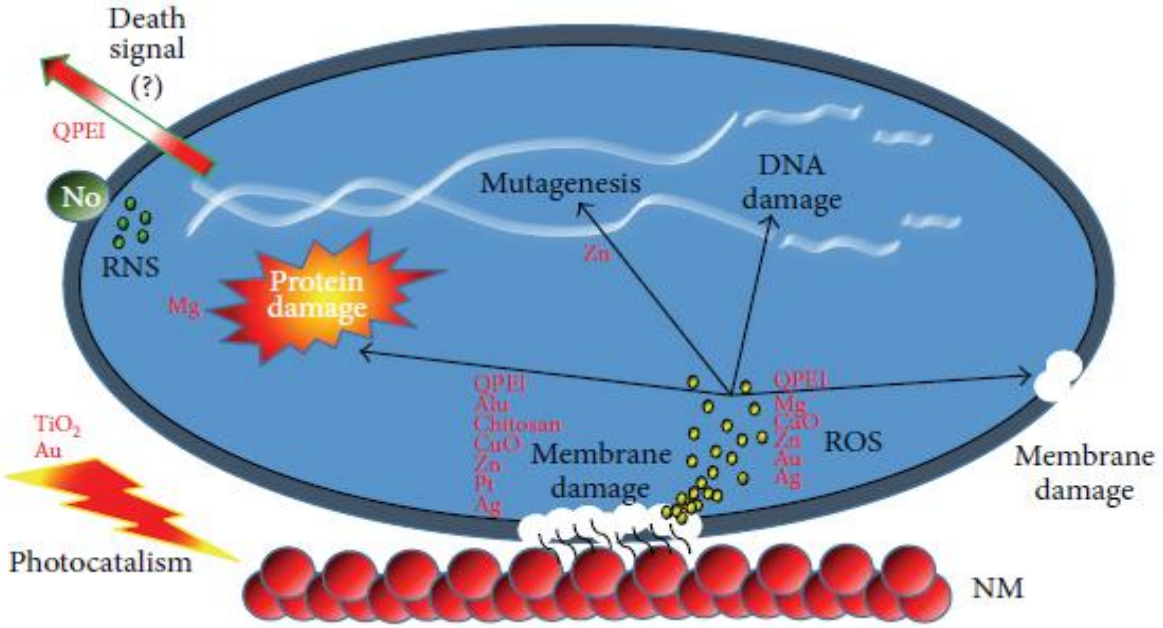

Figure 1-3. Different schemes for antibacterial associated with nanomaterials (Source: [153])

of antimicrobial agents for active packaging, wound healing, and biomedical applications [165,185–191].

1.5 Paper Coating and application methods

Several techniques are available for the application of coatings over substrates, which can be divided into three basic categories based on three metering processes: self-metered, pre-metered, and doctored. In the self-metering process, the coating equipment itself controls the final coverage; example are comma roll, reverse roll [192], and dip coating [193] processes. For pre-metering, all fluid fed to the applicator transfers to the web. The volume of solution supplied to the applicator controls final coverage for the slot die [20] and curtain coaters [195]. Doctored processes such as air knife, mayer rod, and blade and knife coaters use the metering off action as an applicator device

that removes excess applied coatings to control final coverage. Industrially the most commonly used technique for paper coating is the rod or blade metering/doctored method. Blade metering has an advantage over the rod metering process because it can run at higher speeds, up to (~2000

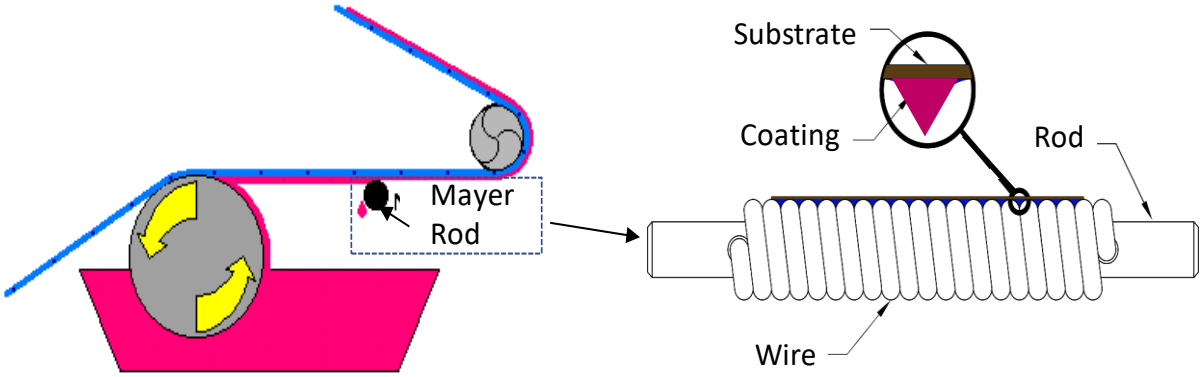

Figure 1-4. Wire wound Mayer rod for bench-top coating

m/min) [196]. Recently a lot of attention is also being given to the curtain coating method. Though there are several coating processes available for paper coating, only a few of them are applicable when nanocellulose suspensions are used as coating materials.

The low solid content (2-3 % for CNF and ~8-10% for CNC) and very high viscosity of nanocellulose suspensions limit high speed and pressure of blades or other metering coating techniques [23]. The most commonly used technique on a lab scale for nanocellulose is the bench-top Mayer rod coating method. [75,76,203–205,117,186,197–202] In the Mayer rod coating method, a wire-wound bar-rod is used to apply a thin film of the coating suspension over the paper substrate (Figure 1-4). This method gives users the ability to fine-tune coating thickness quickly and easily, without altering the chemistry of coating materials and without time-consuming and expensive changeovers. Coating thickness can be controlled with a selection of rod having wire wrappings of different diameters, as specified by the number designation of a selected rod. When wire-wound

rods are used, the approximate wet film thickness over substrates can be calculated by using the following equation: where 'n' is the rod number chosen (Equation 1-3).

$$Coating\ film\ thickness\ (t) = n \times 0.10 \times 0.0254\ mm \ldots\ldots\ldots Eq.\ 1-3$$

For CNF, most coating applications have been done at 0.5-2% solids and very few cases show coatings done at 3% solids [203,204]. The other methods used for nanocellulose coating over paper substrate are size press [206], size press with flooded configuration [207,208], slot die configuration [20], foam coating [209], spray coating [210], filtration and deposition method, [171] etc. These techniques work for nanocellulose coating applications with certain limitations such as low coat weight, slow drying issues, and the handling of high viscous suspensions.

1.6 Conclusion

Nanocellulose is one of the most studied forest biomaterials in recent years for several applications. It has been used for barrier coatings extensively in terms of oxygen barrier properties. However, it lags behind in terms of the water and oil barrier properties. Apart from barrier properties, the scalability of nanocellulose materials for coatings has been a big question due to their low solid concentrations. From the literature, it was found that nanocellulose can be synergized with other antimicrobial agents to add the value to be used as barrier and antimicrobial coatings.

CHAPTER 2. High Performance Nanocellulose-based Composite Coatings for Oil and Grease Resistance

2.1 Abstract

A sustainable packaging system with excellent liquid- and gas-barrier properties and enhanced strength properties was highlighted by a composite coating containing a mixture of cellulose nanocrystals (CNC), a high-aspect ratio nano-filler montmorillonite clay (MMT), an amphiphilic binder soy protein, and a surface-active agent alkyl ketene dimer (AKD). They were tested on various surfaces of commercially available packaging papers and compared with the appropriate control (i.e., CNC-only coating) to determine surface morphology, chemical composition, barrier, and mechanical properties. Scanning Electron Microscopy (SEM) image analysis showed a compact matrix whose defects (cracks) were significantly attenuated compared to the control while FTIR showed fewer exposed hydroxyl (-OH) groups. The compact structure and reduced –OH groups are attributed to the plate-like structure, high aspect ratio of clay, and uniform distribution of additives to help inhibit gas, moisture, water, oil, and grease permeation. The base paper used also had a significant impact on how coatings interacted with various fluids. Overall, sustainable CNC-composite barrier coatings with relatively low-cost additives were fabricated and showed improved barrier and strength characteristics with a strong potential as barrier coatings for packaging.

2.2 Introduction

Nearly 1.3 billion tons of food is wasted each year after the manufacturing, distribution, and disposal of household waste [211]. Furthermore, one-third of food in developed countries such as Britain, Sweden, and the USA are wasted due to expiration of shelf-life [212]. Such waste indicates the overriding importance of packaging for maintaining quality and facilitating movement of food

along the value chain. An ideal packaging material should have substantial barrier properties for gases, water, oils and grease materials to protect food from its surroundings and increase shelf-life.

Cellulose nanocrystals (CNC) and cellulose nanofibrils (CNF) are among the most studied materials over the last two decades due to their intrinsic nanoscale dimensions, excellent mechanical strength, light weight, tunable chemistry and assembly, and biodegradability [75]. However, difficulty in processing due to a very high viscosity of CNC and CNF suspensions at low solids, and susceptibility to moisture have limited their commercialization prospects in applications such as barrier coatings for paper and paperboard. CNFs possess amorphous as well as crystalline regions with diameters in the nanoscale range (5-50 nm) and lengths of several micrometers depending on the source and method of preparation [213]. CNCs are crystalline derivatives of cellulose prepared by acid hydrolysis of various forms of cellulose with diameters in the range 2 to 30 nm and lengths from one to several hundred nm [214,215]. A higher crystallinity provides the potential for superior film barrier properties [216]**.** However, high crystallinity makes this type of structure more susceptible to fractures resulting in defects, including pin-holes.
Several studies have employed nanocellulose materials as composites or fillers for plastic films [217,218] and coating on paper substrates [66,198]. Synthetic films with CNC as reinforcement material have demonstrated an increase in mechanical properties [107].

Regarding oxygen barrier properties, CNFs are promising, but only at lower relative humidity (RH) values (23%-50%). Permeability increases with relative humidity due to the plasticizing and swelling of nanofibrils [105]**.** A reduction in oxygen permeability by adding 50% sulfonated CNC in a xylan and sorbitol matrix has already been observed [219]**.** Luís et al. performed a similar test with a polyvinyl alcohol matrix and used CNCs as filler [220]**.** Though 100% CNC films

have not demonstrated similar results compared to CNF films for improved oxygen barriers, [221] they have a potential advantage due to their higher crystallinity.

The intrinsic nature of cellulose is hydrophilic due to the abundance of hydroxyl groups [222] which must be modified to make them suitable for packaging [223]**.** Modified CNFs such as acetylated and carboxymethylated CNFs have demonstrated excellent oxygen barrier properties at higher relative humidities, but acetylation adversely affects bonding and other mechanical properties [224]. Unmodified CNC has also been a filler in many composite films with higher water barrier properties [225]**.** Bardet et al. showed that when 32.5 % of CNC and nano-clay were filler in CNF matrix, both resulted in similar WVTR values of 85% RH [226]**.** Khan et al. studied the effects of CNC as a filler in methylcellulose films and demonstrated a decrease in water vapor permeability by 25% with the addition of 1 wt% CNC in CMC films [227]**.** Yet, there is still a lack of work in water vapor barrier and oil resistance for nanocellulose-based coatings in paper-based products [77]**.** Substrates for food packaging and serving must show substantial resistance to stains and the passage of oils and grease. Studies have shown that CNF films prepared for oxygen barrier performance tend to provide greater oil/grease resistance [114]. However, more work is required to study the difference in diffusion phenomenon of oil and oxygen through nanocellulose films and coatings.

As already described, chemical derivatizations generally inhibit intermolecular bonding in nanocellulose, resulting in a lower strength [228]**.** However, underivatized cellulose does not dissolve in water, but both liquid water and vapor can pass through its pores. When water passes through this porous structure, it leads to the swelling of the amorphous regions and adversely affects barrier and mechanical properties. The research objective of this study is to therefore develop composite CNC-based barrier coatings with high aspect ratio additives such as nanoclays, naturally occurring

amphiphilic polyelectrolytes (e.g., protein) binders, or cationic hydrophobic agents (alkyl ketene dimer emulsion) to induce CNC impermeability to gases, water, water vapor, oil, grease, and other liquids while maintaining packaging mechanical properties.

2.2.1 Rationale

The theme underlying the current work is illustrated in Figure 2-1 in which the development of a CNC coating layer with compatible additives is demonstrated. Generally, a uniformly aligned arrangement of CNCs in films is expected to give better barrier properties [23]. However, for paper coatings which is dried at very fast rate at high temperature to avoid penetration of water through paper sheet [229]. These conditions will not provide enough time for CNC coatings to attain such align orientations. However, a randomly settled CNC coating may be less permeable to gas, water, oil and grease. It is further proposed that nano-scale fillers, selected to impart desired characteristics to the coating, can be deployed such that film remains dense and relatively defect-

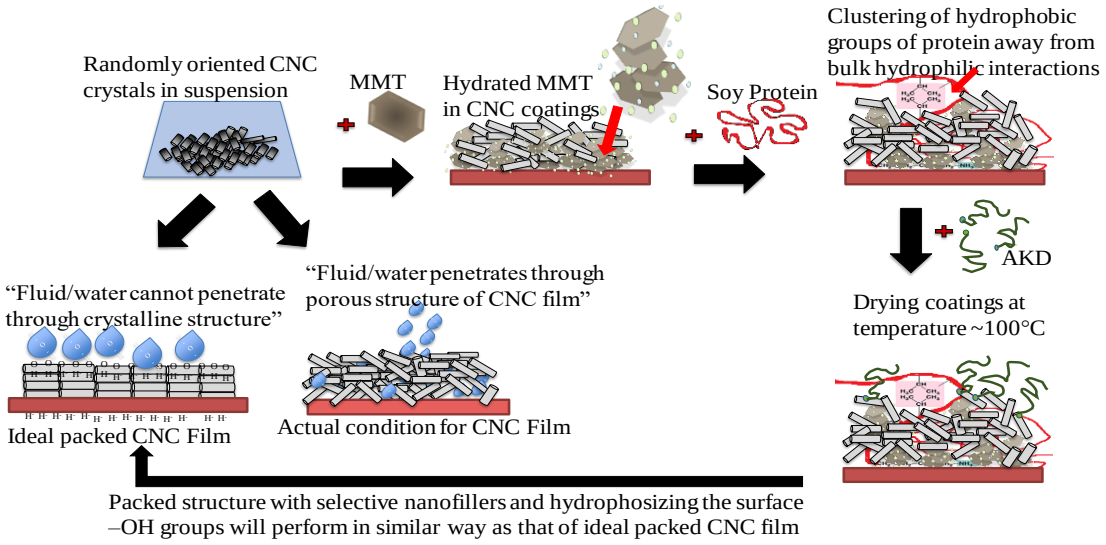

Figure 2-1. Schematic displaying how coating materials such as randomly distributed CNC can lead to high barrier and strength properties.

free, and therefore able to resist air penetration. Sodium montmorillonite, MMT, (i.e., bentonite)

was selected as a co-additive in a blend with CNC suspension because of its nanoscale (~1 nm thickness) platelet structure. Pal et al. have demonstrated that plate-like shaped engineered clays in acrylic-copolymerized coatings help reduce WVTR and air permeation [230]. Rearrangements in MMT were observed as a direct result of the breakdown of MMT particles due to increased hydration. The CNC coating thus has pores filled with plate-like MMT particles that individually block the passage of fluids [231]. The high crystallinity of MMT effectively prevents the penetration of fluids through the mineral phase. The shape and size attributes of MMT clay can change CNC suspension coated layer behavior; therefore, kaolin clay with higher size and lower aspect ratio was selected for comparison. Considering its amphiphilic nature, biodegradability, and conformable and surface-active nature, soy protein was chosen to improve CNC-MMT coating attributes. Finally, AKD in a cationic emulsion form was selected as the hydrophobizing agent. It has been proposed that by adding a reactive cationic hydrophobic agent in the form of an emulsion, spreading will tend to be delayed until late in the heating and drying of the paper (or coating, in the present discussion), at which point a significant proportion of potential hydrogen bonding among the cellulose surfaces would have already had a chance to form [232]. The expected chemical ineraction between selected components of coatings is presented in Figure 2-2.

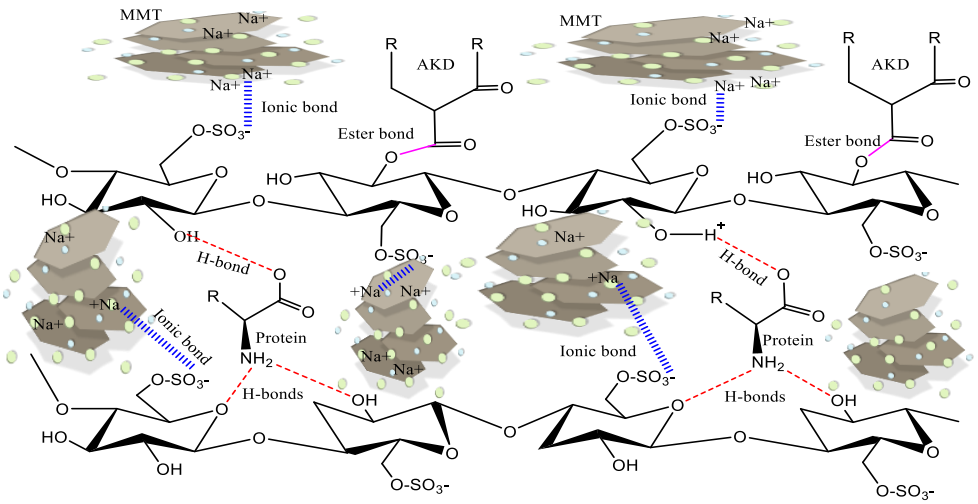

Figure 2-2. Possible chemical interactions among various components of coatings

2.3 Experimental Plan

An experimental procedure was set up based on a lab drawdown method for coating paper to better understand the interactions between CNC and other additives, and to compare the results obtained from CNC-composite coatings with CNC-only coatings. Table 2-1 shows the chemical ingredients and amounts used to prepare barrier coatings in the current study. Three different packaging papers were selected for the coating application to evaluate the functionality of optimized CNC-composite coated layers from each major component combination.

Table 2-1. Chemical ingredients and amounts used to prepare barrier coatings.

Dry Parts	**CNC-only**	**CNC-AKD**	**CNC- S-AKD**		**CNC-S-AKD-K**				**CNC-S-AKD-MMT**			
CNC	100	100	100	100	90	85	80	75	90	85	80	75
MMT	0	0	0	0	0	0	0	0	10	15	20	25
Kaolin	0	0	0	0	10	15	20	25	0	0	0	0
Soy protein	0	**0**	10	20	0 & 20				0 & 20			
AKD	0	2	0 & 2		0 & 2				0 & 2			

2.4 Materials and Methods

The main coating components involved in this study were nanocellulose crystals (CNC), used as a primary coating material together with sodium montmorillonite (MMT), kaolin clay (K), soy protein (S), and alkyl ketene dimer (AKD) as co-components. CNC was procured from the University of Maine in an aqueous suspension form, which was 12.2 wt.% CNC in water. The CNC had been prepared by acid hydrolysis using sulfuric acid, so it had 0.85 wt.% sulfur content based on dry CNC, in the sodium form. Sodium montmorillonite (bentonite), which was obtained from BASF with the trade name HYDROCOL 2D6, is 95-99 % MMT and 1-5% crystalline silica with a bulk density of 2.4 g/cm^3 at 20 ^{0}C. Kaolin clay used in this study is a fine

clay with 95% of particles less than 2 µm. Soy protein, with a neutral pH of 6.3-6.8 used as a binder in this study, was obtained from DuPont USA with the trade name 'SoBind^{TM} Balance HVL Soy Polymer'. A protein solution was prepared by first making a 10% slurry in water under a continuous high shear, and then cooking it at 80 ^{0}C for 30 minutes. AKD emulsion cationic polymer (Hercon™ 100) was procured from Solenis, LLC, Wilmington, USA.

2.4.1 Coating preparation

First, each coating ingredients dry and wet weight was calculated based on the dry parts in Table 2-1 and each ingredient solid contents for a batch size of 250 grams at a target coating solid of 10 wt.%. Second, the water needed to achieve a target solid of 10 wt. % was calculated by subtracting ingredient total wet weight from the target wet batch size (250 grams). The coatings were prepared by first weighing each ingredient according to the desired coating recipe, and then slowly adding it into a small beaker while continuously mixing using a 'constant-torque' lab mixer at 500 rpm. Ingredients were added in the following order: water, MMT, K, CNC, SA and AKD ingredients. This helped avoid agglomeration of the coating suspension. CNC, MMT, and K were considered the main ingredients (100 parts), and other components were added on their basis. After making sure of enough hydration of clay by mixing with water for 1 hour, all other ingredients were added. The overall coating recipe was mixed at 1000 rpm for 2 hours to make a uniform suspension.

2.4.2 Wet coating properties

Rheology testing was done using the TA instrumentation Advanced Rheometer (AR 2000) with a plate geometry of diameter 40 mm. The steady-state viscosity was measured at a shear rate of range 1 to 1000 s^{-1} at a temperature of 25 ^{0}C. For the flow step, steady state flow was selected with 3 points per decade and a sample period of 10 seconds. Apparent viscosity was also measured

using a Brookfield DV-III Ultra viscometer with spindle number 3 and 5 at a speed of 200 rpm at 20 ^{0}C. The water retention value of coatings was determined using the TAPPI T 701 method.

2.4.3 Coating application

CNC-composite coatings were applied on packaging paper using a Mayer rod and dried using hot air (approximately 100 °C) for 5 to 8 minutes. The target wet coating thickness was achieved by changing the Mayer rod. The wet film thickness on the substrate was approximated by using the following equation, where n is the rod-number chosen and directly correlates to the applied wet coat thickness in inches (n × 0.001 inches).

$$Film\ thickness = n_{\,x}\, 0.001_{\,x}\, 25.4 \ldots\ldots\ldots\ldots Eq.1$$

2.4.4 Morphological and chemical properties

The surface morphology of coated samples was examined using a FEI Verios 460L field emission SEM at an accelerating voltage of 2 kv and 13pA current. Prior to imaging, samples were sputter-coated with a thin layer of gold in a low vacuum of 90 mTorr of Ar gas pressure with an accelerating voltage of 600 V for 3 minutes at a coating rate of 7 nm/min. For high magnification imaging, no gold coating was carried out and a biased voltage was used. The chemical characterization of the coated surface was carried out using a Bruker-Opus ATR-FTIR instrument within the range of 400 to 6000 cm^{-1} wavenumber with 4 cm^{-1} resolution for 64 scans. Packaging base paper pH measurement was done by weighing 2 grams of paper and soaking it in 100 ml of deionized water. After slushing in a Waring blender, the resulting pulp was boiled in a hot water bath for 5 minutes, and pH was measured after cooling the pulp to room temperature. Fiber characterization of each paper type was carried out using the TAPPI T271 method with a HiRes fiber quality analyzer (FQA) from Op Test Equipment.

2.4.5 Mechanical & surface smoothness properties

The bending stiffness of papers was measured using a Taber tester as per the TAPPI T566 method. The roughness of the papers was measured using the TAPPI T538 method, which is an indirect measure of smoothness. Results were reported in Sheffield-units.

2.4.6 Barrier Properties

Barrier properties such as water resistance, water vapor transmission rate (WVTR), resistance to air permeance, and oil and grease resistance (OGR) of CNC-containing coated substrates were measured. The WVTR was tested using the water cup method in accordance to the ASTM E-96 test method, by using standard cups from Thwing-Albert Instrument Company. Water absorption (Cobb test) was determined using the TAPPI T441 method. For resistance to air permeance, the TAPPI 'Gurley Densometer method' of air resistance T460 was used. Results are reported as Gurley seconds per 100 ml air displacement (Gs/100ml). The OGR was tested by performing a 3M Scotchban test, which has been adopted under TAPPI T559. Results were reported as kit number from 1 through 12.

2.5 Results and Discussion

2.5.1 Packaging base papers

Three different base papers were selected with different characteristics and labeled A, B, and C, as described in Table 2-2 to study coating behaviors. Base paper A had the lowest roughness that can help more uniform distribution of the coating layer on the surface. Base paper B had the highest water absorption (Cobb), and lowest contact angle, but also the highest air resistance (least porosity). Base paper C seemed to have most hydrophobic surface (highest contact angle and least Cobb60 value), but the least air resistance (highest porosity).

Table 2-2. Three base papers selected for current study and their characterization

Base Paper ID	Base paper A	Base paper B	Base paper C
Basis weight (g/m2)	300	325	195
Caliper (µm)	378±4	428±4	421±8
Fiber length (Lw) (mm)	2.24	1.37	1.62
Roughness *(S.U.)	264±2.6	351±4	428±4
Surface pH	5.7	7.4	5.94
Bulk (cm3/g)	1.26	1.32	2.16
Air resistance *(G.s./100ml)	36.1	212	3.1
Cobb60 (g/m2)	48.3	455.9	27
Contact angle	89.8	71	103

2.5.2 Wet coating properties

Properties such as apparent viscosity, pH, and water retention were measured before applying the coating on base papers by a Mayer rod and then drying. Table 2-3 shows fluid properties measured for selected coating recipes. These were used to select a Mayer rod number to obtain a target coat weight of 5 g/m^2. For convenience, a special abbreviation is given to each selected coating recipe for reference in further discussion.

Table 2-3. Fluid properties of selected coating recipes

Coating Recipe	**Abbreviation used**	**pH**	**Apparent viscosity [cP] @ 200 rpm**	**Water Retention [g/m^2]**	**Mayer Rod no.**
CNC-Only	C100	6.17	1150±84	1349±41	6
CNC100-AKD	C-A	6.75	396±27	1258±23	8
CNC80-AKD-MMT20	C-A/M20	8.76	544±43	1051±67	8
CNC100-S20-AKD	C-SA	6.75	728±16	1196±19	8
CNC80-S20-AKD-K20	C-SA/K20	6.94	394±38	1069±46	12
CNC80-S20-AKD-MMT20	C-SA/M20	7.62	619±48	1062±53	8

2.5.3 Rheological properties

Figure 2-3 shows the rheological power law behavior for major coating formulations

studied as a log-log curve between viscosity against shear rate. From the graph, it is clear that all coating formulations are pseudoplastic following the power law of fluids (slopes of the graphs are less than 1 showing shear thinning behavior of coatings), which is desirable for coating application purposes [233,234.] The steady viscosity of 'C-A' coatings was significantly higher than that of other CNC and additive formulations, indicating stronger networks formed by hydrogen bonding, which keeps on disrupting at high shear rates due to the shear thinning behavior of CNC. This is very surprising that with Brookfield viscometer, apparent viscosity of CNC was found to be much higher as compared to C-A. The possible explanation for this can be that CNC at low shear values presents higher viscosity compared to C-A. However, at high shear rates, steady viscosity decreases due to the disruption of hydrogen bonding and shear-thinning. C-A (where AKD is cationic stabilized as dispersion in water) had more interaction even at higher torque due to additive ionic interaction between CNC and AKD. Also, likelihood of depletion of CNC concentration in the neighborhood of wall boundaries can another reason for lower viscosity in case of plate geometry rheometer [235]. Among multi-component coatings, 'C-SA/K20' showed the least viscosity and stress at the same shear rate, indicating the least coating interactions at a given concentration. Following 'C-A' formulation, MMT in combination with CNC and AKD ('C-SA/M20') showed the highest shear stress and viscosity, which was slightly greater than for CNC-only particles. This was due to structural compatibility and ionic interaction between bentonite's platy structure and CNC's cylindrical shapes, both at nanoscale structures. Such rheological behavior of CNC-containing suspensions gives a stronger point to the microscopic-structural behavior of coatings (Fig. 2-4 and 2-5). For all these coatings, viscosity decreased with shear rate. Upon shearing, the internal structure of coatings breaks down, showing the thixotropic behavior of both CNC and MMT suspension.

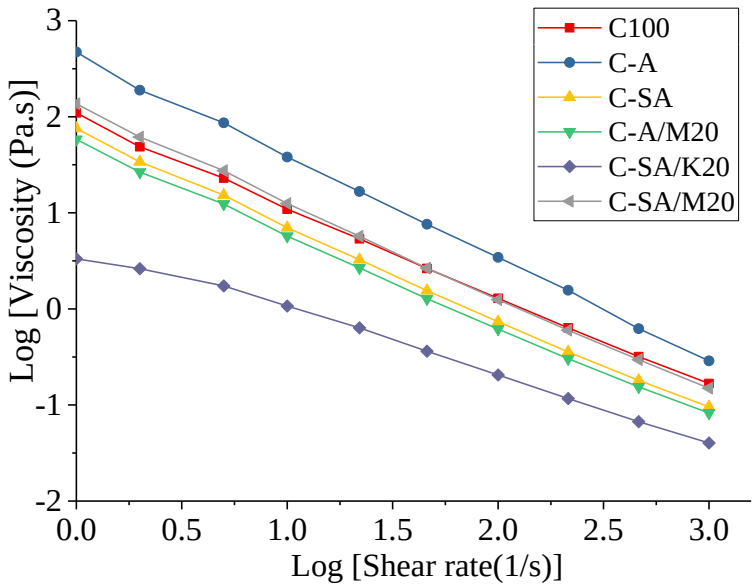

Figure 2-3. Rheological behavior of selected coatings, Viscosity (η) as a function of shear rate.

2.5.4 Morphology of coatings

Figure 2-4 shows the SEM images of CNC coatings with different additives. It can be inferred from the Figure that CNC with MMT (Fig. 2-4e) provided the most compact matrix

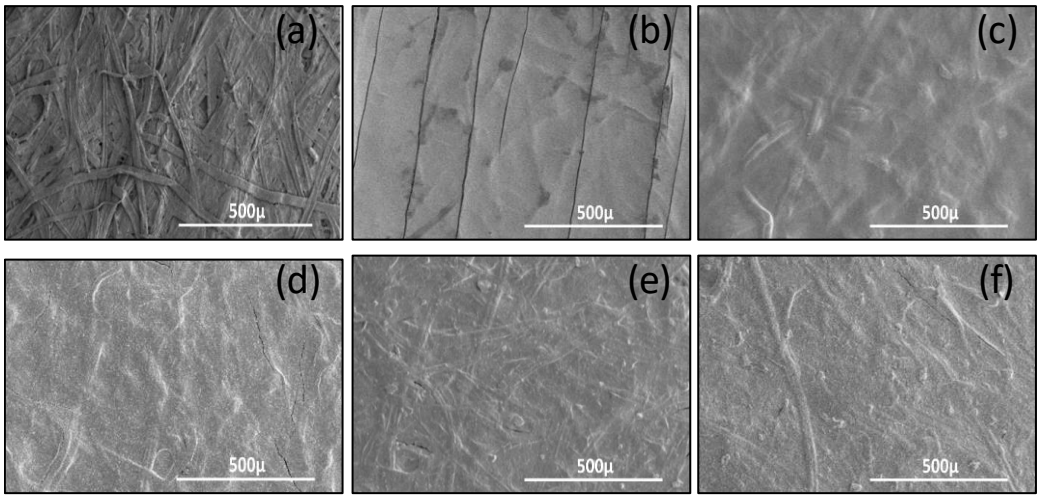

Figure 2-4. SEM images of (a) Uncoated, and coated base paper with (b) C100, (c) C-SA, (d) C-SA/K20, (e) C-A/M20 (f) C-SA/M20 coatings on base paper B at 100x magnification.

covering all the paper types with the least number of defects (cracks). This allows the papers to develop a barrier against the diffusion of moisture and gases. The compact packing structure of CNC and MMT clays can be attributed to the platy structure and high aspect ratio of bentonite clay [226]. An even tighter matrix was observed when soy protein was used as a binder (Figure 2-4f).

However, a combination of kaolinite and CNC gave rise to a defective coating layer over the same base paper due to the incompatible shape and size of kaolin clay with CNC coatings (Figure 2-5b and 2-5d). This can be attributed to large particle size and comparably low aspect ratio of kaolinite. Figure 2-5a and 2-5c shows how MMT platy particles are distributed throughout the paper surface, either embedded into the CNC coatings or covering the outer surface. However, kaolin particles had the tendency to protrude from the CNC-S matrix and, hence, provided no contribution to barrier properties.

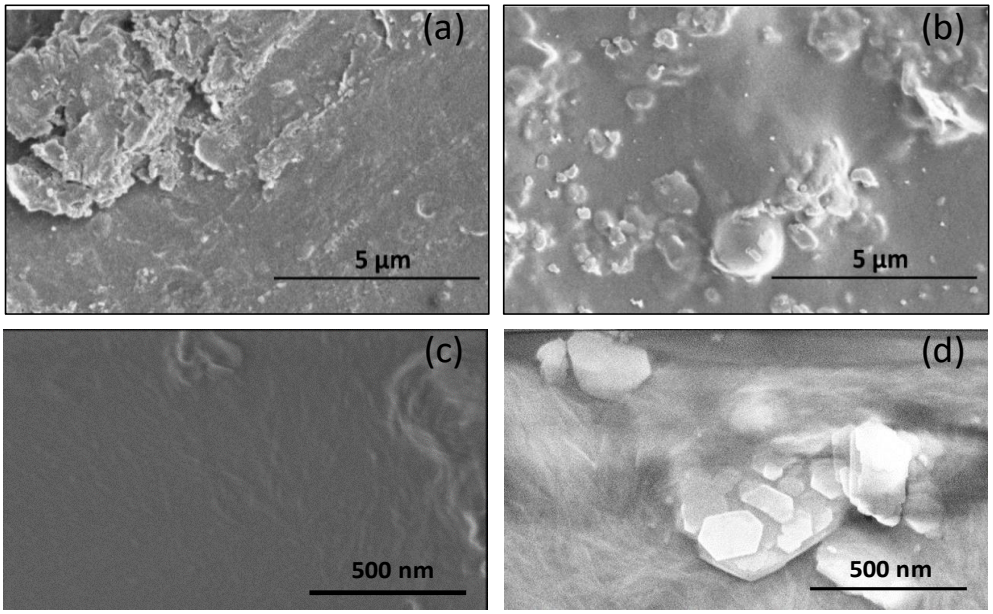

Figure 2-5. SEM images of (a), (c) C-SA/M20 and (b), (d) C-SA/K20 coating layer on base paper B at 10,000x and 50,000x magnification.

2.5.5 FTIR spectroscopy

To confirm the presence of clays on coated base papers, FTIR spectra of CNC coatings with and without clays were compared with respect to their characteristic peaks (Fig 2-6). 'CNC only' spectra reproduce the same CNC characterization as studied by Pei et al [236]. For 'C100' and 'C-SA coated base paper the presence of soy protein in 'C-SA' coating was confirmed by the following peaks: 3200 cm^{-1} to 3500 cm^{-1} corresponds to the stretching vibration of hydroxyl groups present on CNC surface. The peaks in the range of 3000-2800 correspond to the stretching vibration of the -CH and -CH_2 bond in CNC; their intensities were reduced with the addition of

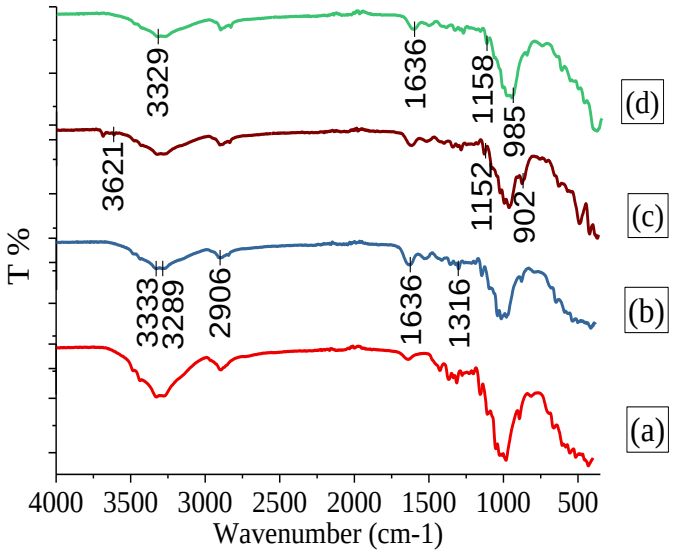

Figure 2-6. FTIR spectrums of a) C100, b) C-SA, c) C-SA/M20, and d) C-SA/K20 coatings on paper B.

clay. Peaks at 1634 cm^{-1} (redundant with water absorption peak at 1636 cm^{-1}) correspond to amide I (C=O stretching), 1537 cm^{-1} for amide II (N-H bending), consistent with the previous reports [237,238]. However, another confirmatory peak for soy protein, which should have been observed at 1234 cm^{-1} for amide III (C-N and N-H stretching), was absent. This confirms the denaturation of the tertiary structure of soy protein while heating during coating preparation and drying. The presence and reaction of AKD in the coating has been confirmed with the ester peak (bending of

C-O) at 1048 cm^{-1}.

The presence of kaolin on the surface of C-SA/K20 coated base paper was confirmed by a stretching peak at 3692 cm^{-1} due to crystalline -O-H and Al—O-H , the Si-O in-plane stretching at 1023 cm^{-1}, and 464 cm^{-1} due to Si-O-Si bending vibration [239]. The intensity of water absorption peak at 1636 cm^{-1} is reduced in the kaolin-containing coating and almost disappeared in the MMT-containing coated surface ('C-SA/M20). This confirms significant interaction between amide I of soy protein and O-H of MMT. The intensity of -OH stretching vibration peaks at 3200-3500 cm^{-1} has been reduced significantly in 'C-SA/M20 coatings. MMT-containing coated surface exhibited almost flattened or no peak between 2800 and 3000 cm^{-1}, confirming the absence of -CH and -CH_2 groups [240] and good coverage of the CNC surface with MMT platy structure as shown in the SEM picture of C-SA/M20 coatings (Fig. 2-5a).

2.5.6 Water absorption

Water absorption was reduced substantially for CNC coatings on the selected base paper (B). Further reduction was observed with the addition of AKD to CNC-MMT coating. MMT was optimized for blending with the CNC at 20 parts for a given coating recipe with CNC and reduced water absorption by 78% on base paper B (Fig. 2-7b). The base paper used had a significant impact on how coatings interacted with the substrate surface. Substrate B, which had the highest air resistance ~212.0 Gs (Table 2-2), resulted in the highest reduction of water absorption from 455 g/m^2 to 100.86 g/m^2 with 'C-SA/M20' coating (Figure 2-7a). However, for substrate A and C, which had very low air resistance (i.e., ~36.1 and 3.1 Gs), little difference existed even at higher concentrations of MMT particles.

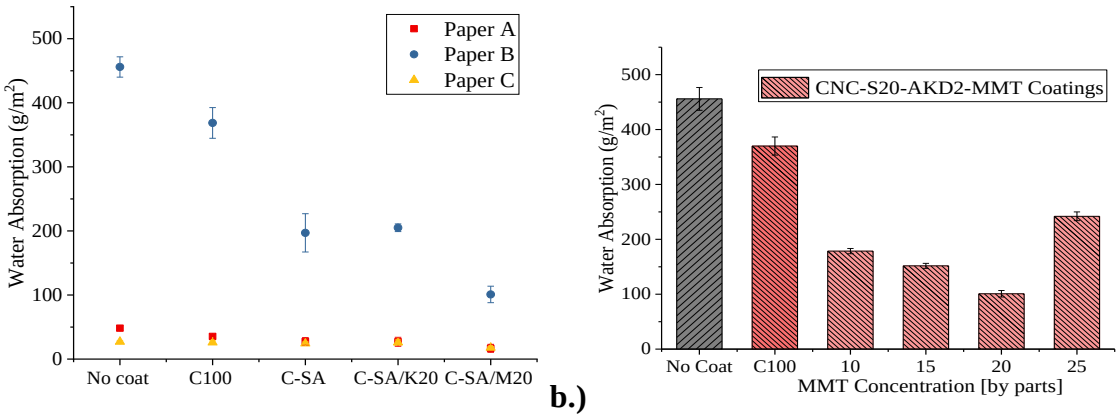

Figure 2-7. Water absorptiveness of: a) Optimized CNC coatings with different combinations of additives on different base papers (A, B, C); b) un/coated base paper B with different concentration of MMT in CNC-S20-AKD2-MMT coatings.

2.5.7 Water vapor transmission rate

In contrast to the significant reduction in water absorption, no significant reduction in WVTR was observed for a kaolin blend with CNC on base paper B. However, soy protein, AKD and MMT in CNC coatings showed a slight reduction in WVTR. As shown in Figure 2-5a, MMT platy particles are distributed more uniformly throughout the paper surface, either embedded into the CNC coatings or covering the outer surface. However, kaolin particles had the tendency to protrude from the CNC-S matrix and, hence, provided no significant reduction in water vapor transmission rate. This could further be explained by a lower viscosity (Table 2-3 & Figure 2-3) of Kaolinite containing coatings in comparison to MMT and soy coatings, potentially leading to more non-uniform coating application. Increasing the concentration of MMT from 10 to 25 parts showed no reduction in WVTR (Fig. 2-8b). Different base papers exhibited a significant impact on the application of functional coatings. For instance, substrate A, which was comprised of unbleached longer fibers and had a smoother surface, showed better results with CNC-blend coatings when compared to rough papers (B &C). A smoother paper surface increases the chances

of a more uniform distribution of coating layer providing a more effective coat weight instead just filling the valleys of rough paper. It can be seen from Figure 2-8a that for substrate A (Red square), WVTR was reduced from 137 g/m^2/day for non-coated paper to 99 g/m^2/day with 'C-SA/M20' coating (reduced by ~27%).

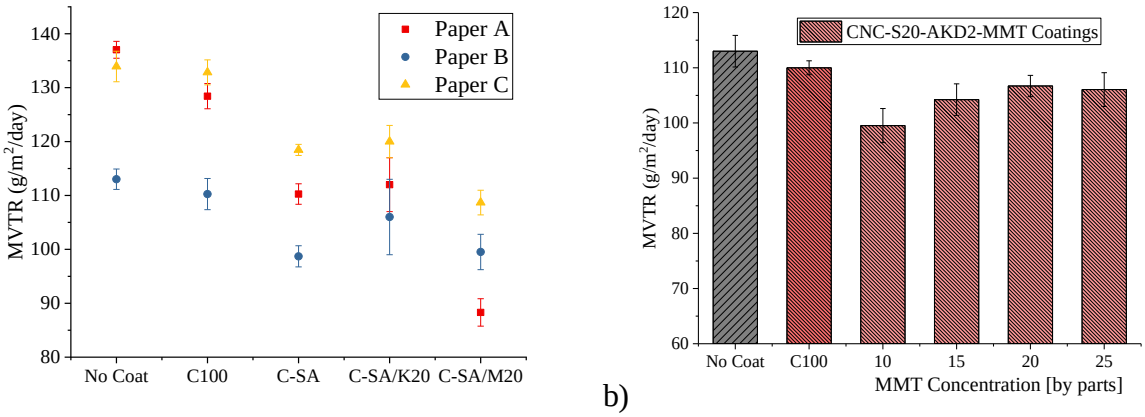

Figure 2-8. WVTR of un/coated base paper B with: a) Optimized CNC coatings with different combinations of additives on different base papers (A, B, C); b) Different concentrations of MMT in CNC-S20-AKD2-MMT coatings.

2.5.8 Gas barrier

Measured air resistance for different coating components on substrate B is shown in Figure 2-9a. Air resistance increased dramatically by CNC and was increased further by introducing other components such as MMT. MMT and other additives were able to provide more tortuosity to the CNC coating, and thus increase the mean free path for air molecules to diffuse through coating and paper thickness. The lowest permeance (highest air resistance) was measured with the 'C-SA/M20' coating as 1,917 Gurley seconds (higher Gurley $\propto$ lower permeance), which dropped from 424 Gurley seconds for non-coated paper (Fig. 2-9a & 2-9b). No significant air resistance improvement was observed with any of the coatings used on substrate C for a given coat weight. The roughness of substrate C was much higher in comparison to the roughness of substrates A and

B. The equivalent coat weight applied on paper C might not be enough to provide functional resistance to permeance. Also, the bulk of base paper C was higher in comparison to A and B, which further reduced resistance to air (Figure 2-9a).

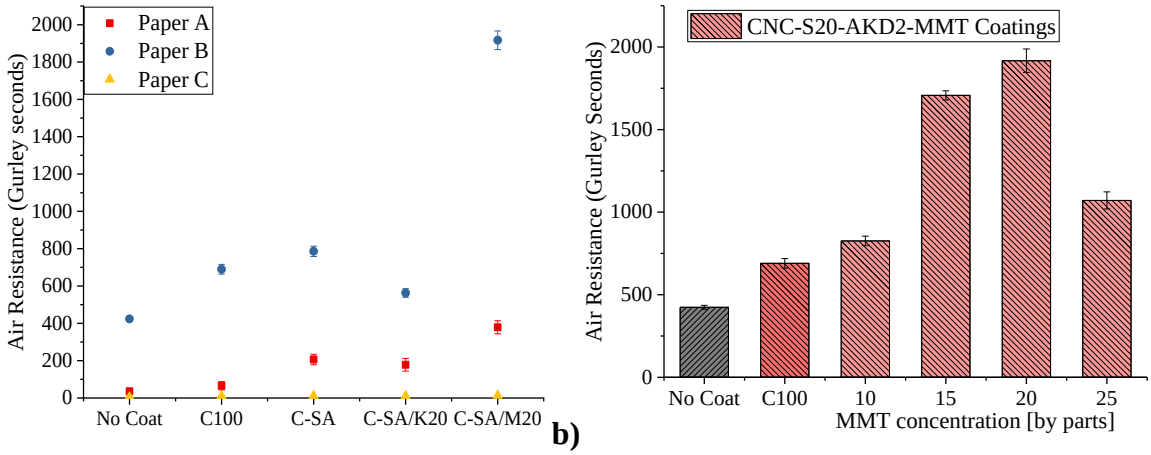

Figure 2-9. Air-resistance of un/coated base paper B with: a) Optimized CNC coatings with different combinations of additives on different base papers (A, B, C); b) Different concentration of MMT in CNC-S20-AKD2-MMT coatings.

2.5.9 Oil and Grease Resistance

Figure 2-10a shows a pass. No dark surfaces after treating the paper with oil/solvents kit solution, indicates no penetration of oil through paper coating. Figures 2-10b and 2-10c show a fail. A dark surface observed after treating the paper with oil/solvents kit solution, indicates oil penetration through paper coating. These are the conditions for a paper specimen with kit numbers 6, 2 and 1, respectively. As kit number increases, the amount of hexane and toluene solvents increases and the amount of castor oil decreases in kit solution. Thus higher kit number, favors the penetration of kit solution through paper due to less viscosity and compratively more non-polar solution. Table 2-4 summarizes all significant results obtained with different CNC coatings on

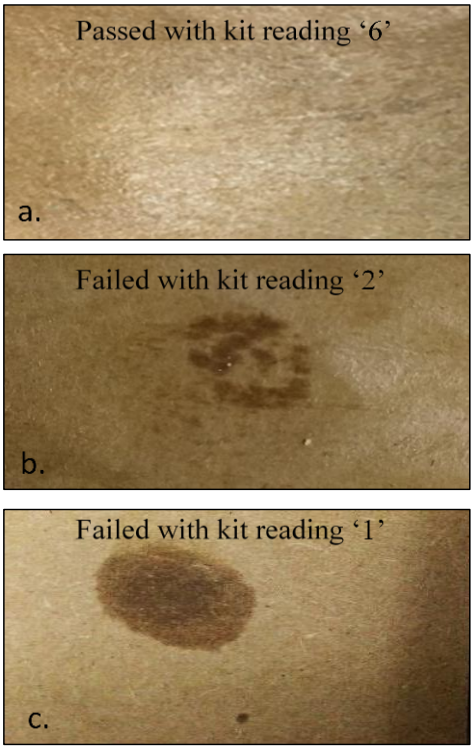

Figure 2-10. Examples of kit testing of paper samples with a.) 'C- SA/M20'- coated, b.) C100 and c.) uncoated base paper B.

three different substrates. For samples A and B, the highest readings obtained were 3 and 6, respectively. Base paper B, with the highest air resistance (212 G.s), showed the highest reading with 'C-SA/M20' coating.

However, with base paper C, which had the lowest air rsistance (3.6 G.s), as mentioned in Table 2-2, no improvements for oil and grease barrier properties were observed with any of the coating recipes studied. A very high porosity affects the consolidation of coating layer over the paper surface negatively. Due to a highly porous paper structure, most of the coating components penetrate through the paper bulk instead of consolidation of coating layer over the surfrace. [229].

Table 2-4. Summary for Kit test results for all three base papers

Coatings	Base Paper A	Base Paper B	Base Paper C	Remarks
No coating	0	0	0	
C100	0	1	0	
C-SA	3	5	0	No cracks
C-SA/K20	2	4	0	
C-SA/M20	3	6	0	No cracks

This shows that the higher the air resistance, the greater the tendency to obtain a grease resistant property after coating the paper [229]. Another challenge faced during this study was the brittleness of the coatings due to the lack of plasticity in the crystalline coating structure of CNC. The coating layer was more prone to fracture, which could be more prominently observed during a test with a partial penetration of solution through the coating layer. This explains the reason for failing the higher number kit even for a compact and tortuous coating layer of CNC-MMT.

2.5.10 Strength properties (Stiffness)

Stiffness was measured to characterize the flexural rigidity of paper, which is very important for packaging purposes and is related to economics. Figure 2-11a and 2-11b indicates that stiffness increased by 30% with a pure CNC coating on base paper B, due to nanoscale structures, packing of CNC, and hydrogen bonding between CNCs and base paper B. The rough surfaces (valleys) of the base paper were filled with the nanocellulose crystalline molecules, resulting in a lower bulk and higher bending moment. Further introduction of additives into CNC matrix reduced the number of hydrogen bonds, resulting in a lower strength. However, coatings with AKD provided better stiffness, which is consistent with the study of Bildik et al. in which AKD wax was dissolved in heptane and applied on filter paper [241].

Stiffness was reduced with kaolin, which can be related to its larger particle size, inhibiting CNC-CNC surface interactions. A rheological study (Figure 2-3) of coatings also supports this behavior (i.e., least viscosity observed with kaolin containing coatings that indicated least interaction between molecules). Surprisingly, stiffness with an increasing concentration of MMT increased from 25.88 mN.m with 10 parts to 30 mN.m with 20 parts (Figure 2-11b). Results can be correlated with platelets and the nanoscale structure of sodium bentonite/MMT, which can fill the CNC coating without inhibiting substantial hydrogen bonding between inter-CNC molecules, leading to a stiffer substrate [226]. Base paper A showed a similar trend as base paper B, but no improvement was observed with base paper C (Figure 2-11a).

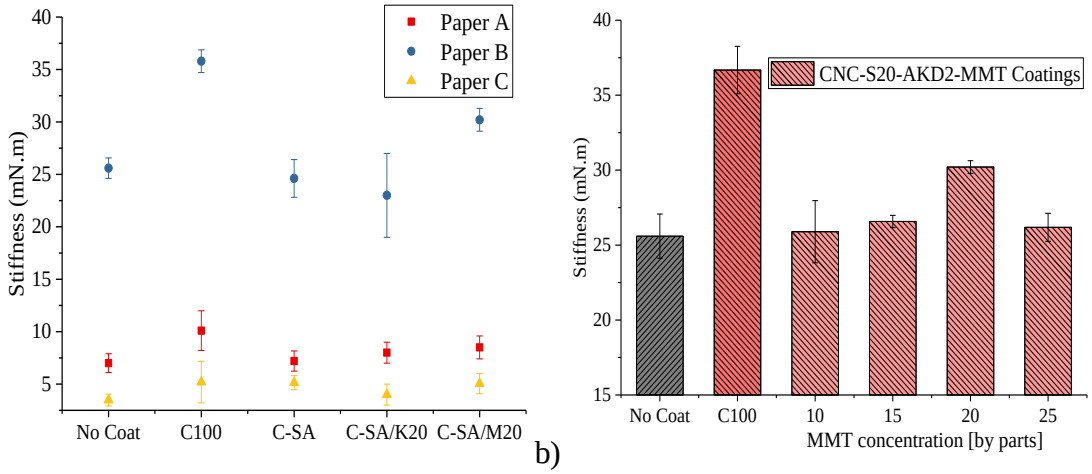

a) b)

Figure 2-3. Stiffness of un/coated base paper B with: a) Optimized CNC coatings with different combination of additives on different base papers (A, B, C); b) Different concentration of MMT in CNC-S20-AKD2-MMT coatings.

2.6 Conclusions

Sustainable CNC-composite barrier coatings were developed using CNC and MMT, protein, and AKD additives. Rheological analysis showed a decrease in viscosity with the addition of MMT and other additives evoking the possibility of making coatings at higher solids. The

morphological analysis of the coated surface showed a uniform distribution and compact packing of additives, which can be correlated with increased tortuosity of a coating layer. Unlike kaolin, MMT has a very high-aspect ratio that has the advantage of interacting with CNC grain bodies and covering surface hydroxyl groups. CNC-composite coatings showed a significant reduction in water absorption (up to 71% compared to surfaces with no coating and up to 27% for surfaces with a CNC-only coating), water vapor transmission rate (up to 27% compared to surfaces with no coating and up to 6% for surfaces with a CNC-only coating), and resistance to air permeation (up to 88% compared to surfaces with no coating and up to 44% for surfaces with a CNC-only coating). Stiffness also increased by 20% compared to surfaces without a coating. The same coating recipe that gave optimum results for water absorption and gas permeability also gave the highest kit rating of 6 on base paper B, while the lowest kit rating of 1 failed on CNC only coated and uncoated papers. The selection of base paper impacted the coating layer performance significantly. The data show that porosity, roughness, and bulk of base paper play important roles for oil and grease barrier packaging coatings.

CHAPTER 3. Nanocellulose-based Multilayer Barrier Coatings for Gas, Oil, and Grease Resistance

3.1 Abstract

Cellulose derivatives such as cellulose nanofibers (CNF) and cellulose nanocrystals (CNC) have enormous potential to reduce or replace petroleum and fluorochemicals for food and other packaging applications. CNFs have been studied for their excellent oxygen and gas barrier properties; however, their performance rapidly decreases in the presence of moisture and higher humidity. CNCs are less sensitive to moisture due to their highly crystalline nature; however, coatings and films made of CNCs are more prone to fractures due to their high brittleness. Our work demonstrates a unique composite barrier coating system of CNF and CNC that synergistically enables oil and grease resistance (a kit rating of 11) comparable to fluorochemicals. It also demonstrates a significant increase in air resistance (~by a factor of about 300), and a reduction in oxygen transmission rate (~by a factor of about 260) compared to uncoated paper. The improvements in oil and gas barrier properties were evaluated with respect to the molecular, chemical, and structural properties of the developed coatings.

3.2 Introduction

Fluorocarbons in the form of polyfluoroalkyl substances (PFASs) are widely used in nonstick, stain-resistant, and waterproof food packaging because of their hydrophobic and lipophobic properties [32]. However, these long-chained fluorocarbons have been found to be responsible for kidney, cancer, and thyroid related diseases [242–244]. Fluorochemical paper additives can migrate to food during actual package use [245]. In response to a petition filed by the Natural Resources Defense Council (NRDC), the FDA has banned the use of three families of long-chain PFASs used for food packaging in January 2016 [246]. As a result, there are strong consumer

demands to the paper and board packaging industries to replace the PFASs with other competitive materials. In the last decade, nanocellulose is one of the emerging sustainable materials that can be considered as an option for oil and grease resistance barrier coatings for food packaging [115,247]. Nanocellulose can be a potential replacement for PFASs materials for food packaging, depending on whether questions related to its high humidity and water sensitivity can be answered [248,249].

Cellulose nanofibers have been shown to exhibit excellent mechanical and oxygen barrier properties when used in composites, films, as well as paper coatings [250–252]. Many bio-based and non-renewable polymers have been used to prepare nanocellulose composite films to improve barrier properties. For example, Dai et al. showed that hydroxypropyl guar and TEMPO (2,2,6,6-tetramethylpiperidine-1-oxyl)-oxidized cellulose nanofibers offer an excellent compatibility for mixing, and exhibited lower oxygen permeability than pure hydroxypropyl guar films [253]. Cellulose nanofibers have also achieved oxygen barrier properties comparable to conventional films when used as a reinforcement in polymers such as PLA [254], borax [255] and bio-based polymers [114]**.** However, there are only a few studies that have focused on nanocellulose as a component in paper coatings [256–259]. A major concern with cellulose nanofibers is their hydrophilicity due to their amorphous structure and the presence of surface hydroxyl groups. At a higher relative humidity, the barrier properties of CNF films become suppressed [260].

On the other hand, films containing a large amount of cellulose nanocrystals provide less oxygen barrier capability when compared to fibrillated nanocellulose films [261]. Saxena et al. have demonstrated a significant reduction in the oxygen permeability of xylan, sorbitol composite films from 189.17 $cm^3.\mu m/(m^2 d.kPa)$ to 0.1799 $cm^3.\mu m/(m^2.d.kPa)$ upon the addition of 50 wt.% sulfonated CNCs [262]. CNC reinforced biopolymers have also been shown to improve the water barrier properties of composite films [170,263,264].

As discussed in introduction, the CNC-containing composites show less sensitivity to humidity when compared to CNFs; however, films containing CNCs are more brittle and offer less interaction possibilities for hydrogen bonding, which results in a higher gas permeability [115]. Moreover, very few studies have compared CNCs and CNFs in terms of barrier properties. Considering the different attributes of CNCs and CNFs, there is a possibility that by combining them, optimal barrier properties can be achieved. There is still a need to improve non-wettability, hydrophobicity, as well as the native oxygen barrier properties of CNFs at higher RH conditions [75]. But since in all these studies CNC and CNF are used as fillers, reinforcement, or a minor component with unsustainable petro-based chemicals, such composite materials are questionable on the basis of their recyclability, biodegradability, and also sustainability [23].

Considering the synergy between CNF and CNC, the objective of this work is to combine both of these nanomaterials for paper coatings and films, in a multilayer system to obtain effective barrier attributes to provide a solution to the aforementioned concerns to develop gas, oil, and grease resistant coating for packaging. The concept adopted in this work is to take advantage of inherent oxygen barrier properties by having an inner/bottom CNF coat layer covered with a less moisture sensitive top coat layer. The amorphous cellulose content of nano-fibrillated cellulose contributes to high flexibility in the wet state, allowing it to attain high density when it dries. High density, in combination with the high cohesive energy density associated with hydrogen bonding, results in better resistance to oxygen. The moisture and high humidity-sensitivity of CNF films can be overcome by using a top layer of CNC composite coating optimized in our earlier work [247].

Figure 3-1 shows a schematic of the hypothesis of using the CNF layer for an oxygen barrier and pre-optimized multifunctional CNC* (CNC 80 parts, MMT (montmorillonite clay) 20 parts, and Soy protein 20 parts) as a top layer [247]. In the top CNC* layer, soy proteins were used with the intention that at specified conditions, clusters of hydrophobic polypeptides would cover the surface, leaving hydrophilic clusters in the bulk with CNC and MMT due to hydrophobic interactions [265].

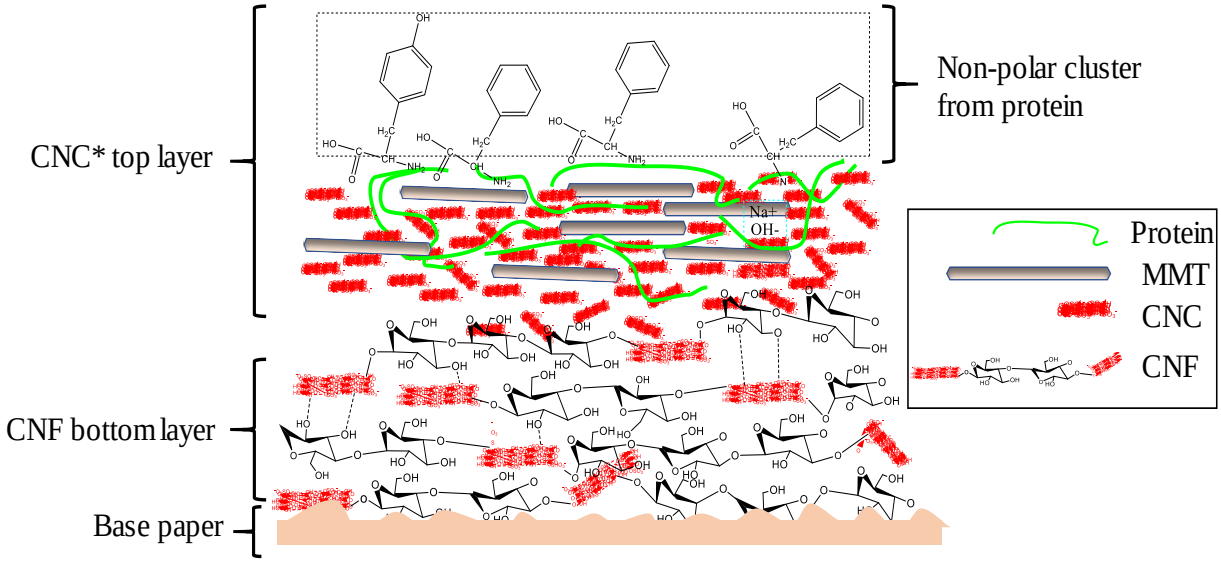

Figure 3-1. Hypothesizing multilayer concept of CNF and CNC* coating.

3.3 Experimental

3.3.1 Materials

The basic coating components used in the current study were CNF, CNC, soy protein, MMT, and dispersant (copolymer of methyl acrylate). CNC was obtained from the University of Maine in an aqueous suspension form with 12.2 wt-% solids. CNC was prepared by acid hydrolysis with sulfuric acid [266]. It had 0.85 wt% sulfur content in sodium form based on dry CNC. The dimensions of obtained CNCs were 5-20 nm wide and 150-200 nm long. CNF obtained from Stora Enso was a 3 wt-% suspension in water. The structural features of CNCs and CNFs were affirmed

with Transmission Electron Microscopy (TEM) using JEOL JEM-2000FX S/TEM at 200kV in TEM mode. Soy protein isolate with the trade name SoBind was obtained from DuPont USA. A protein solution was prepared by first making a 10% slurry in hot water under a continuous high shear at 400 rpm, and then cooking it at 80 °C for 30 minutes. After cooling to room temperature, the pH of the protein solution was measured and adjusted to a pH of 8 before use [267]. Sodium montmorillonite (bentonite) was obtained from BASF with the trade name HYDROCOL 2D6. It is 95-99 % sodium montmorillonite (MMT) and 1-5% crystalline silica with a bulk density of 2.4 g/cm^3 at 20˚C and a melting point of >300˚C. Dispersant (meth) acrylic acid copolymer was provided by SNF-INC with the trade name of Flosperse 3018 CS A50.

A low basis weight white kraft (WK) paper was selected for multilayer coatings as a base and to test required physical properties. In addition, a virgin pulp SBS whiteboard (bleached) and linerboard (unbleached) with a higher basis weight and porosity, and inherently higher contact angle than kraft paper, were also selected to study the contact angle and surface energy of multilayer coated surfaces. The properties of these base papers were obtained using standard TAPPI methods and are provided in Table 3-1.

Table 3-1. Basic properties of selected base papers and coat weight.

Base paper denotation	**Paper type**	**Basis weight (T410) [g/m^2]**	**Caliper (T411) [µ]**	**Bulk (T500) [cm^3/g]**	**Smoothness (T575) [SU]**	**Air Resistance (T460) [G.s]**
WB	White board	250 ± 5	342 ± 5	1.3	153 ± 10	35
LB	Linerboard	120 ± 5	197 ± 5	1.5	390 ± 10	48
WK	White kraft	35 ± 2	44 ± 2	1.3	160 ± 10	30

3.3.2 Methods

CNC* coatings were prepared by first shearing MMT in water and stirring it for 10 minutes at 1000 rpm with a Caframo stirrer similar to discussed in chapter 3. Other ingredients, dispersant,

CNC and soy protein were added sequentially. To prepare CNC and CNF coatings, the respective nanocelluloses were diluted to the required solids % (Table 3-2). All CNC and CNC* coatings were prepared at 10 wt.% solids and CNF coating at 2.5 wt.% solids.

Table 3-2. Coating recipes and their nomenclature definition

Coat Name	Coating recipe/ Multilayer coating setup	Temperature [ºC]	pH	Viscosity [centipoise] @ 100 rpm	Water Retention (Absorption by paper) [g/m^2]
CNC	CNC only	20.02	6.18	1048 ± 45	1669 ± 12
CNF	CNF only	21.2	5.22	480 ± 18	2486 ± 137
CNC* [247]	CNC80/MMT20/Soy20	20.1	8.45	668 ± 52	1278 ± 60
CNC/CNF	[CNC coating as bottom layer, adjacent to paper and CNF coating as top layer]				
CNF/CNC	[CNF coating as bottom layer and CNC coating as top layer facing out]				
CNC*/CNF	[CNC* coating as bottom layer and CNF coating as top layer facing out]				
CNF/CNC*	[CNF coating as bottom layer and CNC* coating as top layer facing out]				

For calculating the required coating component for CNC coating according to the recipes, CNC (80 parts) and MMT (20 parts) were pigments, and their combined concentration was 100. Other ingredients such as soy protein (20 parts) and dispersant (0.1 parts) with respect to total pigments (100 parts), were added as required for the defined recipes and stirred for 30 minutes at 1000 rpm [247]. Table 3-2 shows different coating recipes and their nomenclature as used further in this manuscript.

Water retention plays an important role for coating processes in terms of uniform application and drying [268]. In the current study, an AA-GWR water retention meter was used to perform pressure filtration tests for calculating the water holding capacity of coating recipes using the TAPPI method T-707. Low shear rate viscosity was also carried out to measure apparent

viscosity just before coating application at a speed of 100 rpm at room temperature using spindle number 5 with the Brookfield DV-III Ultra viscometer.

Coatings were applied on the paper surface using the lab drawdown rod coating method. To make equivalent uniform coatings, lab drawdowns were carried out using Mayer rod number 8 for CNC coatings (10% solid) and rod number 12 for CNF coatings (2.5% solids) with a targeted coat weight of 5 g/m^2. CNC and CNF films were prepared by using the solvent casting method under controlled conditions. All coatings were diluted to 1% solids concentration to obtain uniform and thin films. The suspension was stirred at 1000 rpm for 5 minutes using a Caframo constant-torque stirrer before casting into polystyrene petri dishes of a diameter of 130 mm and dried at a temperature of 23 °C for 2 days at flat surface. The amount of suspension used varied from 20 to 40 ml for different CNF and CNC suspensions to achieve the same dry film thickness of approximately 30 µm. To obtain multilayer films, 15 ml of bottom layer suspension was poured in Petri dishes and allowed to stabilize the networked structure by evaporating excess water for 6 hours. Second, the top layer suspension (15 ml) was poured uniformly over the pre-stabilized bottom layer in the petri dish and placed on a leveled surface under pre-specified conditions. After drying, films were conditioned at 23 °C and 50% RH for 24 hours before characterization.

The air resistance of coated and uncoated base papers was analyzed using the TAPPI T460 (Gurley porosity) method. Oxygen transmission rate through coated paper was measured using a MOCON Optech instrument with an atmospheric oxygen concentration of 21% and a 100 cc volume at 23 °C temperature and 70% RH. The water vapor transmission rate (WVTR) was measured using the ASTM E96 wet-cup method with coating side towards the high humidity at 23 °C and 50% RH. Results were reported as g/m^2/day. Oil and grease resistance of the coated paper was evaluated using a 3M Scotchban visibility method, also known as the TAPPI kit test for oil

and grease resistance (TAPPI T559). Results were presented as kit number. Mechanical strength was measured using an Instron tensile tester at 500 kN load with a preset length of 50mm and 25mm strip width at 50% RH and 23 °C.

Contact angle measurements were carried out using the sessile drops method with a SEO Phoenix 150/300 contact angle system) and a CCD camera at room temperature (23 °C). A drop of the probe liquid was placed on the paper surface from a micro-syringe, and images of the contact angle for 150 frames in the interval of 200 microseconds were taken using the attached CCD camera. Advancing and receding quasi static contact angles were also measured using the water droplet method in accordance with Huhtamäki et al [269] using a 27 gauge needle (0.21mm diameter). For simplification, the Owens-Wendt geometric mean equation was used to estimate surface energy from the contact angle (Eq 1.). In the equation, $\gamma_{L-Dispersive}$ taken for liquid 1 (methylene diiodide) is 50.8, and $\gamma_{L-Dispersive}$ for liquid 2 (water) is 21.8, $\gamma_{L-Polar}$ for liquid 1 is 0 and $\gamma_{L-Polar}$ for liquid 2 is 51. Based on these constants, γ_{LV} and γ_{SV} has been calculated.

$$(1 + cos(\theta))\,\gamma_{LV} = 2\sqrt{(\gamma_{S-Dispersive}\gamma_{L-Dispersive}} + 2\sqrt{(\gamma_{S-Polar}\gamma_{L-Polar})} \qquad \text{Eq.1}$$

To verify the multilayer construction of nanocellulose coatings and films, scanning electron microscopy (SEM) was conducted on a FEI XHR-Verios 460L field emission SEM (with 2 kV beam voltage and 13 pA beam current). All samples were sputter-coated with gold nanoparticles prior to imaging, with a thin layer of gold in a low vacuum of 90 mTorr of Ar gas pressure with an accelerating voltage of 600 V for 5 minutes at a coating rate of 7 nm/min. The chemical characterization of the coated surface was carried out using Bruker-Opus ATR-FTIR spectroscopy instrument within the range of 400 to 6000 cm^{-1} wavenumber with 4 cm^{-1} resolution for 32 scans. ToF-SIMS analyses were conducted using a TOF SIMS V (ION TOF, Inc. Chestnut Ridge, NY) instrument equipped with a Bi_n^{m+} (n = 1 - 5, m = 1, 2) liquid metal ion gun, Cs^+

sputtering gun and electron flood gun for charge compensation. To acquire high lateral resolution mass spectral images, a Burst Alignment setting of 25 keV Bi_3^+ ion beam was used to obtain a 500µm x 500µm area with negative ions.

3.4 Results ad Discussion

3.4.1 Wet properties of coatings

Table 3-2 describes the wet coating properties of all recipes described in this study. Brookfield viscosity at 100 rpm was found to be the highest for CNC coatings and the lowest for CNF coatings. Water retention for CNC* coating was also the highest (inversely proportional to water absorption by filter paper) and the lowest for CNF coating. Considering these factors and several trials, rod number 12 was selected for CNC* and CNF coatings, and rod number 8 was selected for CNC coating.

3.4.2 Barrier properties of coated paper

Porosity: Gurley densometer tests evaluated the permeance of air under applied pressure through a substrate in the z-direction (thickness). Figure 3-2 shows a significant increase in the air resistance of substrate with various coatings. Air resistance was increased by a factor of about three-hundred with CNF/CNC* two-layer coating (8846 Gurley seconds/100ml of air) compared to no-coat substrate (30 Gurley seconds/100ml of air). CNF/CNC and CNC*/CNF two-layer coatings also provided comparable improvement in air resistance with the same coat weight of 5 g/m^2. The air resistance for CNF and CNC/CNF is in the same order of ~1000 Gurley seconds.

This shows more open structure generated with CNF relative to CNC with a thin layer of coating [208,270].

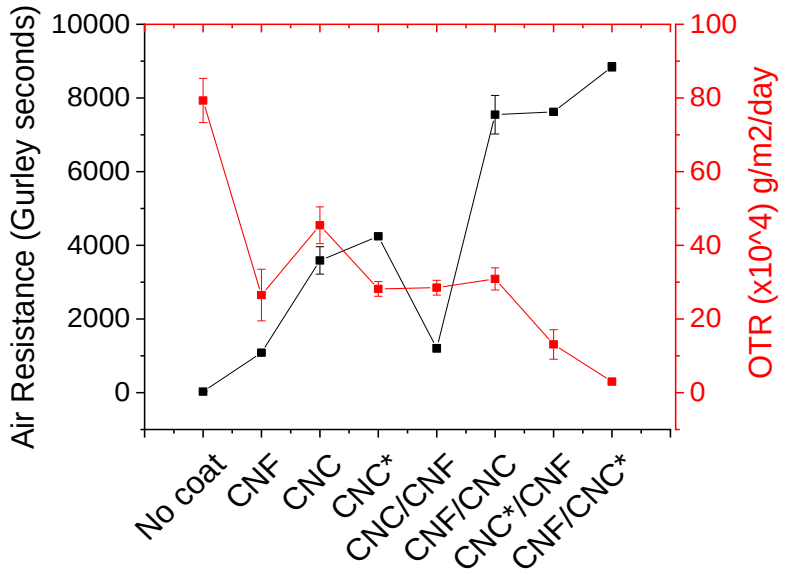

Figure 3-2. Air resistance and oxygen transmission rate of nanocellulose coatings on WK paper.

Oxygen Transmission Rate (OTR): Consistent with the results of air resistance, oxygen transmission showed similar trends with nanocellulose coatings (Figure 3-2). A single layer coating with CNF provided better barrier properties compared to CNC at existing relative humidity conditions. CNC* coatings showed further reduction in OTR compared to CNF, which might be due to the lower sensitivity of CNC* coating to higher relative humidity conditions [247]. The highest reduction in oxygen transmission rate (~by a factor of about 260) was observed with a double layer coating with CNF/CNC* (79 x10^4 g/m^2/day/atm) compared to no-coat substrate (0.3 x10^4 g/m^2/day/atm). Results shown in Figure 3-2 confirm that the CNF coating layer works more efficiently as an oxygen barrier if protected from direct exposure to humid conditions, which is done by using the CNC* as a top layer in the present case [125]. All the gas and oxygen transmission

rate results can be correlated to the morphology, chemical structure and surface chemistry of the different layered structures as discussed later in the surface and chemical characterization section.

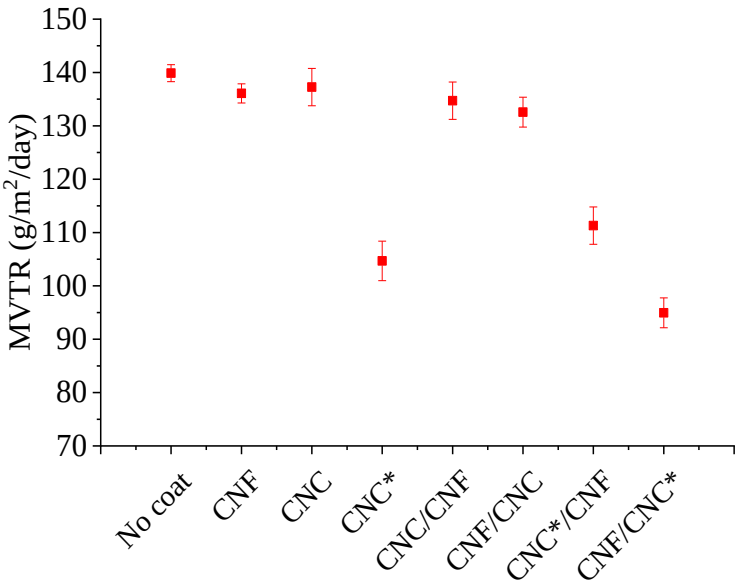

Figure 3-3. Water Vapor transmission rate of nanocellulose coatings on WK paper.

Water Vapor transmission rate (WVTR): No significant improvement was observed with a single layer coating of CNF or CNC and neither with the double coat layer of CNC/CNF, CNF/CNC (Figure 3-3). However, CNC*-containing coatings reduced vapor transmission rate by 20-30%. The lowest vapor transmission rate was obtained with CNF/CNC* coated base paper. The results can be explained based on the hypothesis of this study: the bottom layer of CNF increases resistance to the flow of gases; however, the CNC* top layer inhibits interaction of water vapors with the surface, which results in a reduction in the permeability of coated base papers.

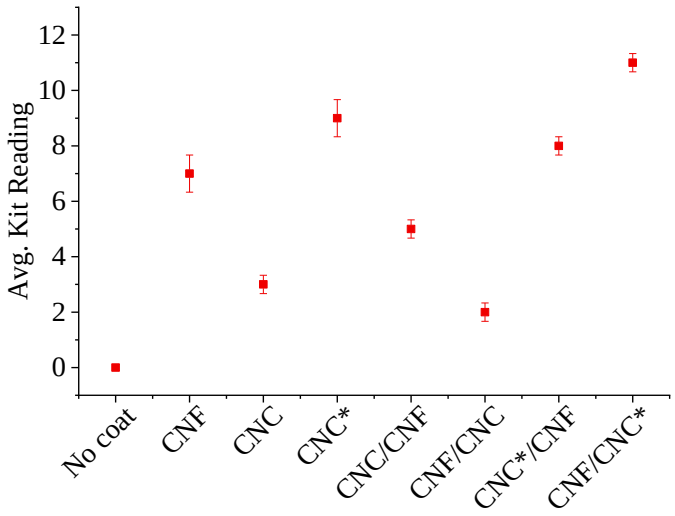

Figure 3-4. Oil and Grease Resistance Kit reading of nanocellulose multilayer coatings on WK paper sheets with CNF, CNC and CNC*.

Oil and Grease Resistance-Kit Test: Figure 3-4 shows the improvement from '0' (with uncoated) to 8 for CNC* coating and to 11 for CNF/CNC* multilayer coating. This provides a great opportunity for the paper and board industry as an effective alternative for fluorocarbons for food packaging applications. As discussed earlier, the reading depends highly upon the porosity and bulk of the paper irrespective of basis weight [247].

Contact angle: Surface chemistry and roughness are key factors that can affect hydrophobicity and hydrophilicity [271]. The water contact angle (WCA) can be defined as the angle at which liquid/vapor interface meets the solid substrate, when the testing fluid is water (Figure 3-5).

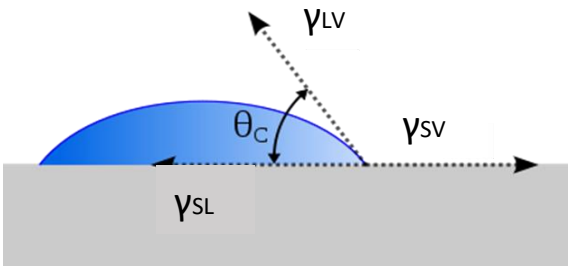

Figure 3-5. Water Contact angle and soild-vapor (γSV), liquid-vapor (γLV) and solid-liquid (γSL) components of surface energy for a given substrate.

However, quasi-static advancing (θ_a) and receding (θ_r) contact angles provide more information about the wettability and the absorption behavior of surfaces [269]. Advancing and receding contact angles are measured by increasing and decreasing the droplet volume in the

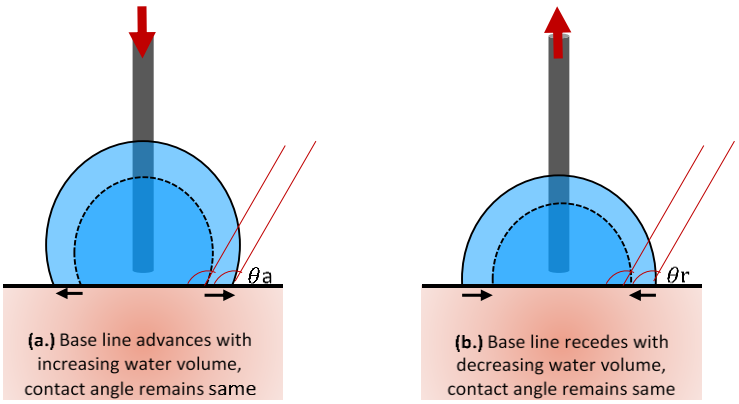

Figure 3-6. Depiction of advancing and receding quasi-static contact angle.

sessile droplet contact angle measurement method (Figure 3-6). Table 3-3 summarizes the θ_a, θ_r and hysteresis (θ_a - θ_r) for water contact angle, which determines the mobility of a drop on surface. The larger the hysteresis, the less mobile the drop is on the surface, which is a function of an interaction of the droplet with the surface. Hysteresis can occur due to reasons such as surface roughness, surface heterogeneity or absorption of the droplet into surface [272]. The uncoated WB surface had a large θ_a, whereas hysteresis was found to be the highest (54.3) due to water absorption and the porous, rough surface of the paper [273]. CNC and CNF coated surfaces showed almost equal hysteresis despite CNC being highly crystalline in nature, which is in line with earlier studies [274]. CNC* coated surfaces showed the highest θ_a with a hysteresis of 13.0, which is much lower than CNC and CNF coated surfaces. All substrates with CNF and CNC coated on the top surface showed similar hysteresis ~25, which proves the importance of the top surface. CNF/CNC* coated surfaces showed the least hysteresis (2.1) and the least absorbency of droplet into surface. The other point to be noticed in following table is that the standard deviation of measurements was found to be the least with CNF/CNC* coated surfaces. The least hysteresis obtained with

CNF/CNC* coated surface can be explained based on the dense, uniform and comparably less polar chemistry of the top surface as described later in SEM and ToF-SIMS spectra (Figures 3-10, 3-11 and 3-12).

Table 3-3. Advancing and receding water contact angle of multilayer based coatings on WB.

Coating	θ_a	θ_r	Hysteresis (θ_a - θ_r)
No coat	85.7 ± 1.15	31.3 ± 2.31	54.3 ± 3.05
CNC	46.0 ± 2.64	20.7 ± 3.78	25.3 ± 6.35
CNF	58.0 ± 1.00	22.3 ± 2 .08	25.7 ± 1.53
CNC*	107.7 ± 2.11	94.7 ± 8.50	13.0 ± 6.92
54.3CNC/CNF	48.7 ± 2.57	25.3 ± 2.52	23.3 ± 3.15
CNF/CNC	47.7 ± 8.12	22.3 ± 4.51	25.3 ± 4.51
CNC*/CNF	46.7 ± 2.88	24.7 ± 4.51	22.0 ± 5.19
CNF/CNC*	65.7 ± 1.16	63.6 ± 2.31	2.1 ± 1.29

The static water contact angle was also measured after 1- and 30-second interval on three different types of paper substrates coated with multilayer nanocellulose coatings (Table 3-4). The results in Table 3-4 coincide with advancing and receding contact angle as shown above in Table 3-3.

Table 3-4. Contact angle of single/double layer CNC & CNF coated paper.

	White Board		Liner Board		White Kraft	
Coating Type	WCA (1 sec)	WCA (30 secs)	WCA (1 sec)	WCA (30 secs)	WCA (1 sec)	WCA (30 secs)
No Coat	93° 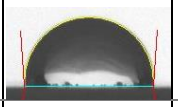	55° 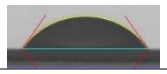	106° 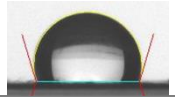	64° 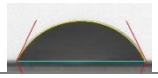	54° 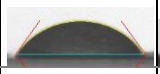	19° 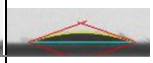
CNC	40° 	36° 	41° 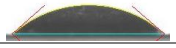	36° 	40° 	30° 
CNF	97° 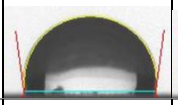	93° 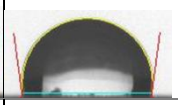	19° 	0° 	43° 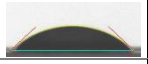	0°
CNC*	97° 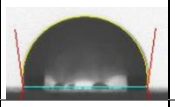	96° 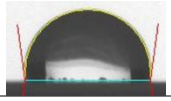	108° 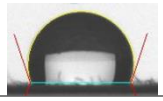	108° 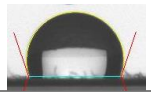	66° 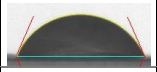	62° 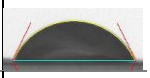
CNC/CNF	44° 	38° 	44° 	36° 	31° 	28° 
CNF/CNC	35° 	31° 	36° 	34° 	40° 	34° 
CNC*/ CNF	60° 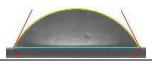	59° 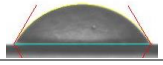	46° 	44° 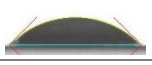	58°	55°
CNF/CNC*	64°	63°	58°	58°	57°	57°

Estimation of surface energy is another approach to reveal unbalanced forces for the molecules at the surface. The contact angle (θ) can be related to interfacial energies between the solid-liquid (γ_{SL}), liquid-vapor (γ_{LV}) and solid-vapor (γ_{SV}) interfaces. These interfacial energies can be described with Young's regimes described by Equation 2:

$$Cos\theta = \frac{\gamma_{SV} - \gamma_{SL}}{\gamma_{LV}} \qquad \text{Eq. 2}$$

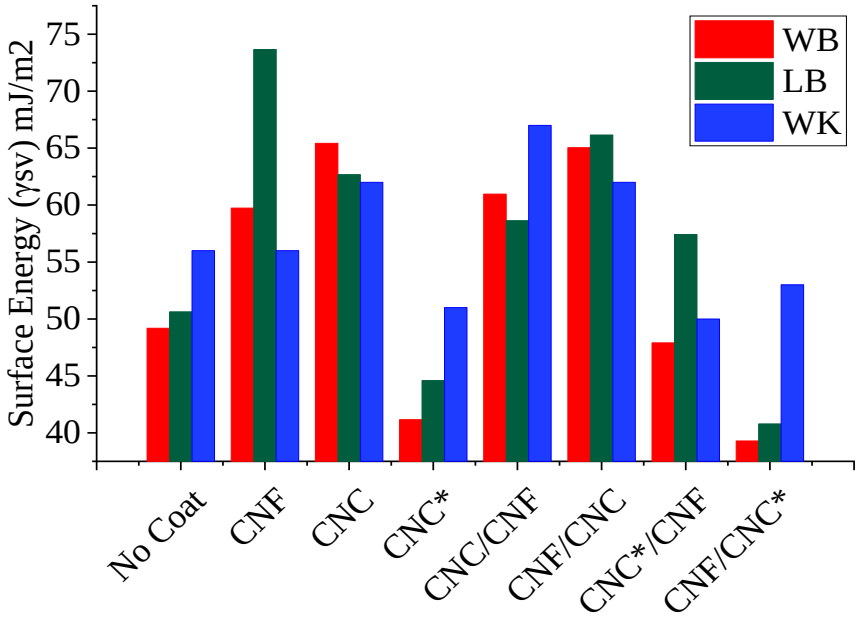

Figure 3-7. Surface energy estimation of single- and double-layer CNF, CNC and CNC* coated papers using Owens-Wendt model.

The total surface energy of the CNC* coated surface was reduced significantly (Figure 3-7). For WB and LB, a reduction in surface energy by >20% with CNF/CNC* multilayer coatings were more prominent as compared to the effect of multilayer coating on WK paper. The value of surface energy was much higher as compared to a super-hydrophobic or superomniphobic, which is around 11-14 mJ/m^2 [275]**.** This gives a platform to make a non-absorbing surface for both polar and non-polar fluids. For example, a drop-in contact angle with methylene diiodide (MI) on CNF/CNC* coated white board surface remains unchanged for a long time without any absorption into the paper (Figure 3-8). This further shows the oil and grease resistance character of the following double layer coating against such a highly non-polar solvent. Similar behavior was observed with CNC* and CNF/CNC* coatings on all three types of selected base papers.

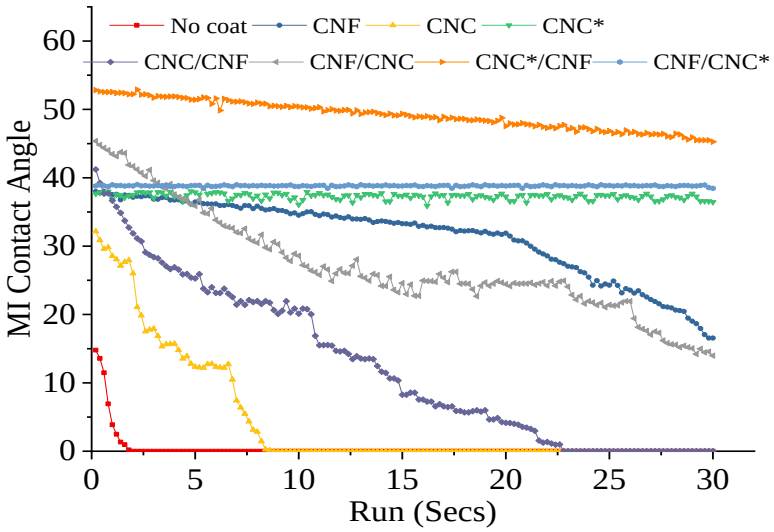

Figure 3-8. Contact angle pattern of methylene diiodide over nanocellulose coated surface over time.

3.4.3 Chemical & Surface characterization

The FTIR spectra of coated papers with all three different base papers was found to be identical. For more clarification, results with WK paper are shown in Figure 3-9. The FTIR spectra of uncoated and nanocellulose (CNF and CNC) coated paper were exactly the same except for the CNC showing an extra peak at 1391 for SO^{-}_{3}. This indicates that there were no new bonds present in the selected nanocellulose [276]. CNC* coating containing CNC, MMT, and soy protein can be characterized with an absorption band of polypetide Amide I (C= O) at 1637 cm^{-1}, which overlapped the water absorption region in nanocellulose and in-plane N-H bending vibration of soy protein [277]. Absorption peaks for polypeptide amide bonds were consistent in CNC*/CNF and CNF/CNC*. Characterization peaks of MMT in CNC* containing coatings at 1040 cm^{-1} for Si-O-Si and vibration peaks for Al-O and Si-O at 625 cm^{-1} could not be seen here due to overlapping peaks of stretching of C-O-C and noise respectively in cellulose [278]. No new peaks were observed

in the FTIR spectra other than that of present species, which can be interpreted as implying that no covalent bonding formation is happening between selected coating components.

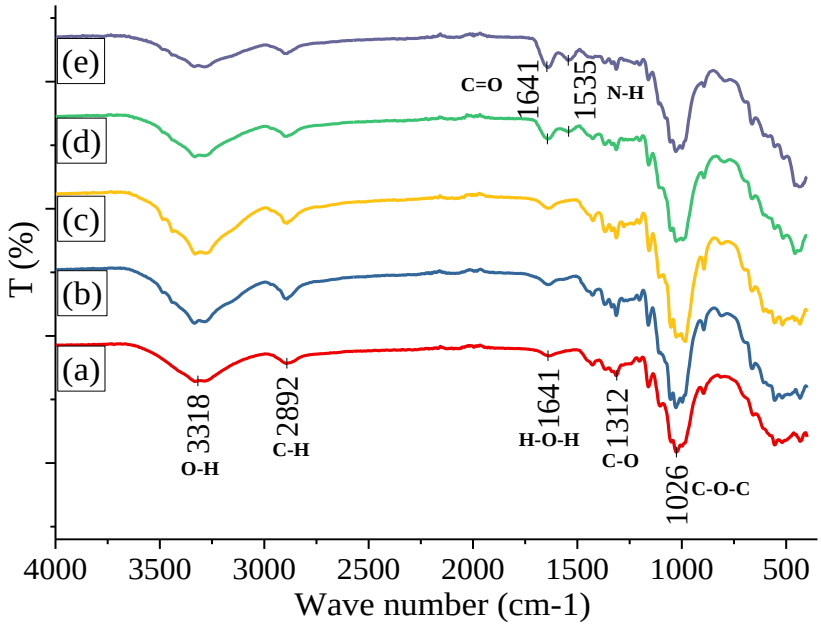

Figure 3-9. FTIR spectra of multilayer coated WK paper of (a) No coat, (b) CNC/CNF, (c) CNF/CNC, (d) CNC*/CNF, (e) CNF/CNC*.

TEM: Structural features of individual CNCs and CNFs used in the current study are shown in figure 3-10. This confirms the size, morphology, and structural features provided in material section.

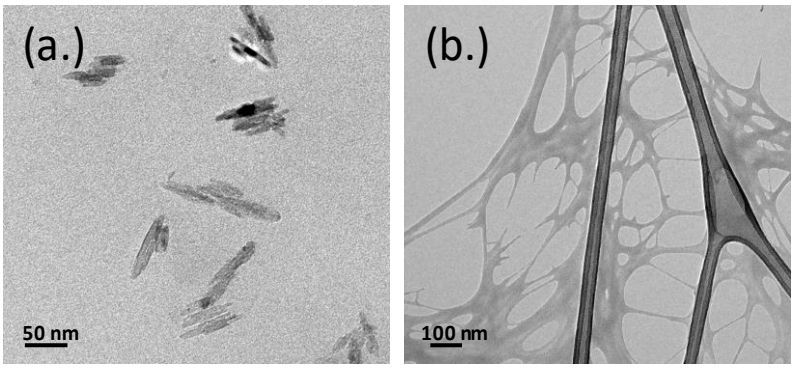

Figure 3-10. TEM images of (a) CNC and (b) CNF used in current study.

SEM: Figure 3-11 shows the SEM images of cross section and top view of multilayer coatings on WK paper. For CNC/CNF, CNF/CNC multilayer coatings-cross section view shows expected results according to the hypothesis (Figure 3-11a & 3-11b). The two-separate layers of CNF and CNC were found to be lying over each other without any major continuous gradient of coating components at the interface. In the CNC*/CNF coating, where the CNF layer was coated over the CNC* layer on base paper, a continuous gradient of clay and CNC particles was observed at the interface against the gravity (Figure 3-11c). CNF/CNC* showed a completely different interfacial behavior with a denser merged layer of CNF and CNC* at the interface (Figure 3-11d).

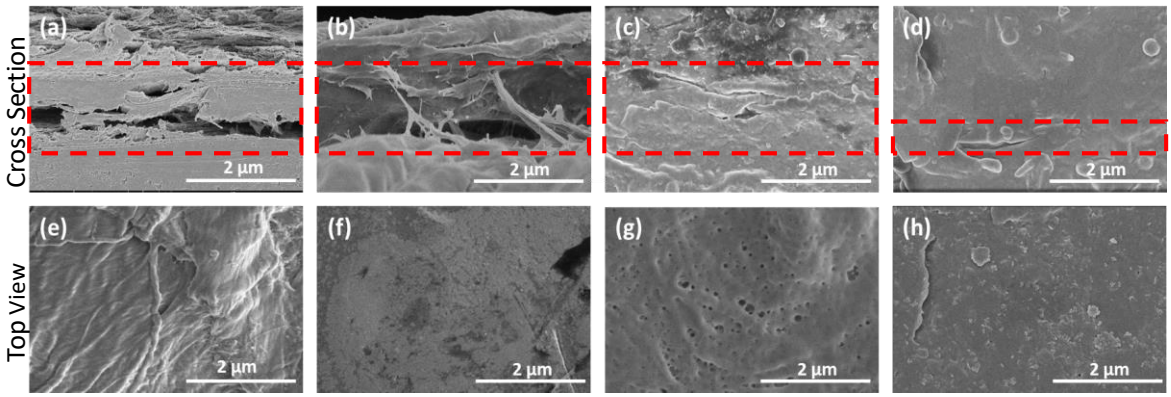

Figure 3-11. SEM images of double layer coated WK paper with: (a), (e) CNC/CNF; (b), (f) CNF/CNC; (c), (g) CNC*/CNF; (d), (h) CNF/CNC* coatings.

This can be either due to physical diffusion and van der Waals, or possible hydrogen bonding between components of CNC* and CNF layer through the CNF bottom layer. There is also the possibility of the formation of new bonds between two layers. A top view of CNC*/CNF showed that defects appeared on the surface as holes (Figure 3-11g). These holes might have appeared due to the quick hydration of the MMT layer in bottom CNC coatings and then, diffusing through the surface with a fast-drying process [279]. The following information supports the data for a reduction in porosity, OTR and kit reading with CNC*/CNF coating compared to CNC* (Figure 3-2, 3-3 and 3-4). Double-layer coatings with CNF/CNC could not form a uniform layer on the

paper surface compared to CNC* coatings, which is consistent with results from earlier studies (Figure 3-12b and 3-12c) [247].

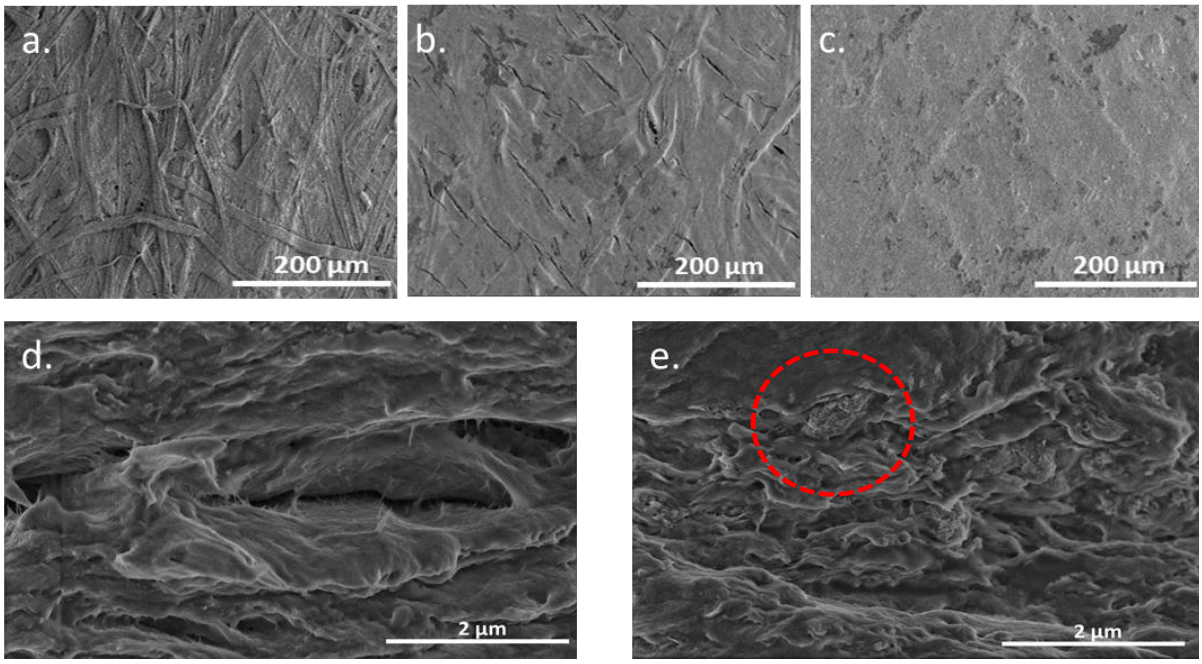

Figure 3-12. Lower magnification (250x) top view SEM images of (a) uncoated, (b) CNF/CNC, (c) CNF/CNC* coated paper; and cross section view of solvent casted multilayer (d) CNF/CNC and (e) CNF/CNC* individual films at interface of two layers on higher magnification

To study the type and nature of interaction between interfaces of double layered CNF/CNC and CNF/CNC* individual films were also examined with SEM at higher magnification (Figure 3-12d & 3-12e). CNF/CNC* coatings present a uniform (Figure 3-12c) and a tight continuous interface (Figure 3-12e). The following results support the data for steady contact angle for MI over the CNF/CNC* coated paper for a longer time (Figure 3-8). Unexpectedly, at the interface of double layered CNF/CNC* film, a reinforcing phenomenon of MMT particles through the bottom CNF layer was observed (Figure 3-12e).

ToF-SIMS: Figure 3-13 shows the TOF-SIMS spectra of uncoated and multilayer coated WK paper. Mass spectra peaks for sulfate and sulfite were observed for all multilayer coatings except for uncoated paper. This shows that CNC particles were diffused through the adjacent layer during the coating application and drying irrespective of their position. Proteins also diffused through the adjacent layer in a similar way, as shown by the presence of CN^- and CNO^- peaks in CNC*/CNF and CNF/CNC* multilayer coatings. These results support the data from SEM cross section images (Figure 3-11). For a non-sputtered mass spectrum, no peaks corresponding to silicates (MMT clay) were observed in either of the multilayer coatings, CNC*/CNF or CNF/CNC*. However, a sputtered mass spectrum of CNF/CNC* coated paper showed a visible peak for SiO_2^- (Figure 3-13f).

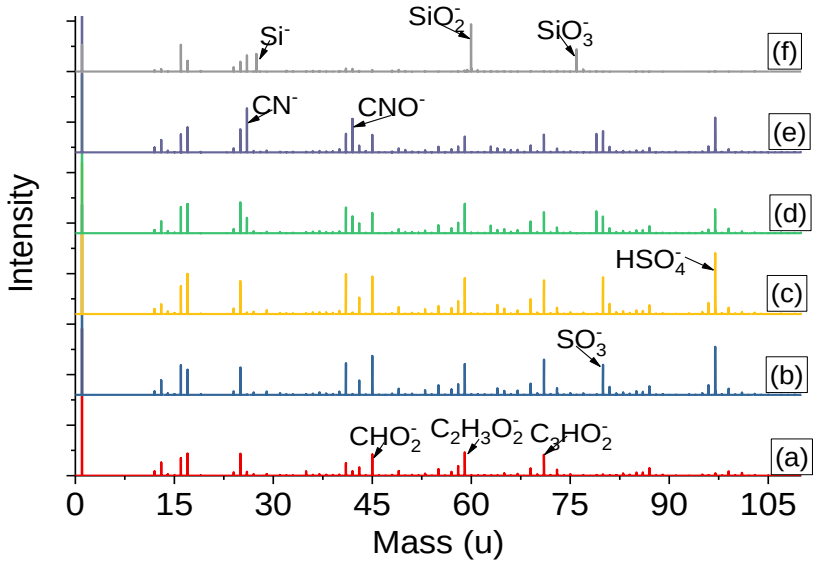

Figure 3-13. TOF-SIMS spectra of non-sputtered (a) No coat, (b) CNC/CNF, (c) CNF/CNC, (d) CNC*/CNF, (e) CNF/CNC* and (f) 1-hour sputtered CNF/CNC* multilayer coated WK paper.

This shows that MMT particles were completely embedded into the protein matrix and no surface of the MMT particles were exposed to the atmosphere. This might be due to the protrusion

of the non-polar clusters of the soy protein from the coating matrix due to hydrophobic repulsion interactions as presented in the hypothesis, which is evidenced by non-sputtered spectra of positive ion fragments from proteins (figure 3-14) [265]. This is also consistent with the reduction in WVTR with CNC* and CNF/CNC* coated paper due to a comparably hydrophobic top surface (Figure 3-3). Figure 3-15 shows a detailed characterization of the chemical properties and morphology of CNC*/CNF and CNF/CNC* coatings with negative ion sputtered TOF-SIMS. In TOF-SIMS images, the distribution of a specific chemical is shown based on the color intensity; the lighter the color, the higher the presence/distribution of the chemical components (Figure 3-15). In

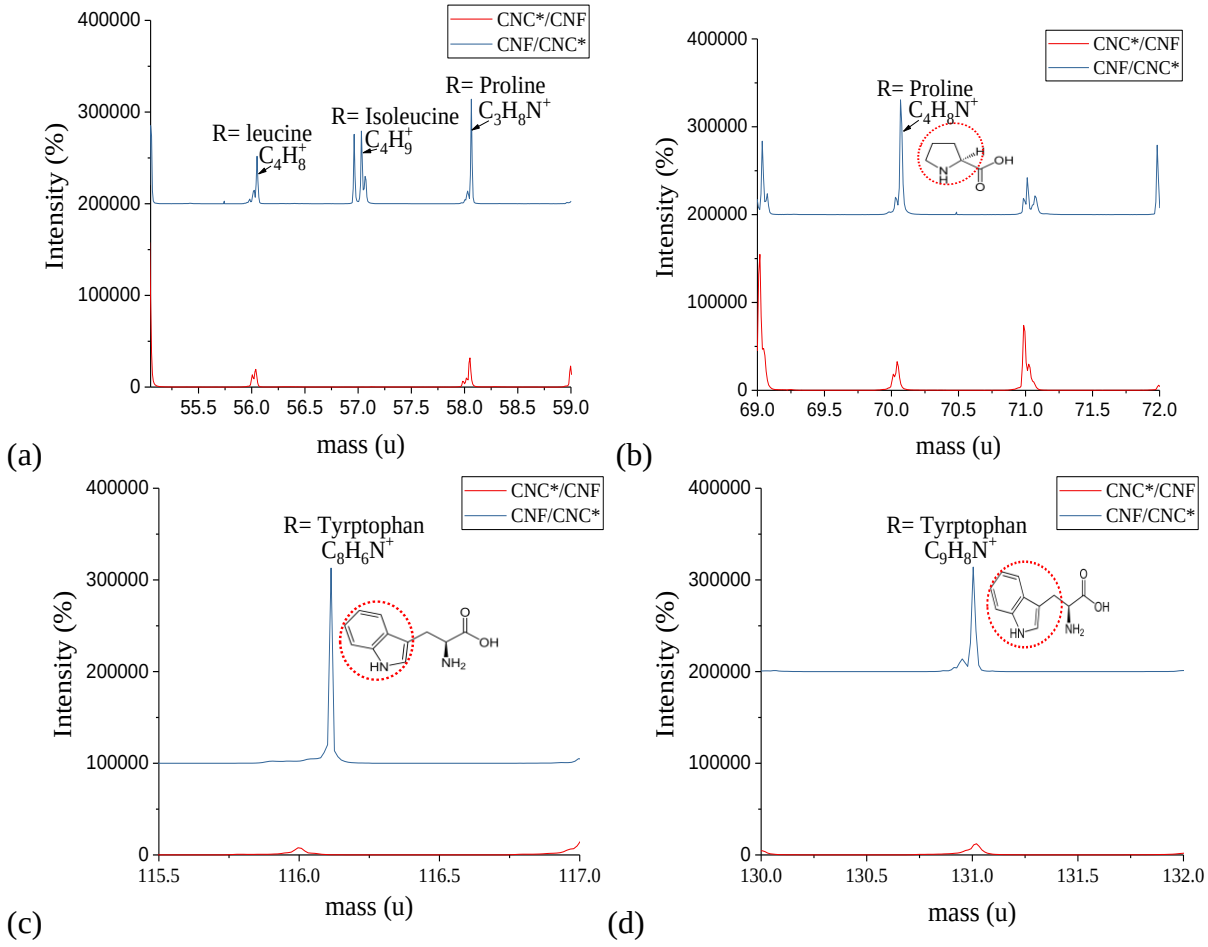

Figure 3-14. TOF-SIMS of CNC*/CNF and CNF/CNC* coatings with noticeable fingerprints in terms of fragments from hydrophobic amino acids.

CNC*/CNF coatings, $C_2H_3O_2^-$ (from CNF) shows a uniform and significantly higher distribution and very lower distribution for CNO- (Protein) and almost no presence of SiO_2^- (Clay). Unexpectedly, a very low distribution of $C_2H_3O_2^-$ (from CNC) was observed in CNF/CNC* double layer coated paper. A uniform and higher distribution of CNO^- (Protein) and SiO_2^- (Clay) was observed in CNF/CNC* coatings (Figure 3-15). This shows that MMT clay was hydrated and separated in thin layers, leading to a more uniform distribution throughout the coating surface. This also demonstrates that a successful multilayer coating system was attained with this method. Figure 3-13 and 3-14 supports the explanation for the hypothesis of multilayer coatings, as no peaks for $Si/SiO_2/SiO_3$ were observed without sputtering the coating layer (Figures 3-13d & 3-13e). However, peaks for silica and silicates were observed after 1-hour sputtering of coated paper (Figure 3-13f).

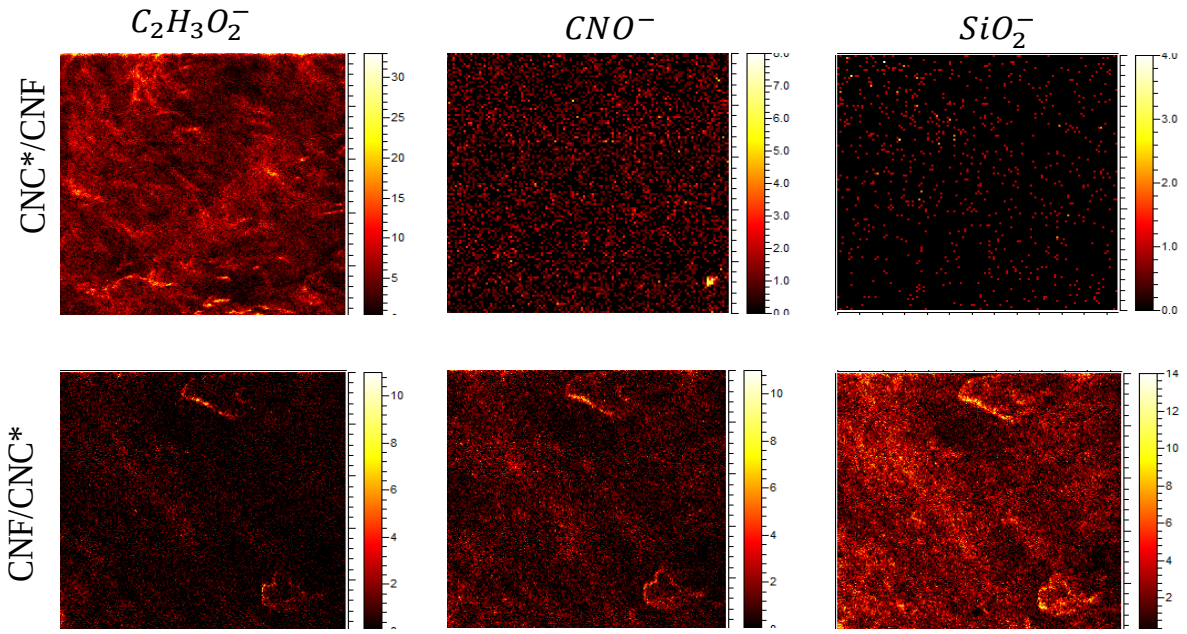

Figure 3-15. Surface-sputtered TOF-SIMS images of CNC*/CNF and CNF/CNC* double layer coated paper to prove the formation of two separate layers in terms of constituents.

3.5 Conclusions

CNF and CNC layers were successfully obtained in a multilayer coating system to exploit their unique properties. The CNF/CNC* double-layer coating system provided the best results for the development of a sustainable solution for gas, oil, and grease resistance packaging. The CNF/CNC* double layer coated paper resulted in a reduction of air-permeability by a factor of approximately 300, OTR by a factor of approximately 260, and WVTR by 30%. An improvement in kit reading was also observed from a kit number of 0 to a kit number of 11, compared to uncoated paper.

Water contact angles measured on different model surfaces showed increases with a single coating layer of CNC*. However, the contact angles dropped in any combination with a CNF layer. Though the contact angles with the CNF/CNC* coating layer on different model surfaces were lower than contact angles with CNC* coated papers, the contact angles remained unchanged when observed after 30 seconds (i.e., water or MI remained unabsorbed after an observation of >30 seconds). All these aforementioned improvements in gas and oil barrier properties were consistent with the molecular, chemical, and structural behaviors of these coatings. SEM images show that CNF/CNC* or CNC*/CNF coatings had no distinct layer separation between CNF and CNC* layers. However, coatings with CNF and CNC layers exhibited a distinct layer interface. These multilayer coatings provide a new pathway for delivering sustainable gas and oil resistant coatings.

CHAPTER 4. High Strength Antibacterial Chitosan-Cellulose Nanocrystals Composite Tissue Paper

4.1 Abstract

A heightened need to control the spread of infectious diseases prompted the current work in which functionalized and innovative antimicrobial tissue paper was developed with a hydrophobic spray-coating of chitosan (Ch) and cellulose nanocrystals (CNC) composite. It was hypothesized that the hydrophobic nature of chitosan could be counterbalanced by the addition of CNC to maintain fiber formation and water absorbency. Light-weight tissue handsheets were prepared, spray coated with Ch, CNC and their composite coating (ChCNC), and tested for antimicrobial activity against gram-negative bacteria *E. coli* and a microbial sample from a human hand after using the restroom. Water absorption and strength properties were also analyzed. To activate the surface of cationized tissue paper, a helium gas atmospheric plasma treatment was also employed on the best performing antimicrobial tissue papers. The highest bactericidal activity was observed with ChCNC coated tissue paper, inhibiting up to 98% microbial growth. Plasma treatment further improved the antimicrobial activity of the coatings. Water absorption properties were reduced with Ch but increased with CNC. This "self-disinfecting" bactericidal tissue has the potential to be one of the most innovative products for the hygiene industry because it can dry, clean, and resist the infection of surfaces simultaneously, providing significant societal benefits.

4.2 Introduction

Increasing infection rates are creating higher demand for the development of effective hygienic products [280,281]. For example, infections caused by *E. coli* (gram-negative bacteria), which alone leads to an estimated 73,480 illnesses each year in the United States, results in 2,168

hospitalizations and 61 deaths annually [282], and is the main reason for acute renal failure in children [283,284]. Many solutions are available to cure these diseases, but they carry a high monetary and health cost. Vaccination, an effective method to address these infections, bears a large USD 4 billion annual cost for the 72 most impoverished countries, and costs are approximately six times more in developed countries [285]. Each year about 30 million children globally lack access to vaccination [286].

The present work is based on the premise that a number of the associated aspects of these issues can be solved in a frugal and practical manner by taking advantage of papermaking technology. Toilet papers and napkins are essential products in developed countries. A recent study determined that the average annual consumption of toilet paper in the United States is 50 lbs. per person.[8] Indeed, the market for hygiene tissue paper is increasing annually due to growing healthy lifestyles, but there are very few tissue products with bactericidal properties. As an example, a USA patent (20030143372) demonstrates the process of making an antimicrobial toilet paper. This tissue is composed of intermediate planar-shaped absorbent layers and a dry antimicrobial layer that is activated by moisture [287]**.** However, these products tend to have a high price point due to the incorporation of antimicrobial agents in specified manner.

Biomaterials have gained increasing attention over the last two decades due to sustainability and ecological considerations. Cationic functional polysaccharides are promising from biomedical and hygiene product perspectives. Chitosan, which is a > 70% deacetylated derivative of chitin, is one of the most sustainable and abundant polysaccharides that has been studied for its antimicrobial properties for many years [288–290]. To obtain chitosan from chitin, acetyl groups are hydrolyzed from amine functional groups located at the C2 position of the glucosamine residue. This is done by hydrolysis of acetyl groups in the presence of alkaline

solution, yielding the deacetylated form. If the deacetylation of these copolymers (1 → 4)-2-amine-2-deoxy-β-D-glucan and chitin unit is greater than ~65%, the polymer is referred to as chitosan. The pKa of glucosamine -NH_2 (in chitosan) is ~6.3. Thus at pH lower than 6.3 more than half of such groups in chitosan are protonated (-NH3+), as shown in figure 4-1 [289]. (-NH^{3+}) groups on chitosan can result in three types of cellular denaturation: (i) change in cell permeability, which provokes internal osmotic imbalance and thus inhibits cell growth;[291] (ii) hydrolysis of peptidoglycans in a microorganism's wall, which leads to leakage of electrolytes out of the cell and eventually kills the cell [292]; and (iii) after a longer time, protonated-chitosan chelates metals and suppresses elements by binding to nutrients required for microbial cell growth [293,294].

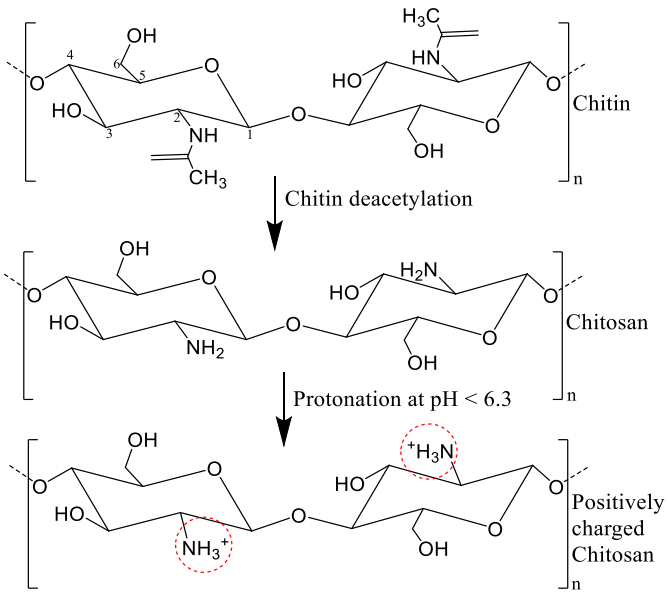

Figure 4-1. A simplified rendition of the molecular steps leading to a protonated chitosan moiety when starting from chitin.

A number of studies have explored the antimicrobial properties of chitosan against bacteria (gram positive and gram negative) and fungi [294–301]. However, most of these studies evaluate the antimicrobial property of chitosan associated with other co-factors such as silver, gold

nanoparticles, other antimicrobial agents (terpenes) or chemically modified chitosan [295–298,300,302,303]. For instance, Badawy et al. studied very moderate antimicrobial properties of chitosan films on bacteria such as *A. tumefaciens*, *E. carotovora*, *C. fascians*. An improvement in antimicrobial property was observed only when monoterpenes (geraniol and thynol) were added in film preparations [295]. Very few studies have shown reasonable antimicrobial activity of chitosan as an individual component, but limited to a narrow range of microbes [304,305].

Besides the positive charge on an antimicrobial agent, size and morphology are other important factors that lead to a disruption of microbial cells. For example, metals such as Ag, Au, Zn, and Mg, etc., can act as effective antimicrobial agents when used in suitable size, morphology and chemical form [306,307]. Cellulose nanocrystals (CNC) possess an unusual morphology that is characterized by a rigid, narrow, rod-like structure (figure 4-2) [23]. This peculiar morphology is similar to antimicrobial agents such as silver and gold nano-particles that damage the microbial cell membrane and cause osmotic imbalance inside the cell, resulting in cell apoptosis. However, due to commonly used preparation methods, CNC particles generally bear negative charge, which tends to cause repulsion between a negatively charged cell membrane and CNCs. El-Samahy et al. have studied the effect of addition of CNC in chitosan on antimicrobial activity when used as bagasse pulp paper-additive. Other studies have shown good synergy between CNC and chitosan as a composite for mechanical and water vapor barrier properties [131,227,308–310]. Increasing the concentration of CNC in chitosan resulted in increasing antimicrobial activity against *S. typhimurium* [311]. However, no logical understanding for the antimicrobial effect of CNC was provided.

The current work is based on the hypothesis that chitosan and nanocellulose crystals (CNCs) composited networks of a specific ratio will provide synergistic antimicrobial effects when

used in tissue paper. More specifically, it was speculated that when a bacterium encounters rigid, narrow, stiff, rod-like CNC particles, it will undergo significant cell membrane damage [312]. This harm to the cell-membrane would make microbial cells susceptible to protonated (cationic)-chitosan (figure 4-2). Thus, CNC will be able to work synergistically with the chitosan by enhancing its antimicrobial effect and will compensate for its hydrophobic character. Additionally, CNC and chitosan have been demonstrated to be good dry strength reagents for paper making when allocated as individual units [15,300,313]. Yet, combinations of negative CNC and

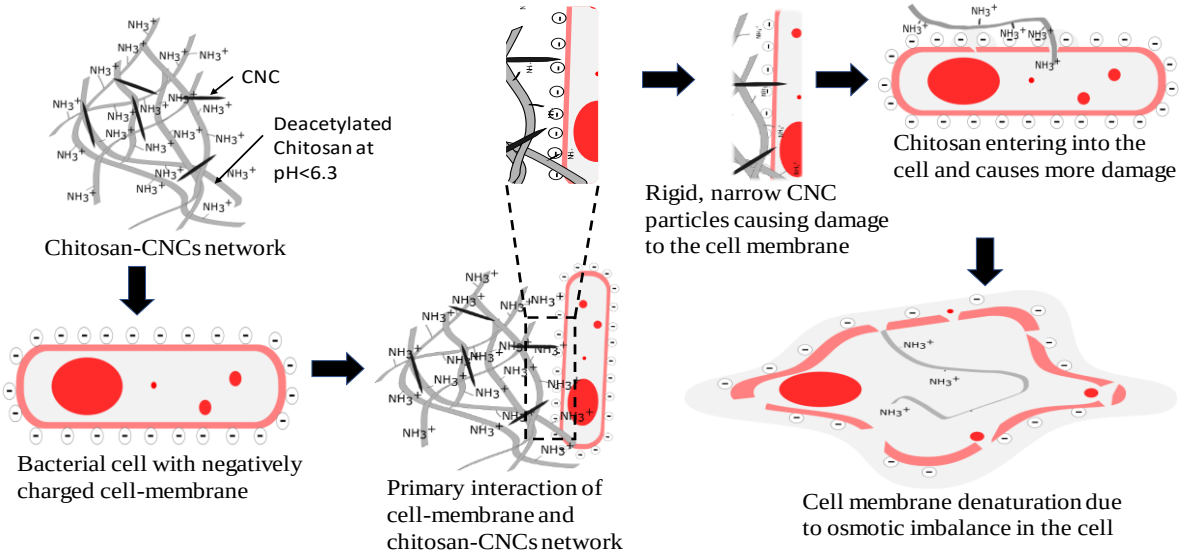

Figure 4-2. Schematic diagram of objective and theory of using nanocellulose and chitosan together for tissue coatings for antimicrobial and superabsorbent tissue papers.

positive chitosan can work synergistically similar to the effect of polyelectrolyte complexes used in paper making to improve dry strength.[314–316]. The combination of Ch and CNC will endow the tissue paper composites with a significant synergistic advantage with respect to antimicrobial agency, increased water absorbency, and mechanical strength.

4.3 Experimental

4.3.1 Materials

Chitosan was purchased from Sigma-Aldrich (medium molecular weight) with 97% deacetylation. Nanocellulose crystals in the form of a gel with 12% solids was procured from the University of Maine. The CNC had been prepared by acid hydrolysis using sulfuric acid, so it had 0.85 wt.% sulfur content based on dry CNC, in the sodium sulfate form. To prepare tissue handsheets, recycled deinked office pulp (DIP) was procured from Resolute Forest Products recycling with a kappa number = 15.2 and a stickies content = 145 mm^2/kg.

4.3.2 Methods

Tissue paper sheets with a 15 g/m2 basis weight were made from recycled bleached de-inked pulp (DIP) using a British handsheet mold. The pulp was a deinked office paper grade. The handsheets were conditioned at 23 °C and 50% RH for 24 hours before surface coating. For the preparation of CNC and chitosan coating complex, a solution of chitosan was prepared in 1% acetic acid solution. Then, it was mixed with CNC (in a Chitosan:CNC ratio as 80:20 by weight) using a constant torque mixer at 500 rpm for one hour. For convenience, the composite of Chitosan and CNC is referred to as Ch-CNC. All coatings were brought to 1% solids concentration for spray coating application. During the entire process pH was measured and maintained at < 6.3. Antimicrobial nanocellulose coatings were spray-coated on the prepared handsheets and dried using a "Chromalox 2110" dryer system at 'zero' load and 110 ºC with a speed level of 10 rpm. Tissue sheets were also surface treated using a Surfx® Atmflo 400 atmospheric plasma system equipped with an automated RB200-XYZ robot stage. The plasma composition was comprised of helium as an inert gas and oxygen as a reactive gas. The use of atmospheric plasma was investigated to study the influence on antimicrobial properties.

The surface morphology of chitosan-treated samples was examined using a FEI Verios 460L field emission SEM at an accelerating voltage of 2 kv and 13pA current. Prior to imaging, samples were sputter-coated with a thin layer of gold in a low vacuum of 90 mTorr of Ar gas pressure with an accelerating voltage of 600 V for 3 minutes at a coating rate of 7 nm/min. ToF-SIMS spectra were obtained using a TOF SIMS V (ION TOF, Inc. Chestnut Ridge, NY) instrument equipped with a Bi_n^{m+} (n = 1 - 5, m = 1, 2) liquid metal ion gun, Cs^+ sputtering gun and electron flood gun for charge compensation. To acquire high lateral resolution mass spectral images, a burst alignment setting of 25 keV Bi_3^+ ion beam was used to obtain a 500µm × 500µm area with a resolution of 300 nm using negative ions to show the distribution and entanglement of CNC particles into the chitosan matrix over tissue paper.

Auger electron microscopy was carried out using a beam voltage 2 kV, emission current 3 mA, resolution 512 x 512 at 250x magnification for the gold coated aluminum substrate treated with Chitosan and CNC complex. The images were taken with a secondary electron detector, and mapping data were taken with a cylindrical mirror analyzer. Contact angle measurements were carried out using the sessile drops method with a SEO Phoenix 150/300 contact angle system) and a CCD camera at room temperature (23◦C). A drop of the water was placed on the paper surface from a micro-syringe and images of contact angle for 75 frames in the interval of 200 microseconds were taken using the attached CCD camera.

Charge estimation on the un/treated tissue paper was carried out using colloidal titration method. Un/treated tissue paper was disintegrated into pulp and brought to a 0.075% consistency in deionized water. The colloidal charge of 200 ml of the resulting pulp suspension was evaluated by titration using a CHEMTRAC ECA 2000 P streaming current analyzer. The charge neutralization point of untreated and treated paper was determined by the addition of cationic

polymer (poly diallyl dimethyl ammonium chloride (poly-DADMAC)) and anionic polymer (potassium polyvinyl sulfate (PVSK)), respectively to the suspension.

Spray-coated and plasma-treated papers were tested for antimicrobial activity using the ASTM E2149 method [317] and disk diffusion assay [318]. For the quantification of antimicrobial activity of developed bactericidal tissue paper, the ASTM E2149 method was used. In this method, an *E. coli* (strain TOP10) culture was grown overnight in LB media and diluted to obtain a culture with 2.1 × 105 CFU/ml in a phosphate buffer solution. The media were transferred to six different conical flasks (75 ml each) and incubated for 1 min in a shaking incubator. After 1 minute (0 contact time with tissue paper), the samples were serial diluted 5 × 10X and plated on petri dishes and incubated for 24 hours. The coated/uncoated tissue specimens (equal area) were transferred to their respective conical flasks and incubated for 2 hours. Again, plating of bactericidal treated cells was carried out and the system was incubated. After 24 hours of incubation, bacterial colonies were counted, and CFU/ml was calculated. The results were presented as a Reduction % for CFU/ml. Antimicrobial activity with a disk diffusion assay of coated paper was tested against *E. coli* and a virtual hand sample (culture of tissue paper used by a person after using the restroom). Water absorbency was tested using the DIN 54540-4 standard test method. Paper samples of size 100 × 100 mm (with basis weight variation in the range of < 1 g/m^2) were prepared and transferred into a 1000 ml beaker containing 100 ml of DI water and kept for 60±3 s. Water was removed from the samples by straining for 120 s, after which time they were weighed. Results were reported as an amount retained in the paper as g/m^2. Spray coated tissue papers were also tested for burst strength and stiffness using the 'Emtec' tissue ball burst analyzer.

4.4 Results and Discussion

4.4.1 Distribution of ChCNC over tissue paper

The SEM image in figure 4-3b shows the distribution of a ChCNC network throughout tissue paper (white spots shown in red square). The high magnification (500×) image shows the ChCNC network associated to the paper cellulosic fibers. Comparing images of uncoated (figure 4-3a) and coated (figure 4-3b and 4-3c) tissue paper, it can be easily gleaned from the microphotographs that the porosity did not change. Most of the ChCNC networks seem to be present on the surface of cellulose fibers instead of filling the pores, which is confirmed in water absorbency data. To confirm the manufacture of a ChCNC composite as shown in figure 4-2, a gold coated aluminum substrate was treated with ChCNC composite (figure 4-3d and 4-3e). Figure 4-3d shows the morphology of spray coated ChCNC composite. Substantial amount of CNCs could be seen as protruded sharp edge particles on the substrate surface, coming out of chitosan matrix as suggested in hypothesis. To compare the morphological difference between Ch and ChCNC composite coatings, SEM image of Ch coating on aluminum substrate is shown in figure 4-3f and 4-3g. Ch coating illustrates the continuous film formation property.

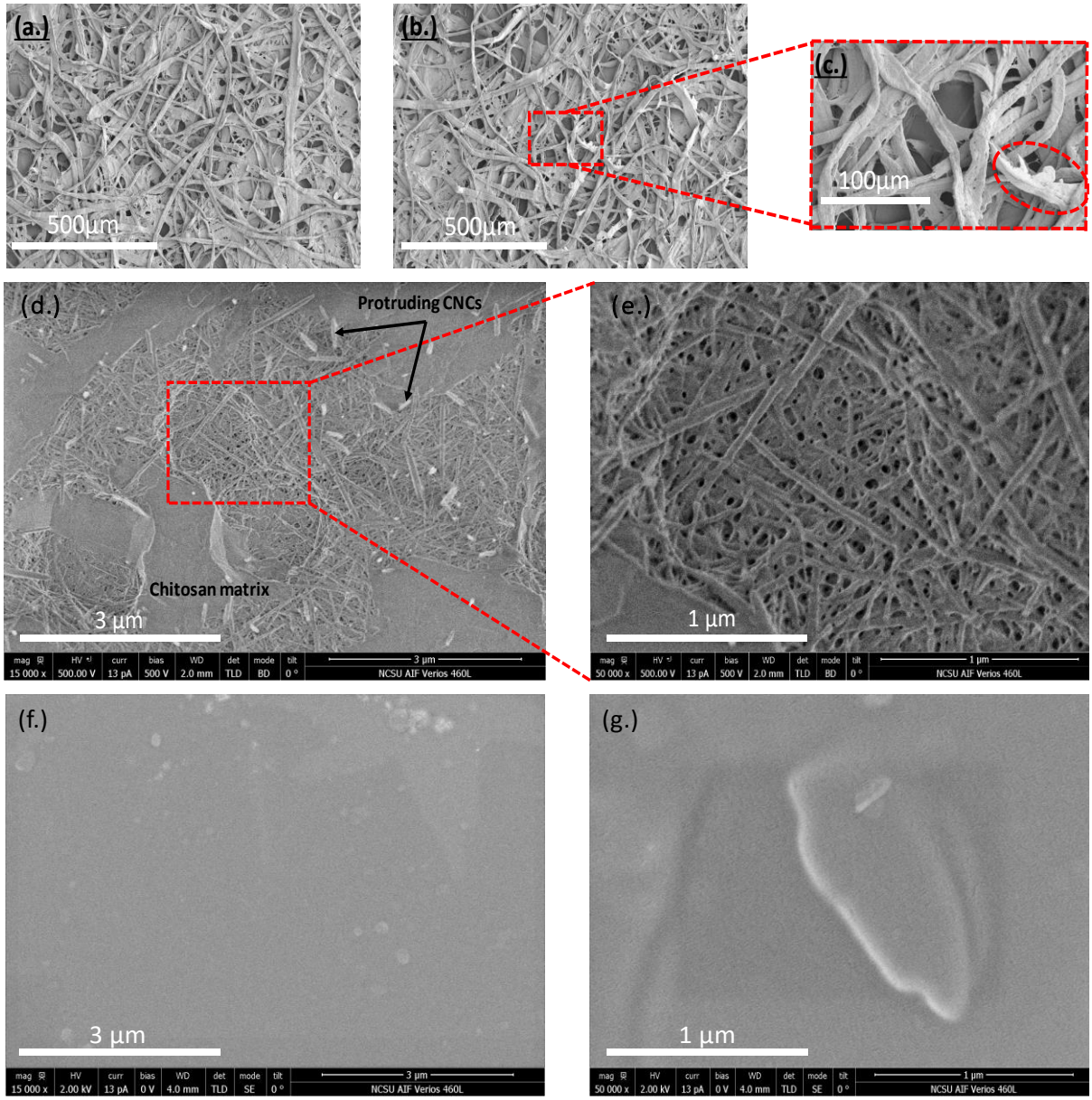

Figure 4-3. SEM images of (a) uncoated, (b) ChCNC treated paper at 100x and (c) 500x magnification; (d), (e) ChCNC composite and (f), (g) Ch treated aluminum substrate, at higher magnification 15,000x and 50,000x respectively.

In the ToF-SIMS spectra for ChCNC, the dominant peaks for CN^- (25.99amu), CNO- (42.20amu), SO_3^{-2} (79.63amu) and HSO_4^- (96.51amu) confirms the presence of the ChCNC complex on the ChCNC treated paper. The CN^- and CNO^- fragments are generated from chitosan, and SO_3^{-2} and HSO_4^- are generated from CNCs. The peaks for CN^-, CNO^-, SO^{3-} and HSO_4^- are absent on the 'No coat' paper (figure 4-4).

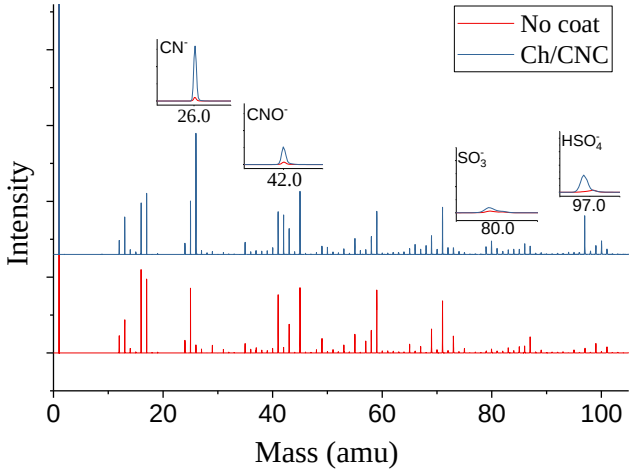

Figure 4-4 TOF-SIMS spectra of untreated (No coat) and ChCNC-treated tissue paper.

To see the distribution of ChCNC over tissue paper, negative ion 'ToF-SIMS microscopic images of tissue paper were studied (figure 4-5). The lighter shade for CN^- and HSO_4^- shows that chitosan and CNCs are distributed uniformly throughout the surface with higher saturation at certain areas (yellowish) compared to others. These observations support the SEM images showing ChCNC complexes associated with cellulosic fibers. Also, in the porous structure of paper, no CNC and Ch particles (black color) are observed, further supporting the data from SEM images. In figure 4-5c, overlay of CN^- and HSO_4^- (dark green area in white circles) depicts how the chitosan and CNCs are present together in the form of a complex structure, CNCs clusters were found mostly where chitosan is present.

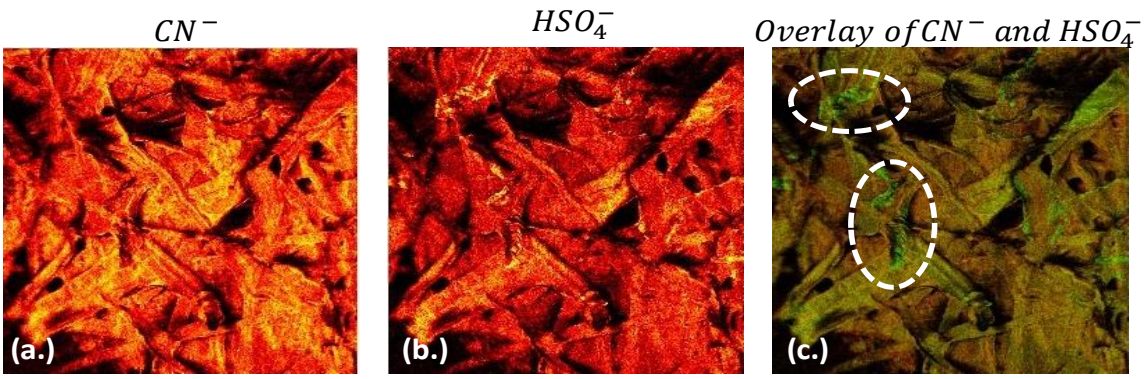

Figure 4-5. High resolution ToFF-SIMS images (500x500µm) of ChCNC treated tissue paper showing distribution of (a.) chitosan (CN-), (b.) CNC (HSO4-), and (c.) complex of Chitosan and CNC.

Figure 4-6 depicts the distribution of CNCs (sulfur scan in blue color) in chitosan matrix (nitrogen scan in yellow color) using auger electron microscopy. Ch treated aluminum substrate shows no traces for sulfur, which confirms the absence of CNCs (figure 4-6a). ChCNC treated substrate shows the presence of CNCs into the Ch matrix, which confirms the SEM images shown earlier. CNC particles can also be seen distributed throughout the chitosan matrix rather than inside

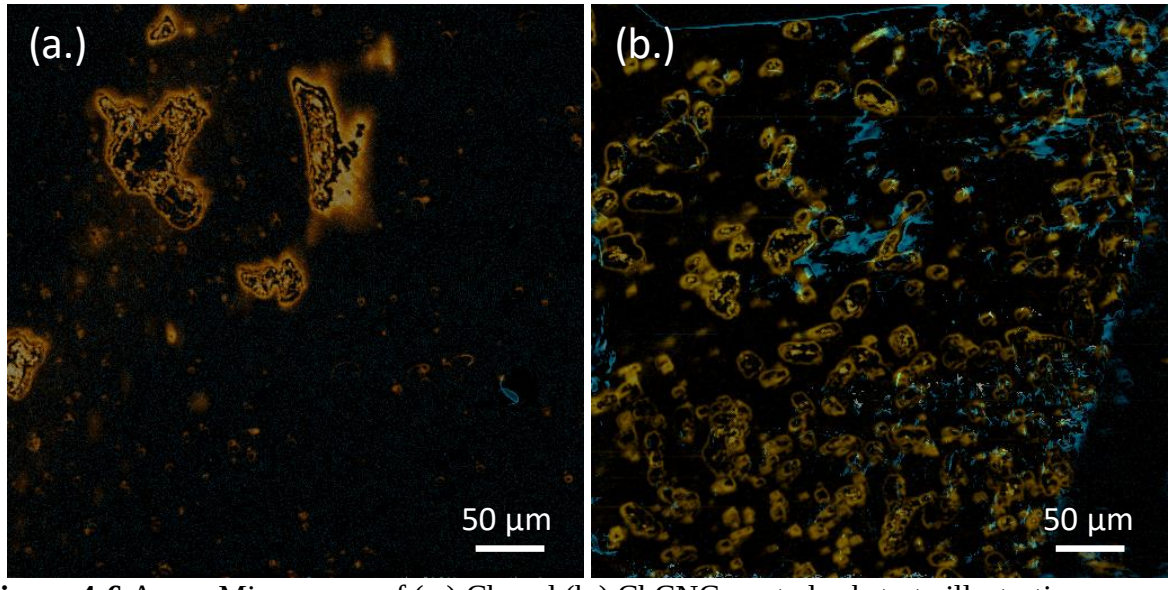

Figure 4-6 Auger Microscopy of (a.) Ch and (b.) ChCNC-coated substrate illustrating nitrogen (yellow) and sulfur (blue) scans.

the chitosan microparticles. Having the CNC particles distributed on the surface of the chitosan matrix enables a greater functional opportunity for antimicrobial activity. Surprisingly, the ChCNC treated substrate shows a more uniform distribution of chitosan particles on the surface (figure 4-6b). Additionally, the Ch-only treated substrate resulted in greater agglomeration of chitosan particles, which resulted in less surface area coverage (figure 4-6a). This could result in the chitosan being less effective as compared to the ChCNC composite, as it pertains to the antimicrobial activity of Ch, as shown later in figures 4-9 and 4-10.

4.4.2 Contact angle

To evaluate the hydrophilic-hydrophobic balance of the coatings, contact angles for pure water were obtained on three glass slides coated with Ch, CNC and ChCNC, respectively, as shown in figure 4-7. The chitosan-only coated slide showed slight hydrophobic character with contact angle of ~93° with a base line of 1.61 mm. The contact angle on a CNC coated glass slide was reduced drastically to 23° with a baseline of 2.88 mm, which is in keeping with past reports.[319] This was consistent with its more hydrophilic character and nanoscale structural texture, providing enormous surface area. More interestingly, the hydrophobic character of chitosan was superseded by the hydrophilic character of the CNC in the ChCNC complex. The contact angle on ChCNC coated glass slide was found to be as 41° with a base line of 2.38 mm. This implies that even a small amount of CNCs can upset the hydrophobicity induced by Ch in the ChCNC complex. This

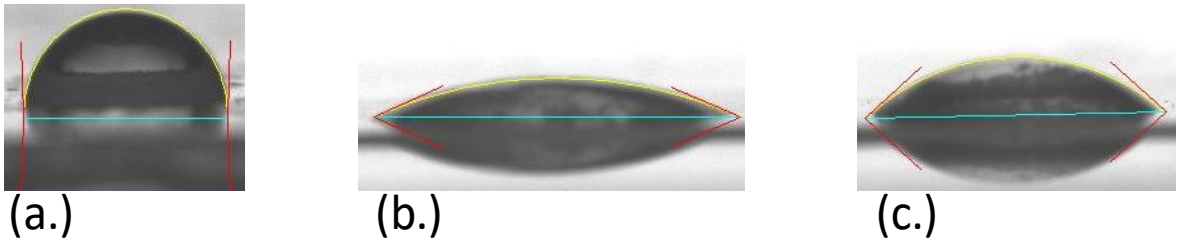

Figure 4-4. Contact angles of glass slides coated with (a.) Ch, (b.) CNC, and (c.) ChCNC.

can also be correlated to the distribution of CNCs into the chitosan matrix in ChCNC composite as shown in figure 4-3d and 4-3e. CNCs are present protruding out of the surface through chitosan matrix instead getting entrap into the matrix. This overcomes the hydrophobic character of chitosan by presence of hydrophilic CNCs on surface. This characteristic finding was further confirmed by measuring the absorbency of tissue paper treated with these test coatings.

4.4.3 Charge determination

The final charge on the ChCNC complex treated tissue paper was hypothesized to play a governing role in the current study. To identify the sign and magnitude of ionic charge present on ChCNC treated tissue paper, polyelectrolyte titration was carried out using the streaming current method for endpoint determination (figure 4-8). Quantification of net positive charge was done using anionic PVSK polymer (potassium polyvinyl sulfate) and expressed as demand of micro-equivalents charge per liter. Not surprisingly, the streaming potential of untreated (non-coated) tissue paper was found to be negative (-1.65 mV), which implies that the net charge on 'non-coated' paper is negative. In that case cationic polymer (poly-DADMAC) was used to neutralize the colloidal charge of the system; during the quantification of charge (4 micro-equivalent charge/liter). The streaming current output for CNC-treated sample was also found to be negative (-3.26), with a cationic demand of 14 micro-equivalent charge/liter. On the other hand, the streaming current output for Ch-treated tissue paper was found to be positive with anionic (PVSK) polymer demand of 135 micro-equivalent charge/liter. The streaming current output of ChCNC treated tissue paper was also found to be positive (+2.54 mV), which signifies that the total charge on ChCNC treated paper is still positive even with the presence of sulfonated CNCs. Following neutralization with PVSK, the approximate charge demand on treated fibers was found to be as 67 micro-equivalent charge/liter (90 micro-equivalent charge/g-fibers).

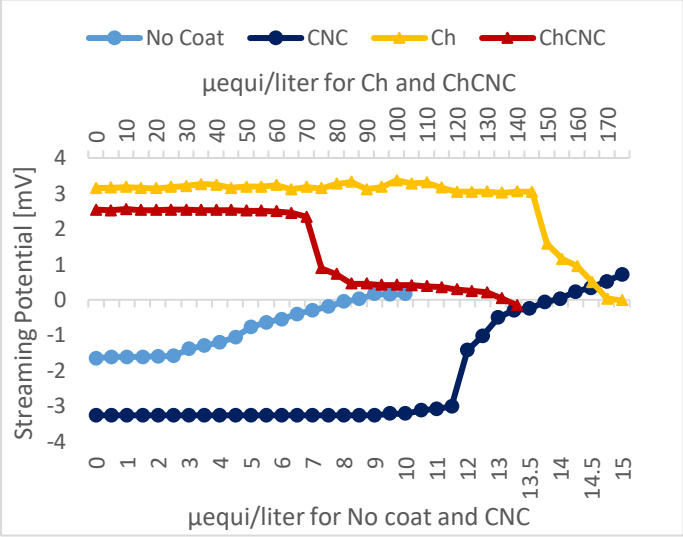

Figure 4-5. Streaming current test output and oppositely charged equivalent volume to neutralize Uncoated and treated tissue paper with CNC, Ch and ChCNC.

4.4.4 Antimicrobial activity of Ch-CNC coatings

Disk Diffusion Assay Results. Table 4-1 summarizes the results of disk diffusion assay in terms of zones of microbial growth against specific gram-negative bacteria (*E. coli)* and the unspecified microbial culture from the unwashed hand sample. A disk diffusion assay was carried out using uncoated, CNC- only (CNC), Ch-only (Ch), ChCNC composite, plasma treated uncoated (p-No coat), and plasma treated ChCNC coated (p-ChCNC) tissue paper against *E. coli* (strain N022) and a microbial sample taken from an unwashed hand after using the restroom. No zone of inhibition for microbial growth was observed with the uncoated and 'CNC' coated tissue paper against the *E. coli* plated culture. However, a slight zone of inhibition (0.87 and 0.85 cm diameter) was observed with the untreated 'Ch' coated and plasma-treated uncoated tissue paper against *E. coli*. The highest zone of inhibition with a diameter 2.34 cm, against *E. coli*, was found with p-ChCNC treated tissue paper. This was followed by untreated ChCNC, which had an inhibiting

zone diameter of 1.74 cm. For a microbial sample collected from human-hand, no zone of inhibition was found with any of the coated or uncoated tissue paper, except for p-ChCNC coated tissue paper. Microbial sample collected from human-hand after using rest room is expected to have a number of different types of microbes including fungi, virus, gram-negative and gram-positive bacteria [320–322].

Table 4-1 Inhibition zone diameter of microbial culture (E. coli and unspecified microbes) on agar plates using spray coated tissue paper.

Coating type	**Zone of microbial growth inhibition/diameter (cm)**	
	E. Coli	Microbes from human-hand sample
No coat	0	0
CNC	0	0
Ch	0.87	0
ChCNC	1.74	0
P-ChCNC	2.34	1.85
P-No coat	0.85	0

However, chitosan has been studied as antimicrobial agent against a limited number of microbes such as gram positive bacteria (*Listeria monocytogenes, Bacillus megaterium, B. cereus, Staphylococcus aureus, Lactobacillus plantarum, L. brevis, L. bulgaris*, etc.) and a very few gram negative bacteria (*E. coli, P. fluorescens, S. typhymurium* etc) [289]. This might be the reason that Ch and ChCNC treated tissue seemed not to show the antimicrobial activity using disk diffusion assay. On the other hand, it has been demonstrated in earlier studies that the hydrophilicity of microbes and substrate is one of the key factors that increases the sensitivity of chitosan as antimicrobial agent [323–325]. Treatment of ChCNC treated tissue paper with oxygen plasma, increases the hydrophilic character of paper [326]. This might be the reason that P-ChCNC samples resulted in a

significant reduction of microbial growth by increasing the inhibition zone in the disk diffusion test.

Antimicrobial activity was evaluated using the ASTM 2149 method. In figures 4-9 and 4-10, spray-coated, and plasma-activated tissue paper inhibited up to 99% of bacterial growth. The samples are considered to be bactericidal if they inhibit greater than 75% of microbial growth [304]**.** The plasma-treated p-ChCNC coated sample showed the highest reduction in the microbial count after 2 hours of treatment, although no inhibition was observed against CNC coated tissue paper in the disk diffusion assay. The reactive oxygen species generated by the plasma systems have shown bactericidal activity against a variety of pathogens in various studies [327–329]. However, unexpectedly, cellulose nanocrystals (CNC) also showed inhibitory action against *E. coli* culture with this method. The mechanism of bactericidal activity needs to be further understood to use this treatment more effectively [311].

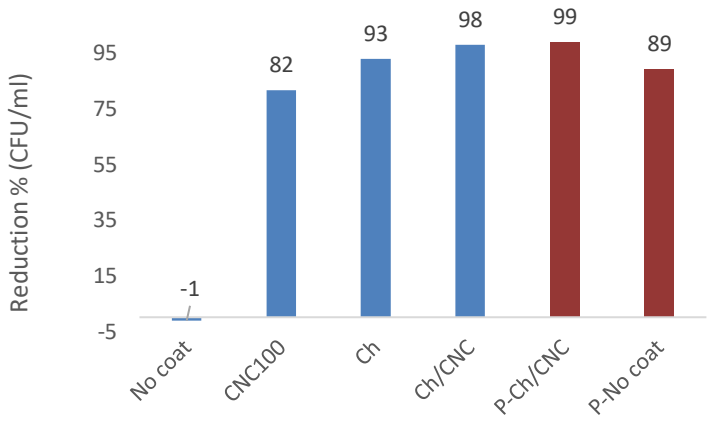

Figure 4-9 Percent reduction in microbial culture growth with spray coated tissue paper against E. coli culture.

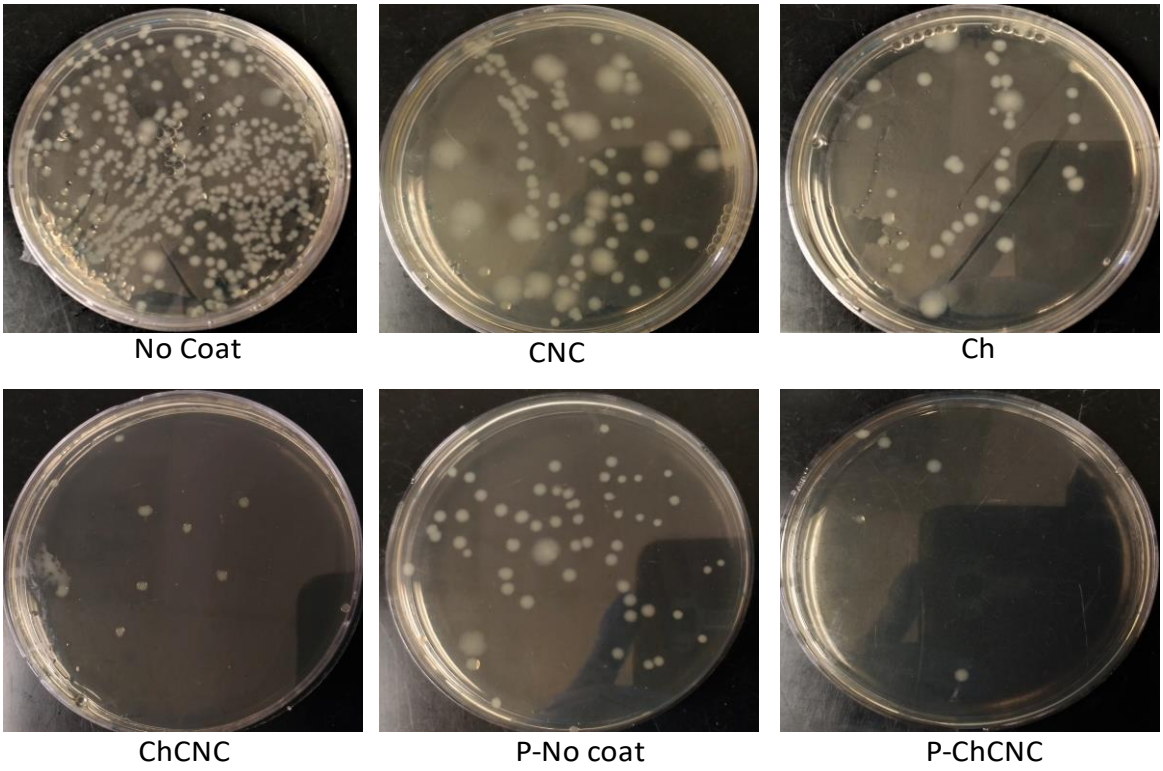

Figure 4-6. Bacterial (E. coli) growth on agar plates after treating the culture with different coated samples.

4.4.5 Water absorption

One of the main purposes of tissue paper is to absorb water and retain it. Water is taken up by capillary action through the cell cavity and fiber walls of the cellulosic fibers [330, 331]**.** The capacity of water absorption depends on several factors such as fiber types, chemicals used in the paper making process and types of creping process. More porous structures have a better water absorption capacity. Increased beating or refining of fibers decreases the rate and amount of water absorption due to a reduction in the porosity of the final paper [332]. CNC and Ch work similarly to a highly refined pulp if added during paper formation, which would result in reduced water absorption [333]**.** However, in the current study, CNC-containing coated papers showed similar or slightly better water absorption when compared to non-coated papers (figure 4-11). This is because, the treatment of CNC and Ch on tissue paper was done using a spray coating method,

which resulted in most of the hydrophilic CNCs and Ch on the fiber surface instead of getting trapped into the porous structure of fibers and thus not affecting the porosity of sheet (figure 4-3b and 4-3c, figure 4-5). Water absorption was reduced with the Ch-coated paper due to its hydrophobic nature and a reduction in the bulk and porosity of paper, which is consistent with the results by Zemljic et al [304]. Synergistic results were obtained with ChCNC coatings, as expected, and an increase in water absorption was observed. The spray coating method resulted a unique morphology of final ChCNC, in which CNC remained exposed to outside the chitosan matrix instead getting within the matrix (figure 4-3d). Due to the presence of hydrophilic CNC particles on the surface, there was an increase of water absorption [334,335]. Plasma treatment did not affect the water absorption capacity of coated or uncoated paper.

4.4.6 Strength properties of coated tissue paper

The ball burst test is one of the commonly measured strength tests for sanitary tissue paper.

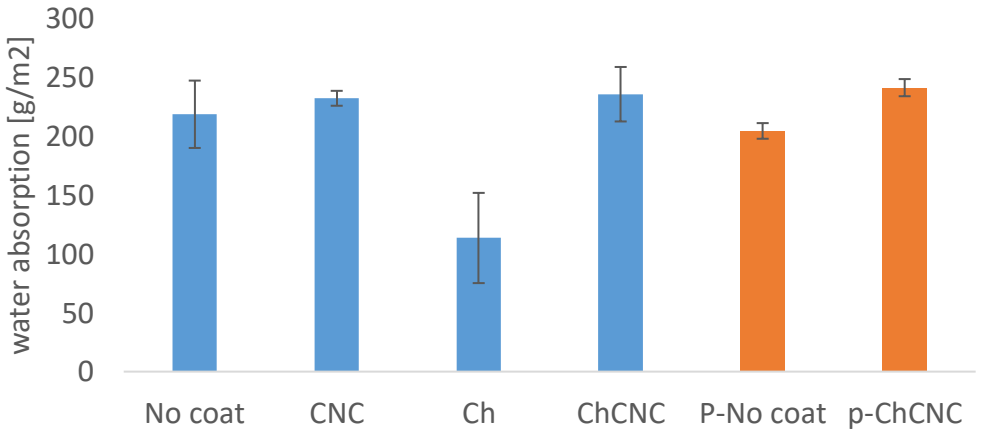

Figure 4-7. Water absorption capacity of Ch-CNC coated paper.

It measures the resistance to mechanical penetration through a tissue paper, which is an important characteristic of napkins or tissue paper for end use. For tissue papers, a very high ball burst strength is not required, but it should possess sufficient strength for handling and usage purposes.

Low dry burst strength can also cause problems in manufacturing and the converting processes. Figure 4-12 shows that dry ball burst strength properties were increased significantly with ChCNC spray coated tissue paper. With CNC coatings, the burst resistance of tissue paper improved by 48%. Further improvement was observed with CNC and Ch. However, as plasma treatment does not impart any modification through the bulk of tissue paper, inter-fiber bonding of tissue paper remained unchanged; thus, strength properties remained uninfluenced. Overall, the burst resistance of tissue paper with spray coating was significantly higher compared to tissue products in this range. Also, there is a linear relationship between burst and tensile strength for the case of tissue papers [336]**.** These findings are favorable for manufacturing and converting processes.

The stiffness behavior of ChCNC coated paper was found to be similar to that of burst

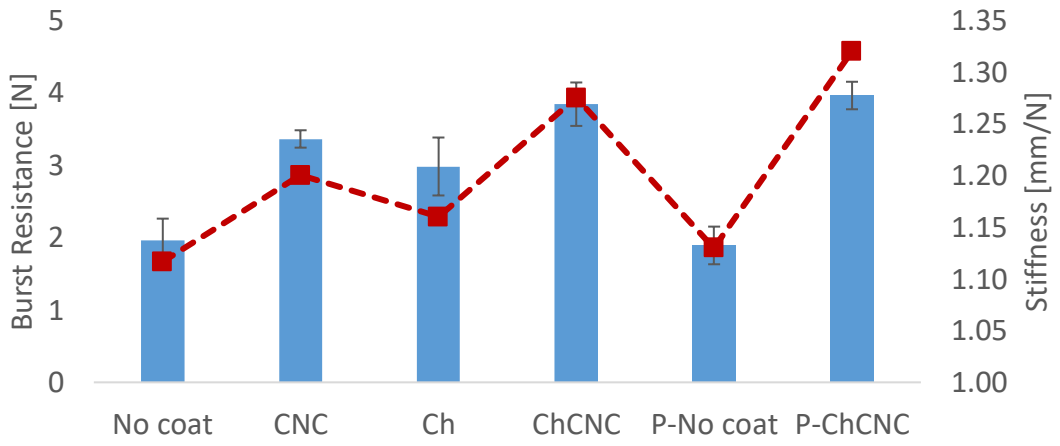

Figure 4-8. Ball burst strength of spray coated and plasma-treated tissue paper.

resistance, as shown in figure 4-12. The principle behind this behavior of stiffness can be different than burst strength. The burst strength of CNC-coated paper may increase due to its nanoscale structure and integral hydrogen bonding between paper and within CNC particles. Another reason for the increase in stiffness is due to the higher aspect ratio of CNC particles [337].

4.5 Conclusions

A recycled tissue paper was prepared by spraying it with sustainable CNC and chitosan-based coatings to render bactericidal activity without significantly disrupting functional properties such as water absorption and strength. The morphology and chemical characterization of ChCNC-treated substrate was validated using SEM, ToF-SIMS and Auger electron microscopy. Successful antimicrobial activity against specific *E. coli* cultures and unspecified microbial cultures taken from a soiled hand was tested qualitatively (disk diffusion assay), as well as quantitatively (ASTM 2149 method). Spray-coated CNC and chitosan paper could inhibit the growth of *E. coli* up to 99%. CNC coatings improved water absorption due to the higher surface area and hydrophilicity of nanocellulose increasing the rate of absorption. Also, the strength of the paper increased. This was especially true of CNC-containing coated paper. The significant boost in strength properties with CNC-containing coated tissue could pave the way for ultralight weight tissue papers with antibacterial properties, thus reducing the overall cost of the final product.

CHAPTER 5. Lignin Containing Cellulose Nanofibers for Barrier and Antimicrobial Packaging Products

5.1 Abstract

This study includes the effects of the selection of feedstock and processing conditions on chemical and morphological properties of the produced cellulose nanofibers and their barrier and antimicrobial properties. A non-wood feedstock from hemp hurd fibers is selected for producing lignin-containing cellulose nanofibers. The hemp hurds are obtained from industrial hemp stalks and defibrillated/pulped using four different pulping processes, namely autohydrolysis (with water), alkaline/carbonate (4% Na_2CO_3), unbleached kraft (Na_2S + NaOH), and bleached kraft. Lignin-containing and bleached hemp cellulose nanofibers (CNF) were produced using a high-speed mechanical grinding process. For comparison of hemp CNF, hardwood (Eucalyptus) was used and processed in a similar fashion to obtain hardwood (HW) CNF. The morphological properties characterized using SEM showed that lignin containing CNF were more fibrillated compared to bleached CNF from both hemp and HW fibers. The obtained CNF were used to prepare films and serve as coatings over linerboard paper for barrier and antimicrobial property measurements. The chemical characterization of CNF films carried out using ToF-SIMS showed a progressive reduction in surface lignin for carbonate (C), unbleached kraft (UK) and bleached kraft (BK) CNF. When HW fibers were compared, hemp fibers were observed to be more fibrillated, which was evident from CNF diameters. Hemp authydrolyzed (A) pulp containing highest lignin content (23.9%) was observed with relatively lower surface lignin compared to hemp-C, and hemp-UK CNF. The Crystallinity Index (CI) of hardwood CNF was observed, increasing in a progressive manner for HW-C < HW-UK < HW-BK. However, no big difference in CI of hemp-C, hemp-UK, and hemp-BK was observed. The highest water contact angle (WCA)

was measured for hemp-K CNF films (104º) followed by hemp-C (102º), HW-K(86º), and HW-C (84º). A similar trend of contact angle was observed with coated paper, though with lower contact angle ranging between 74º-81º. The water absorption was also found to be lower for lignin containing CNF coated paper compared to bleached CNF. However, when relative water absorption for hemp and HW CNF films was measured, BK CNF was found to accept less water compared to C and UK treated paper due to very high density of BK CNF films. The water permeability (WVP) was also found to be more related to the density rather than the lignin content of CNF coatings and films. The lowest WVP was observed with hemp-BK and HW-K CNF films as 5.85 mm.g/m^2/day and 6.12 mm.g/m^2/day, respectively.

For testing antimicrobial activity of hemp hurds and processed fibers, the extractives were extracted. The characterization of hemp hurds for the presence of antimicrobial active compounds was carried out using GC-MS. In GC-MS chromatographs of hemp hurd powder (hemp-P), CBD was observed, compared to and confirmed by commercially obtained standard CBD chromatographs. The CNF films and coated papers were tested against *E.Coli* for their antimicrobial activity. However, no significant antimicrobial activity was observed. Then, the sterilized paper discs and hemp-A films were treated with the extractives obtained from hemp-P, hemp-A, hemp-C, hemp-K and hemp-B. Hemp-P and hemp-A extractive treated paper showed a significant reduction bacterial growth that resulted in a zone of bacterial inhibition of 1.85 and 1.05 cm respectively in disk diffusion assay. The results were confirmed by doing a colony forming assay, and a 98% and 55% reduction in colony forming units was observed for hemp-P and hemp-A extractive treated paper. The results of using hemp CNF as barrier and antibacterial coatings create a great potential for valorizing industrial hemp waste for value added products.

5.2 Introduction

Hemp is a non-psychoactive variety of *Cannabis sativa L.* [338] The crop is one of historical and worldwide importance as manufacturers seek hemp as a renewable and sustainable resource for a wide variety of consumer and industrial products [339]. *Cannabis sativa* is a straight, annual herb that is mostly dioecious and grows up to 1-6 m in height [340,341]. The stems are green, hollow, cylindrical, and longitudinally ridged. Hemp stems are made up of two parts. The inner core of woody (xylem core body) materials is also known as hurd or shive and outer layer consists of fiber bundles known as bast fibers [341,342]. The woody or hurd fibers are lignified and generally used as animal bedding due to their high absorption capacity and insulation of concrete-like materials [33]. The outer bast fibers are bound by a central lamella and arranged in bundles, which are separated by the cortex parenchyma cell with a pectic and hemicellulose rich cell wall [342]. Bast fibers are used for cordage, rope, netting, canvas, bio-composites, and textiles [343]. Bast fibers represent a smaller percentage of total biomass of hemp stems compared to the xylem core/hurd fibers, which account for 70% of total biomass of hemp [344].

Antimicrobial activity is one of the well-studied properties of hemp fibers, with numerous contradictions and anecdotal information. Few studies show that the antimicrobial activity of hemp fibers is linked to their chemical compositions, such as esterified sterols, triterpenes (β-sitosterol and β-amyrin), which possess antimicrobial properties [345–347]. However, other studies show that hemp contains numerous biologically active compounds known as cannabinoids, which are responsible for their antimicrobial activity [33,348]. Cannabinoids are carboxylic acids of C21 or C22 compounds in the form of analogs and transformation products [349]. There are more than 40 cannabinoids that have been found in hemp plants. Among these, five major cannabinoids (namely cannabidiol (CBD), cannabichromene (CBC), cannabigerol (CBG), Δ^9-tetrahydrocannabinol (Δ^9

THC), and cannabinol (CBN)) have been well studied in terms of their structures and properties (Figure 5-1) [349]. CBD and THC both have demonstrated antimicrobial activity against gram positives, gram negatives, and a few varieties of fungi.[350] However, CBD is the primary therapeutic component of hemp, unlike THC, which is the psychoactive component. Regarding hemp hurds from medicinal cannabis sativa varieties such as Futura 75, they have higher content of lignin and phytochemicals than bast fibers and are thus superior in their antimicrobial activity [349,351].

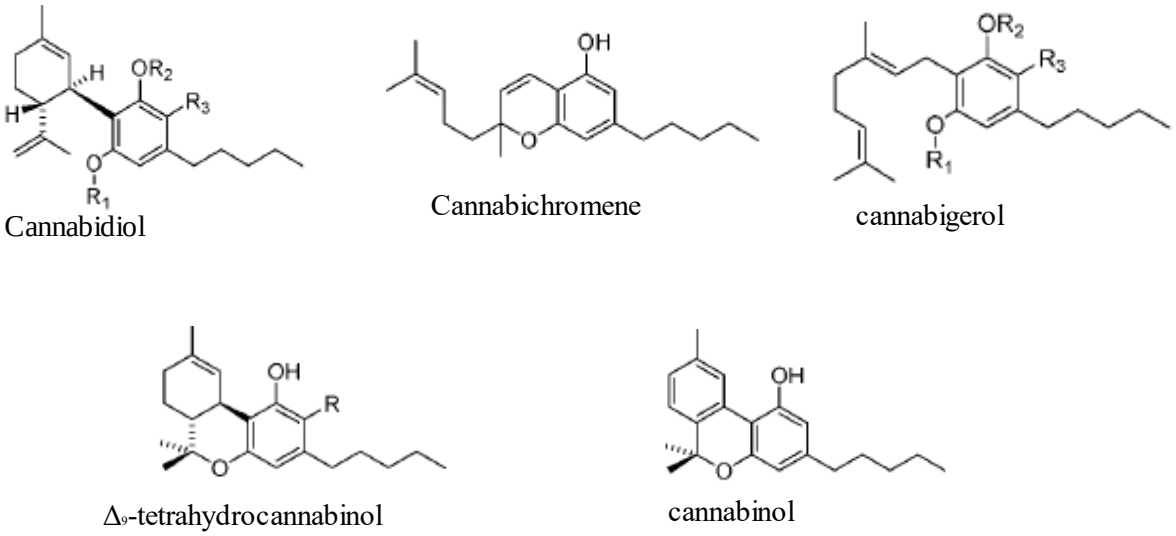

Cannabidiol | Cannabichromene | cannabigerol

Δ9-tetrahydrocannabinol | cannabinol

Figure 5-1. Five major cannabinoids present in hemp (Cannabis sativa L.).

Most of the studies on antimicrobial activity of hemp is focused on their polar and non-polar solvent extractives. The solvents used for extraction of phytochemicals from hemp and cellulosic fibers for antimicrobial functionality are petroleum ether, acetone, methanol, ethanol, hexane, and water [349,352–358]. Ali et al. studied the effects of petroleum ether and methanol extracts of whole *Cannabis sativa L.* plants for antimicrobial activity against Gram positives (*B. subtilis and S. aureus*), Gram negatives (*E. coli and P. aeruginosa*) and fungi (*A. niger and C. albicans*). They found that both petroleum ether and methanol extractives showed pronounced or good antimicrobial activity against all selected microorganisms. Mathur et al. showed that aqueous and

ethanolic extract of cannabis sativa exhibited good antimicrobial activity against *P. aeruginosa* and *S. aureus* but were inactive against *E. coli* and *C. albicans*. However, Wasim et al. showed that aqueous extract of hemp did not perform antimicrobial activity against any of the microorganisms tested including Gram positives, Gram negatives and fungi. A few studies have focused on antimicrobial activity of hemp fibers using different treatments with associative antimicrobial agents. These treatments include incorporation of silver nanoparticles (AgNPs) on oxidized hemp fibers [359], chemisorption of AgNPs on hemp fibers [360], and grafting of hemp fibers with antibiotics such as β-cyclodextrin, etc [361].

As discussed above, hemp extractives with non-polar solvents and physically or chemically modified hemp fibers have shown pronounced antimicrobial activity against a wide range of microorganisms. Very few studies show the antimicrobial activity of hemp fibers themself [351]. To our knowledge, solely Khan et al. studied the antimicrobial activity of hemp hurd powder against *E. coli* [351,362]. Khan et al studied the effects of particle size and pre-heat treatment of hemp fibers on antimicrobial activity. It appears that lignin content and particle size played important roles in the antimicrobial activity of hemp hurd powder.

As described in 'Chapter 1,' lignin containing cellulose nanofibers (LCNF) are more hydrophobic compared to bleached nanocellulose fibers [93,94]. Very few studies have reported the production and properties of LCNF from softwoods (*Thuja plicata, Norway spruce,) and* hardwoods *(Aspen/Populus, eucalyptus)* [87,92,94,363,364]. Rojo et al., showed an increase in contact angle with higher lignin content in cellulose. Similarly, Wei et al and Peng et al. also showed that lignin containing nanocellulose is more water repellent compared to non-lignin containing nanocellulose. However, Ferrer et al. 2012, studied residual kraft lignin in nanocellulose and found that higher residual lignin in nanopaper resulted in higher water absorption and no difference in

contact angles. In response to that, Rojo et al. 2015, studied pulp produced with different types of digestion processes to produce LCNF. In his study, Rojo et al. found that residual lignin present in cellulose fibers has different hydrophobicity and hydrophilicity characteristics. In his study, the hydrophobicity of residual lignin was ranked as follows in increasing order: Kraft pulp < Chemithermo-mechanical pulp (CTMP) < Thermo-mechanical pulpTMP < SO2–ethanol–water (SEW) in terms of water contact angles. Companies such as American Process Inc. have also shown interest in producing LCNF due to its low cost and comparatively hydrophobic nature. Exploring lignin containing nanocellulose from hemp hurds provides another opportunity to impart barrier and antimicrobial coatings with one composition and the least required chemical modification.

The objective of the current study is to obtain an antimicrobial coating and a film from hemp hurd fibers that has the potential to be used as a barrier for packaging also. Hemp hurd wood/shives were defibrillated to lignin containing CNF using chemical free and other conventional pulping methods. Nanoscale hemp fibers would expose more cannabinoids (if present in hemp hurds) and lignin on the coatings and film surface. These LCNF films and coatings were expected to have improved water barrier and antimicrobial properties compared to bleached nanocellulose fibers (BCNF).

This work was divided into two parts: First, LCNF produced from hemp hurds includes exploring barrier properties of hemp LCNF, primarily focusing on water sensitivity. Eucalyptus LCNF was also investigated to compare the effect of raw material on barrier properties. The second part of the study included the testing of antimicrobial properties of hemp LCNF. Since only Khan et al. confirmed the antimicrobial activity of hemp hurd powder without extraction, the hemp hurds extractives were also extracted from hemp hurd powder and tested for their antimicrobial property.

The detailed steps for valorizing barrier and antimicrobial properties of hemp hurds fibers into LCNF has been described in detail in the following experimental section. A detailed description of plan of work for exploring the barrier and antimicrobial properties of hemp hurd waste is summarized in figure 5-2.

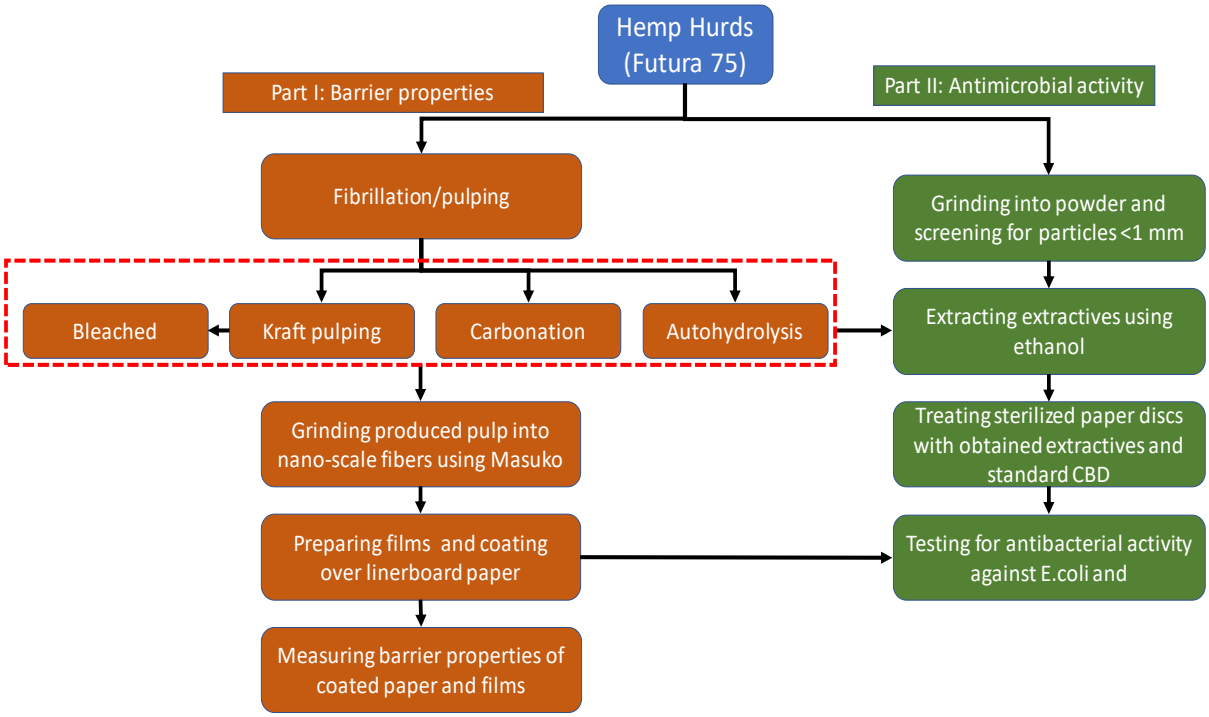

Figure 5-2. Plan of work for testing barrier and antimicrobial properties of hemp hurd extractives and nanocellulose.

5.3 Experimental

5.3.1 Materials

Dew retted and decorticated, Futura 75 hemp (*Cannabis sativa L.)* hurds stems were procured from the Netherlands and cut into small pieces before use. Sodium carbonate, sodium hydroxide, and sodium sulfite used for carbonate and kraft pulping were procured from Sigma-Aldrich at 98% purity. Chlorine dioxide and hydrogen peroxide used to bleach kraft pulp were obtained from Sigma Aldrich at 99% purity. A masuko grinder was used to prepare nanocellulose.

Eucalyptus (hybrid of *E. grandis* and *E. urophylla*) chips were obtained from Brazil. A brown linerboard with a basis weight of 130 g/m^2 and bulk of 1.5 cm^3/g was used as a coating substrate. A wiley mill grinder was used to grind the hemp hurds into powder, and then they were screened through 40 mesh screens to get 1 mm snippets. Ethanol and benzene were used for the extraction process and was procured from Sigma-Aldrich at 99.98% purity. Abn-CBD ($C_{21}H_{30}O_2$) solubilized in methyl acetate (5 mg/ml) was procured from TOCRIS Biosciences at 99.7 % purity.

5.3.2 Methods

The autohydrolysis (A) pulping was carried out by soaking cut pieces of hemp hurd stems in distilled water with a hemp to water ratio of 8:1 at a temperature 160 °C for 3 hours in a stainless-steel reactor at pressure 90 psi. After three hours, the softened hemp hurd stems (pulp) were washed and refined on the laboratory disc refiner at disc gaps of (0.1-0.05) mm with two passes before screening on a 0.15-mm slotted laboratory screen. For a mild alkaline/carbonate (C) pulping, 4wt.% sodium carbonate (Na_2CO_3) was used under the same conditions: 160 °C for 3 hours with 8:1 ratio of hemp to 4% Na_2CO_3. Unbleached kraft (UK) pulp fibers of hemp were obtained using 12% active alkali-25% sulfidity (NaOH+Na2S) (as Na_2O) with a 6:1 solid to liquor ratio under the same conditions. To obtain bleached kraft (BK) pulp fibers, the $D_O(EP)D_1$ sequence was used to obtain a final product of 85% ISO brightness. To compare the hemp hurd fibers with hard wood fibers, similar pulping and bleaching processes were used to obtain cellulose fibers from eucalyptus chips. However, a lower (4:1) solid to liquor ratio was used for defibration of eucalyptus chips due to its high bulk density compared to hemp hurds. Due to the high density and intact structure of eucalyptus chips, the autohydrolysis process could not result in fibers, and only alkaline, unbleached, and bleached kraft pulping processes were used for defibrillation. Extractives wt.% and lignin wt.% in samples were estimated using TAPPI T204 and T236 methods

respectively. The ratio of soluble and insoluble lignin in all pulp samples was determined using the NREL Laboratory Analytical Procedure (LAP) (NREL/TP-510-42618) and TAPPI T222 method.

To achieve a similar diameter range of nano-scale fibers, fibrillation of differently processed cellulose fibers was carried out using a Masuko grinder at 1500 rpm using 16-30 passes. The details of energy consumption in production of each type of nanocellulose is given in table 1.

Table 5-1. Conditions and energy consumption for producing LCNF.

Pulp type	Number of passes	Energy consumption (kWh/tons)	Final (%)	Consistency
Hemp-A	30	4213	2.48	
Hemp-C	25	4584	2.39	
HW-C	25	3885	2.18	
Hemp-UK	15	6661	2.13	
HW-UK	10	6010	1.63	
Hemp-BK	16	4911	2.54	
HW-BK	16	3197	1.96	

The morphological characterization of produced LCNF was carried out using scanning electron microscopy (SEM) under FEI XHR-VERIOS 460L field emission SEM. ToF-SIMS spectra and images were obtained using a TOF SIMS V (ION TOF, Inc. Chestnut Ridge, NY) instrument to show the distribution of lignin on fibers. The X-ray diffraction spectra were obtained with a Rigaku SmartLab diffractometer to obtain crystallinity of LCNF films. The angle was varied to 0.05° per step starting at 2θ angles from 5° to 50°. The diffraction data obtained for each sample were deconvoluted to obtain the area for amorphous peaks and crystalline peaks. The chemical characterization of extractives from differently processed hemp hurd was carried out using gas

chromatography and a mass spectrometer (GC-MS). Extractives were dissolved in ethyl acetate before being analyzed with GC-MS.

Prepared nanocellulose samples at 1.5% consistency were coated over the selected linerboard packaging paper using a lab scale benchtop rod coater using Mayer rod number 16, as described in chapter 2 and 3 and dried with hot air. This coating process was repeated 3-4 times to obtain ~5 g/m^2 of coat weight. The linerboard papers were calendared before and after coating at 100 ºC temperature and 1000 psi pressure. The nanocellulose films with thickness 50 µm were prepared by using the solvent casting method in teflon petri dishes under controlled conditions [248]. The coated linerboard paper and films were conditioned at 23°C and 50% RH for 24 hours before testing.

To analyze the hydrophobicity of LCNF coated papers and films, water contact angle was measured using the sessile drops method with a SEO Phoenix 150/300 contact angle system) and a CCD camera at room temperature (23 °C). The water vapor transmission rate (WVTR) was measured at 23 ℃ and 50% RH using the ASTM E96 wet-cup method with coating side towards the high humidity. Water absorption (g/m^2) of coated paper was determined using the Cobb60 TAPPI T441 method. Relative water absorption (RWA%) was determined by immersing 5 cm diameter films in deionized water and recording the sample weight after 2 hours. The excess water was removed by means of a standard roller using blotting paper on both sides of the film samples before weighing the samples. The RWA was determined using the following equation:

$$RWA\ \% = \frac{wt_{0h} - wt_{2h}}{wt_{0h}}$$

where wt_0 and wt_{2h} are the weights of the sample before and after 2 hours of immersion in water, respectively.

Air permeance of the coated substrate was determined using TAPPI T460" Gurley Densometer method."

The antimicrobial activity of differently processed hemp nanocellulose coated linerboard papers was tested against *E. coli* using a Disk diffusion (Kirby–Bauer) assay. For the disk diffusion assay, the overnight grown culture of *E. coli* in lysogeny broth (LB) media was diluted to 0.5 McFarland concentration (0.5 OD at 600 nm) using a KH_2PO_4 buffer. The 100 µl culture was transferred to the LB agar plates. The extractives obtained from hemp hurd powder and processed pulps were used to treat a sterilized filter paper substrate. The 200 µl of each extractive sample (1mg/ml) were added to different filter discs and dried before being placed over the *E. coli* culture spread on LB agar plate. The treated *E. coli* plates were incubated overnight at 37ºC. The inhibited bacterial growth was measured using a ruler by subtracting the diameter of the original disk from the diameter of the zone of inhibition (a transparent area devoid of *E. coli* growth). The antimicrobial activity of hemp-hurd extractives was also confirmed using ASTM E2149 method, which is the same as that discussed by khan et al.[317,351] For comparison, the antimicrobial test of pure CBD oil procured from TOCRIS Biosciences as positive control was also carried out.

5.4 Results and Discussions

5.4.1 Part I: Barrier properties

5.4.1.1 Lignin and extractives content

Table 5-2 provides the content (wt.%) of lignin and extractives in differently treated pulp fibers. The extractives and lignin amount present in untreated hemp hurd ground powder and auto-hydrolyzed hemp hurd pulp were found to be comparable. As desired, most of the lignin and extractives were retained with the fibers after pulping and washing steps. However, with carbonate pulping, a significant reduction in extractives was observed, while lignin content was found to be

similar to that of auto-hydrolyzed pulp fibers. Compared with carbonate pulping, kraft pulping resulted in the reduction of lignin amount by 35% and 60% for hemp and HW pulp fibers respectively.

Table 5-2. Lignin and extractives composition of treated fibers.

Sample	Klason lignin [%]	Acid soluble lignin [%]	Total lignin [%]	Extractives [%]
Hemp-P	23.78	1.069	24.849	5.9
Hemp-A	23.02	0.878	23.898	5.8
Hemp-C	22.03	1.077	23.107	2.6
Hemp-UK	14.01	1.034	15.044	2.6
Hemp-BK	0.06	0.778	0.838	1.2
HW-C	21.63	1.502	23.132	6.9
HW-UK	8.13	1.074	9.204	6.5
HW-BK	0.06	0.837	0.897	2.6

Surprisingly, the wt.% of extractives remained the same for carbonate and kraft pulping treatments in both hemp and HW fibers. For both hemp and HW pulp, bleaching of kraft pulp resulted in traces or almost no amounts of lignin; however, extractives were still found to be relatively higher. The key point that should be noticed here is the amount of acid soluble lignin (ASL) present in differently treated hemp and HW fibers. ASL is considered to be relatively hydrophilic compared to klason lignin (KL).[365] It has been observed that ASL is typically composed of low-molecular weight products and hydrophilic lignin derivatives formed during lignin degradation while the pulping/defibration process occurs.[366] Among unbleached fibers, hemp-A pulp was observed to have the least amount of ASL and highest amount of KL. Though bleached hemp and HW pulp had almost no KL, they were found to have significant amounts of ASL compared to others.

5.4.1.2 Morphological and chemical characterization of LCNF

The SEM images in figure 5-3 differentiate the morphology of nanocellulose fibers obtained from differently pre-treated hemp and HW (eucalyptus) fibers. When compared to the same pre-treated fibers, nano cellulose fibers obtained from hemp were found to be more fibrillated than hardwood fibers. The small spherical particles appearing in LCNF from hemp and hardwood were identified as lignin using SEM-EDX. In the EDX spectra, the 69% and 31% of total round globular particles are constituted of carbon and oxygen respectively (Figure 5-4). Which eliminates the probability of being this particle as part of ceramic or other polymer coming out of stones while grinding in Masuko grinder. Also, LCNF appeared to have lower diameters compared to bleached CNF, which is consistent with earlier studies and was confirmed by measuring diameter of 100 fibers from SEM images using ImageJ software. The diameter of Hemp-A, Hemp-C, Hemp-K, Hemp-B, HW-C, HW-K and HW-B were found to be 45±10, 67±14, 98±11, 138±26, 72±14, 136±34, 104±18 nm respectively. This can be related to the antioxidation scavenging ability of the lignin to prevent the back crosslinking of cellulosic mechano-radicals produced during the mechanical fibrillation process. This results in more fibrillated and reduced diameter fibrils. In summary, the lignin containing fibers were found to be fibrillated more extensively compared to bleached fibers.[94] Comparing hemp and HW, CNF from hemp were observed to be more fibrillated. This can be related to the higher hemicellulose and pectin content present in hemp compared to HW.[367] Higher amount of hemicellulose should correspond to a higher negative charge on fibers that facilitate the easier fibrillation due to more swellability of fiber walls.

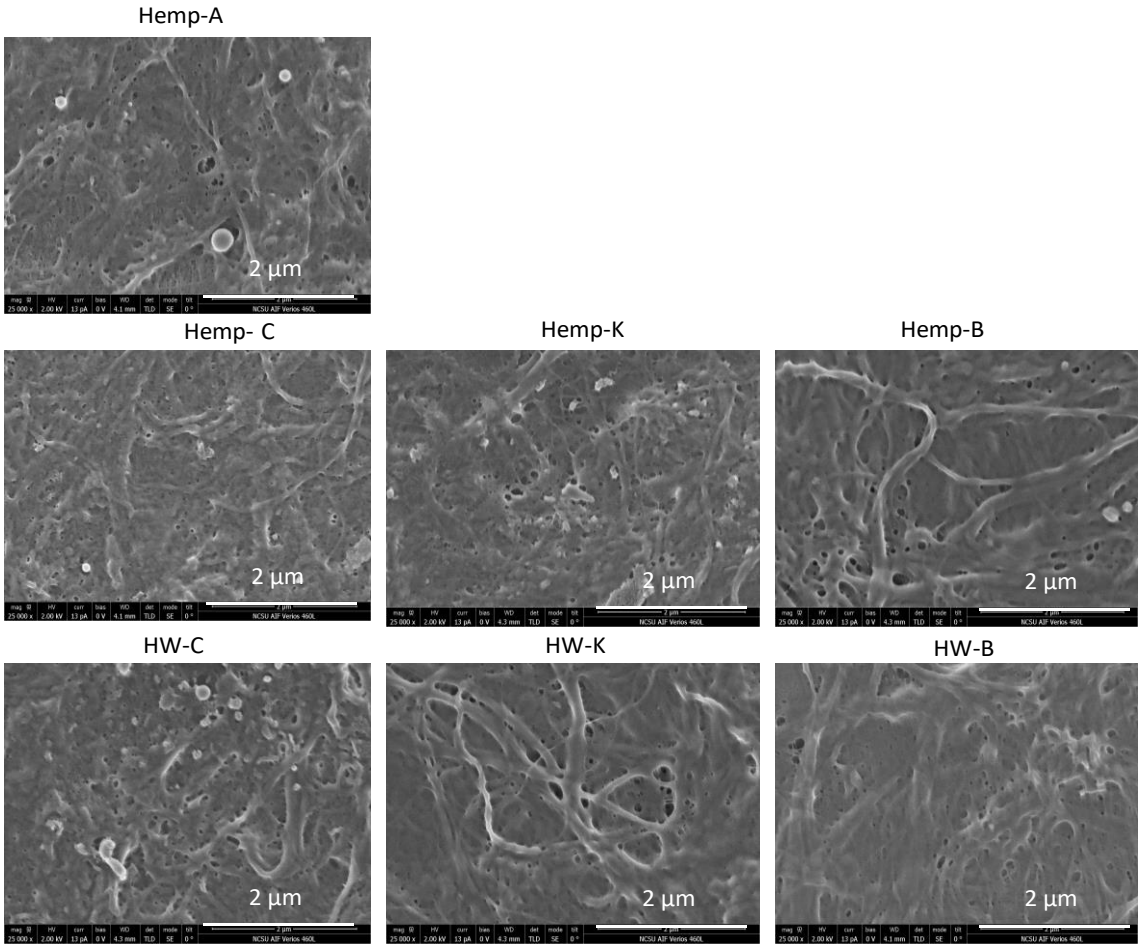

Figure 5-3. 25,000X SEM images of LCNF obtained from differently processed hemp and hardwood pulp.

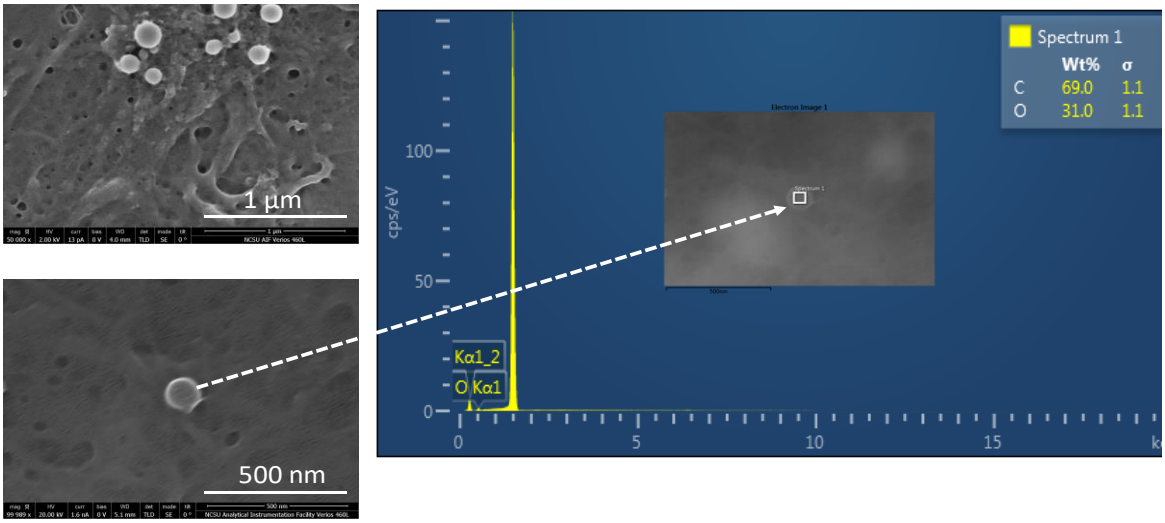

Figure 5-4. SEM images of Hemp-C at (a) 50,000X, (b) 100,000X magnification and (c) EDX of lignin particle.

5.4.1.3 Lignin distribution on the surface of nanocellulose films

In ToF-SIMS spectra of nanocellulose films, the lignin was identified using their prominent G ($C_8H_9O_2^+$, $C_8H_7O_3^+$) and S ($C_9H_{11}O_3^+$, $C_9H_9O_9^+$) fragments.[368] To study the distribution of lignin, RGB overlay of ToF-SIMS lignin fragment images over total fragments image was carried out (Figure 5-5). For RGB overlay (Figure 5-5: o, p, q, r, s, t and u), the total fragment images (Figures 5-5: a, b,c,d, e, f and g) and lignin fragments images (Figures 5-5:h, i, j, k, l, m & n) were given red and green colors respectively. As the lignin concentration decreased with carbonate, unbleached kraft, and bleached kraft pretreated fibers (Table 5-2), the surface lignin distribution on CNF was also found to be reduced. This can be confirmed by a reduction in green color intensity in overlay images. Though hemp-A pulp fibers were confirmed to have highest amounts of lignin (~24wt.%) compared to raw material (Table 5-2), LCNF obtained from the hemp-A appeared to have lower amounts of surface lignin (Figure 5-5o). Though ToF-SIMS is not a quantitative analytical technique, a relative comparison of the amount of lignin present in the CNF films can be carried out conveniently. A 1 μm deep sputtered spectra of LCNF films shown in figure 5v depicts how hemp-A, hemp-C and HW-C possessed the highest amounts of lignin present in them. This confirms the lignin wt% numbers shown in table 5-2. Though the amount of lignin present in hemp-A LCNF was observed as highest in terms of spectral intensity but surface lignin distribution was significantly low compared to hemp-C fibers, the surface lignin distribution was expected to have a significant impact on barrier properties shown in a later section.

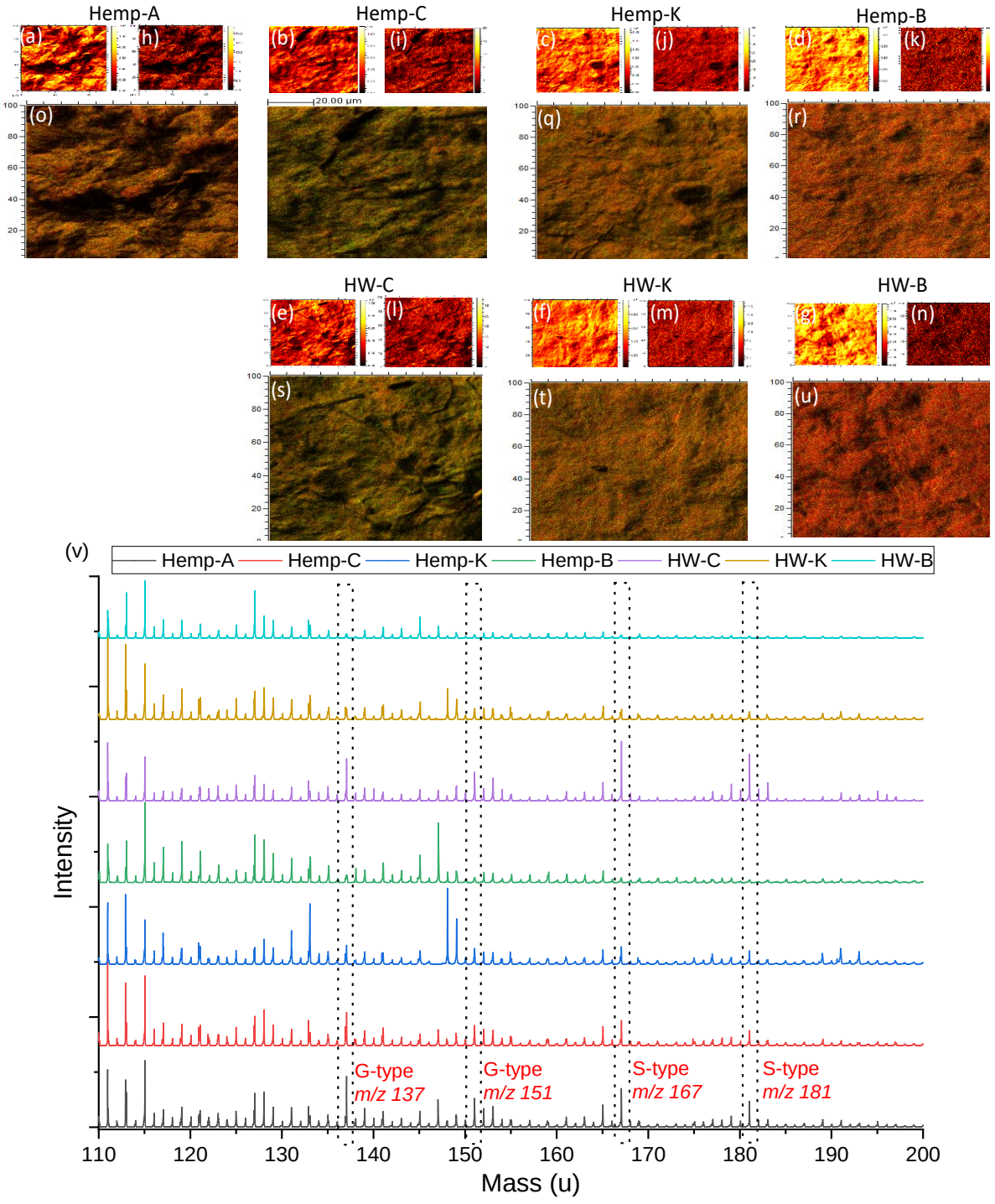

Figure 5-5. Total positive fragments ToF-SIMS images of hemp and HW nanocellulose films (a, b, c, d, e, f, g)., G (C8H9O2+, C8H7O3+) and S(C9H11O3+, C9H9O9+) lignin fragments images (h, i, j, k, l, m, n)., RGB overlay of lignin images (as green) over total (as red) fragments images (o, p, q, r, s, t,u)., and spectrum of all films.

5.4.1.4 Crystallinity of nanocellulose samples

The crystallinity of the nanocellulose films was expressed as the crystallinity index (CI), which is the mass ratio of the crystalline substance in the total dry sample based on the crystallographic two-phase model (Figure 5-6).[369] The CI values were determined by evaluating the ratio of the sum of the crystalline peak areas to the total area, assuming broad peak like nanocrystalline (amorphous) scatterings centered at 20.6° (Figure 5-6b). The peak shape and center of the two amorphous scatterings was determined by maximizing both their height and full width at half-maximum before separating the crystalline diffraction peaks. A significant difference between the crystallinity of LCNF films obtained from differently pretreated HW cellulose fibers was observed. This can be related to the amorphous lignin content in the nanocellulose.[369] Reduction in lignin content with HW-C > HW-UK > HW-BK pulp resulted in increasing CI of HW-C < HW-UK < HW-BK LCNF films. For hemp nanocellulose, a significant difference in CI was observed only between hemp-A (CI: 30%) and hemp-C (40%) CNF films. In contrast, no significant changes in CI were observed between hemp-C, hemp-UK, and hemp-BK CNF films.

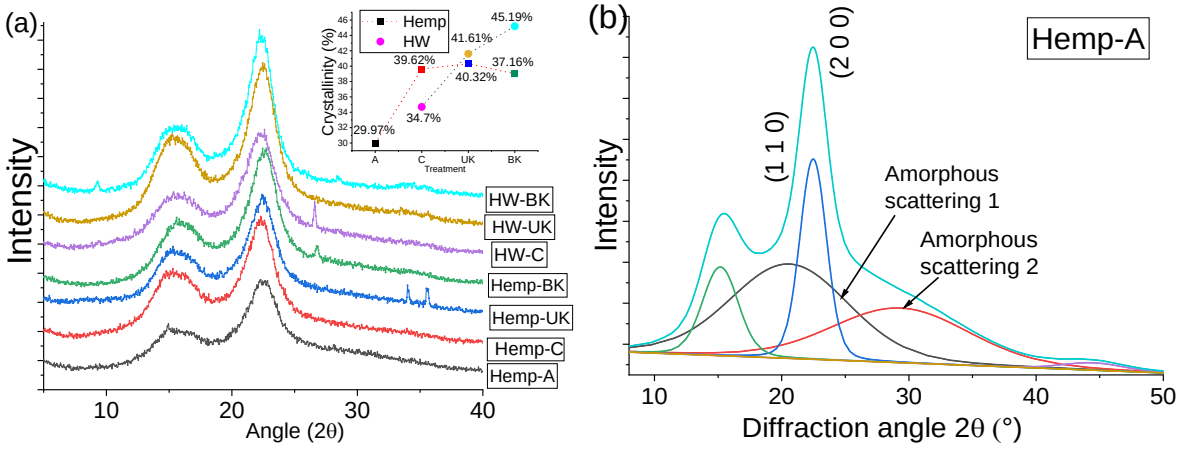

Figure 5-6. (a) XRD profiles and CI measurements of hemp and HW nanocellulose films and (b) Peak separation of a XRD profile for determination of the CI.

5.4.1.5 Water barrier properties

Water Contact angle: Considering that a significantly higher amount of lignin is present in A, C, and UK treated hemp and HW nanocellulose fibers, it was expected that these CNFs would be more hydrophobic compared to BK CNFs. A similar expected trend was observed for hemp and HW, and both C, UK and BK CNF films and coated papers (Figure 5-7). However, hemp-A films resulted in much lower contact angles compared to hemp-C films instead of having similar lignin content (~23 wt.%). This can be explained based on surface lignin distribution of hemp-A films shown in ToF-SIMS image figure 5-5a. Though total lignin concentration present in hemp-A CNF was found to be highest but a lower amount of surface lignin was observed on hemp-A films compared to hemp-C and hemp-UK films. The contact angle of hemp-C and hemp-K CNF films was observed as 102° and 104° respectively, which is similar to the contact angle of organosolv lignin containing CNF films studied by Agrawal et al.[93] Hemp-BK and HW-BK films showed the lowest WCA, 66° and 51° respectively. Despite the big difference between the lignin content of C and UK treated hemp and HW CNF films and coated papers, no significant changes in contact angle was observed. It can be expected that distribution of lignin content over UK CNF films is optimum and sufficient to provide maximum hydrophobicity to the coated surface and films.

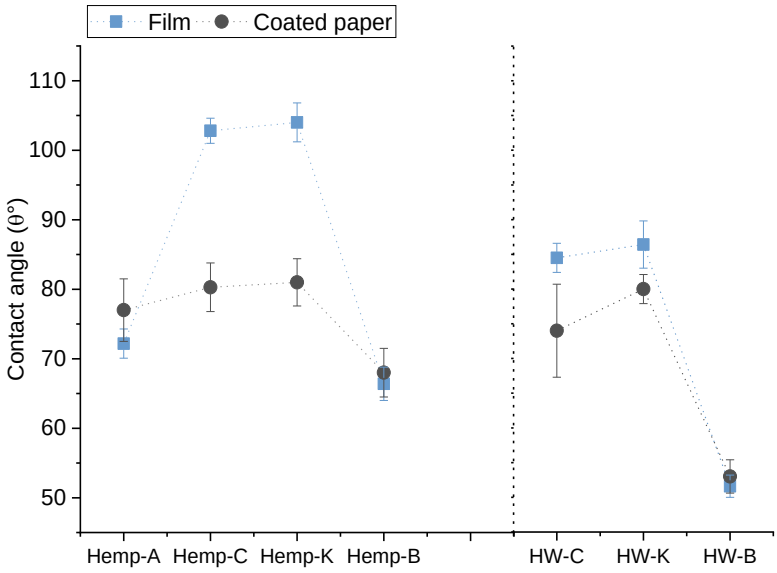

Figure 5-7. Contact angle of nanocellulose films and coated paper.

Water absorption: Water absorption (g/m^2) measured on coated paper increased with a decrease in lignin and extractives content for autohydrolyzed, carbonate, and kraft hemp CNF (Figure 5-8a). A similar trend of relative water absorption (RWA%) was observed with CNF films (Figure 5-8b). However, water absorption measured for hemp-BK and HW-BK CNF was lowered even after having much lower content of surface and bulk lignin. This was surprising and contradictory compared to the results shown in earlier studies.[94,127,364] Water absorption and water contact angle are known to be dependent on the surface energy and pore structure near the surface. But the surface energy for bleached CNF should be lower than unbleached CNF based on the contact angle in figure 5-8 and earlier studies. To explain this behavior of decrease in water absorption, a decrease in pore size can be the expected as the probable reason. This is supported by the increase in apparent density of hemp-BK CNF (Figure 5-9a). However, the reduction in RWA% for HW-BK CNF could be understood based on the crystallinity. As shown in figure 5-6a, the CI of HW-BK was found to be the highest depicting has and had lowest amorphous region.

Since crystalline regions absorb no or much less water compared to the amorphous regions,[125] water absorption by HW-BK was found to be much lower compared to HW-UK CNF films.

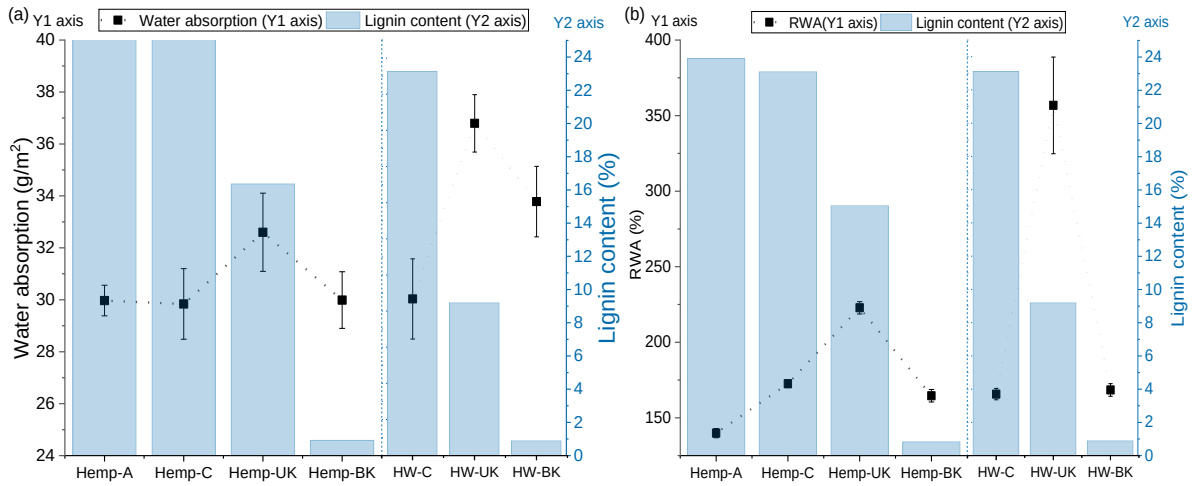

Figure 5-8. (a) Per unit area water absorption (g/m2) on coated paper and (b) Relative water absorption of nanocellulose coated paper and films.

WVP: Water vapor permeability of CNF films and coated papers did not show a similar trend of reduction with bulk lignin content or surface lignin distribution (Figure 5-9a and 5.9-b). On the other hand, WVP was found to be correlated more significantly with film density (Figure

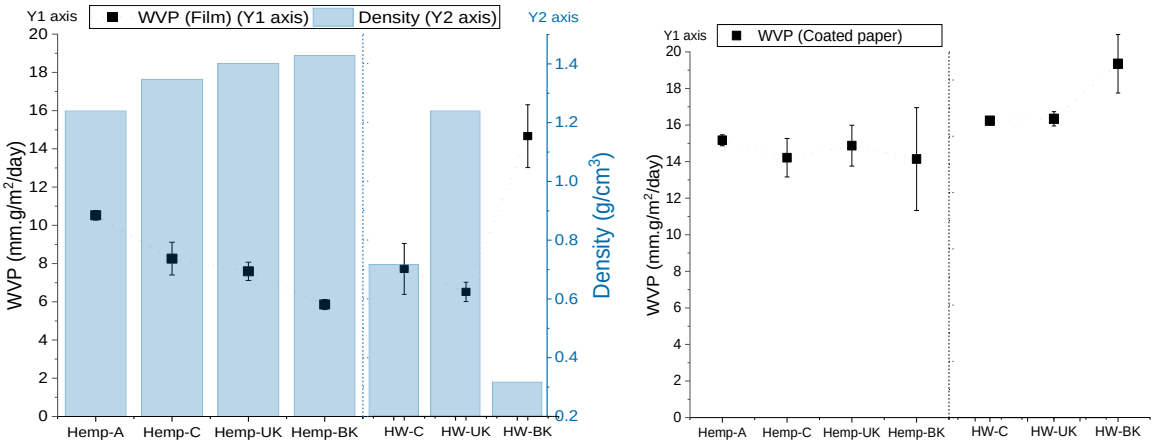

Figure 5-4. Water vapor permeability (WVP) of nanocellulose (a) films and coated paper (b) and coated paper.

5-9b).[127] Samples with higher density possess more compact structures and are found to be less water vapor permeable, regardless of the lignin content and distribution.

Air resistance: The air resistance measured for CNF coated paper at 50% RH showed the linear relationship with lignin and extractives content in CNF (Figure 10). The air resistance was observed to be lower for CNF having higher lignin content. The key factor for suitability of CNF films as gas barriers is attributed to its ability to form the dense structure of high crystalline order.[370] The higher the density and crystalline order of films, the higher the air resistance that was observed.

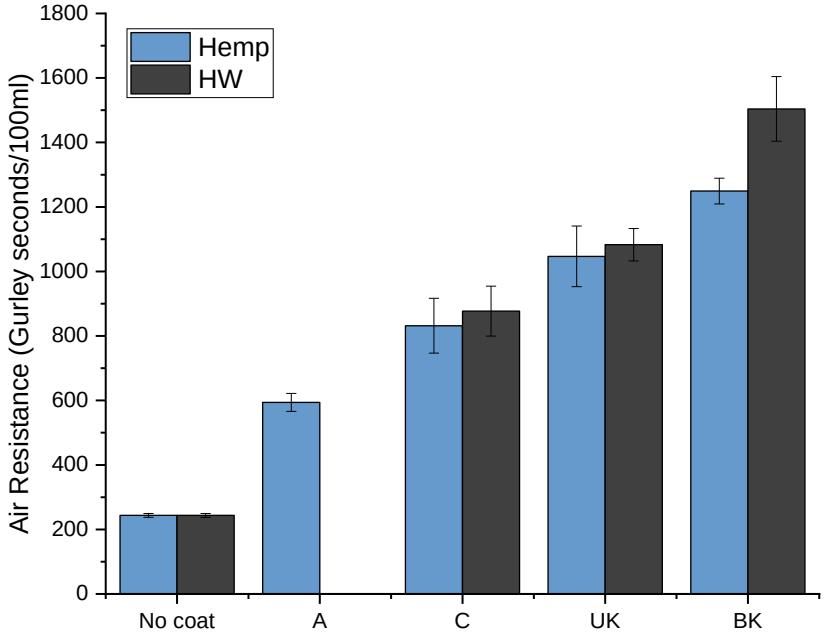

Figure 5-10. Air resistance of hemp and HW nanocellulose coated paper.

5.4.2 Part II: Antimicrobial properties

5.4.2.1 Characterization of extractives

The extractives from hemp hurd powder and processed pulp were analyzed using GC-MS. The chromatogram shown in figure 5-11a shows that the extractives from hemp-P and hemp-A

includes fatty acids, alkanes, aldehydes, sterols, and phenols such as clionasterol, and coumarin etc. However, extractives from hemp-C, hemp-UK, and hemp-BK were observed to have a lower

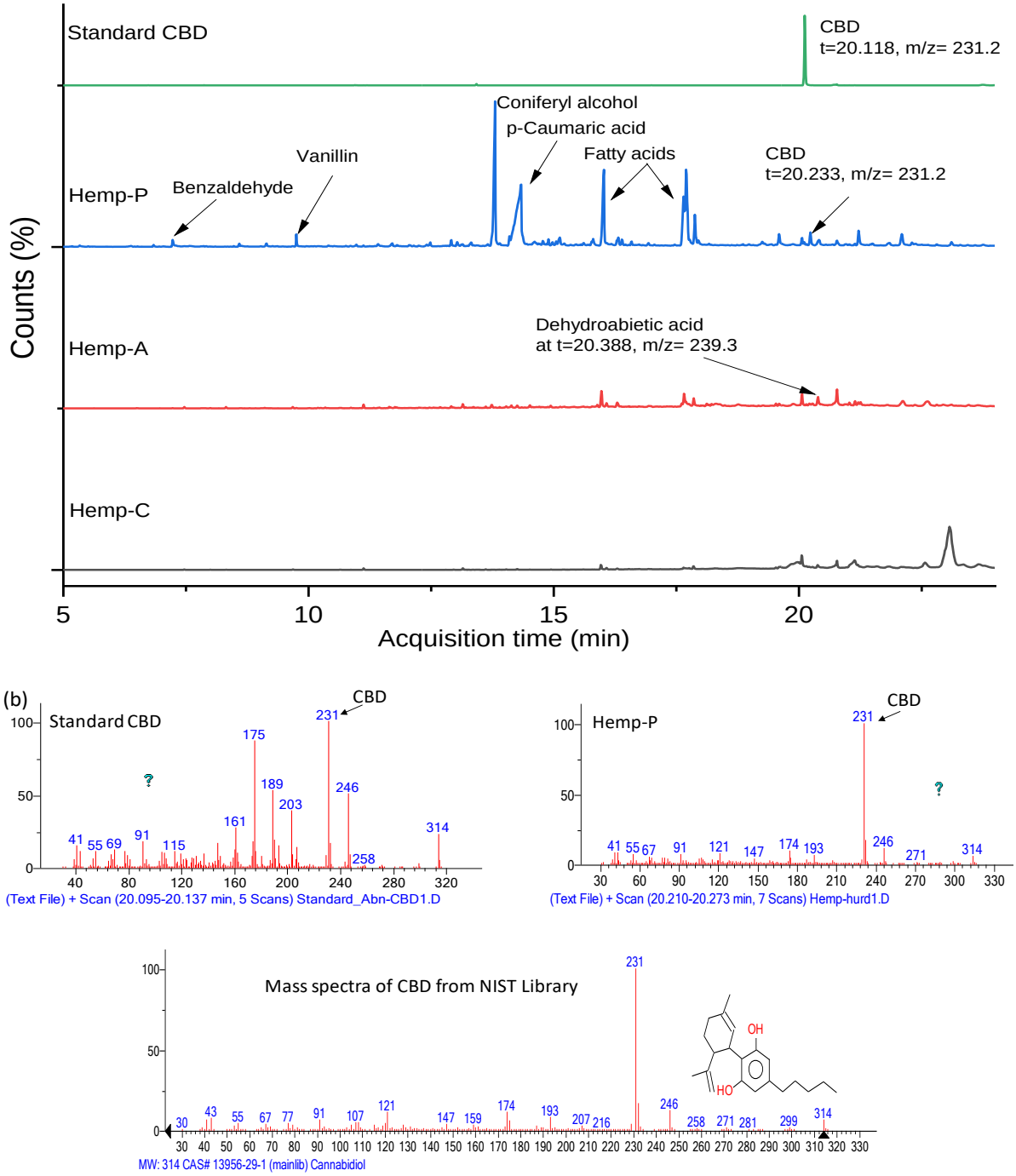

Figure 5-11. (a) GC-MS chromatograms of hemp-P,hemp-A,hemp-C and standard cannabidiol (b) Detailed mass spectrs of hemp-P and its comparison with standard CBD and NIST library mass GC-MS mass spectra.

number of active compounds. Earlier, it had been studied that the possession of CBD found in flowers is highest and progressively lower in leaves, petioles, stems/hurds, seeds and roots. Thus, the study of CBD concentration in stems, seeds and roots is generally excluded.[371] In figure 5-11b, we confirmed the presence of CBD in hemp-P extractives. The probable peak for CBD in the hemp-P extractives sample was confirmed with the standard CBD peak and GC-MS NIST library.

5.4.2.2 Antimicrobial activity

The antimicrobial activity of extractives from differently processed hemp hurds is presented in figure 5-12 (disk diffusion assay) and figure 5-13 (colony forming assay). The clear transparent zone around the treated paper discs presents the zone of inhibition. Table 5-3 presents the zone of inhibition, where d_2 is the diameter of the bacterial devoid (transparent) circle formed around the disk and d_1 is the diameter of the paper disk. It is evident that the hemp-P extractives treated paper disks showed the highest zones of inhibition and higher than standard CBD. The higher antibacterial activity of hemp-P extractives can be related to the fact that apart from CBD hemp hurds also contain other extractives, mainly phenolic acids, aldehydyes and fatty acids such as vanillin, syringaldehyde, p-hydroxybenzaldehyde, vanilic acid, p-coumaric acid, acetosyringone and gallic acid.[348,372] Though no studies have been done in the past to show the antibacterial activity of individual mentioned extractives from hemp, Khan et al. discussed the possibility of extractives other than CBD having antimicrobial activity.[348] Hemp-A extractives also resulted in zone of inhibition of around 1.05 cm against *E.Coli* for one test but not for the replicates. However, hemp-C, hemp-UK, and hemp-BK did not show any antibacterial activity. The results can also be related to their extractives content provided in table 5-2 and GC-MS plots shown in figure 5-11. After consulting the results, it won't be wrong of us to state that other than the autohydrolysis pulping process, most of the active compounds (extractives) washed away with

the carbonate and kraft pulping processes. Thus, no antibacterial activity was observed with the extractives from carbonate and kraft pulped fibers.

Table 5-3. Zone of bacterial growth inhibition (d2-d1).

Sample Id.	Zone of inhibition (cm)
negative Control	0
CBD	1.55 ± 0.22
Hemp-P	1.85 ± 0.15
Hemp-A	1.05 ± 0.71
Hemp-C	0
Hemp-UK	0
Hemp-BK	0

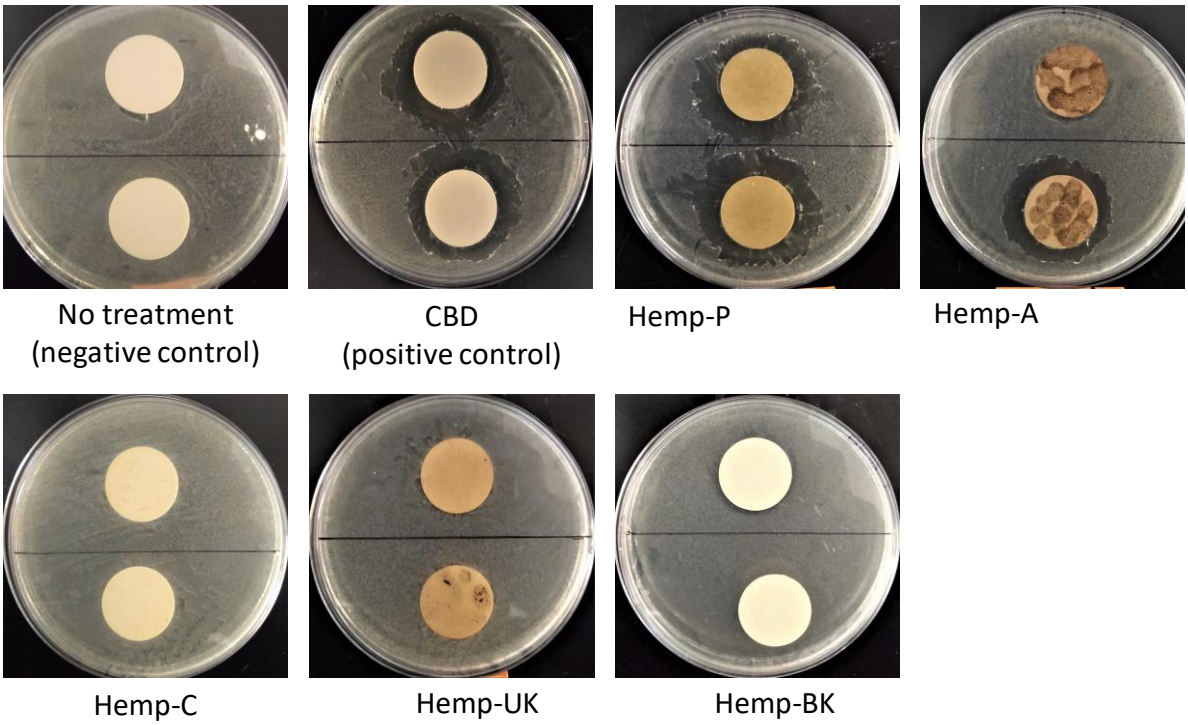

Figure 5-12. Disk diffusion assay for hemp extractives treated paper

To confirm the antimicrobial activity of hemp hurd and processed pulp extractives, a colony forming assay was carried out using treated paper disks (Figure 5-13). The colony forming assay confirmed the reduction in bacterial colony forming units (CFU) by 98.54% for hemp-P extractives, which was similar to the antibacterial activity of pure CBD (98%) (figure 5-13b). The hemp-A extractives treated sheet also showed reduction in CFU by 55%, which confirms the zone of inhibition shown in the disk diffusion assay. The antimicrobial test was also carried out for hemp nanocellulose films and coated papers; however, no antimicrobial activities were observed, not even for hemp-A CNF film. This can be due to the absence of sufficient amounts of active compounds in the used CNF films and coated paper. To study the potential for antimicrobial hemp nanocellulose films, hemp-A CNF film was treated with hemp-P extractives (200 µg of extractives/mg of dry CNF). A 99.7% in CFU reduction was observed with Hemp-A CNF treated film with hemp-P extractives (Hemp-A+P).

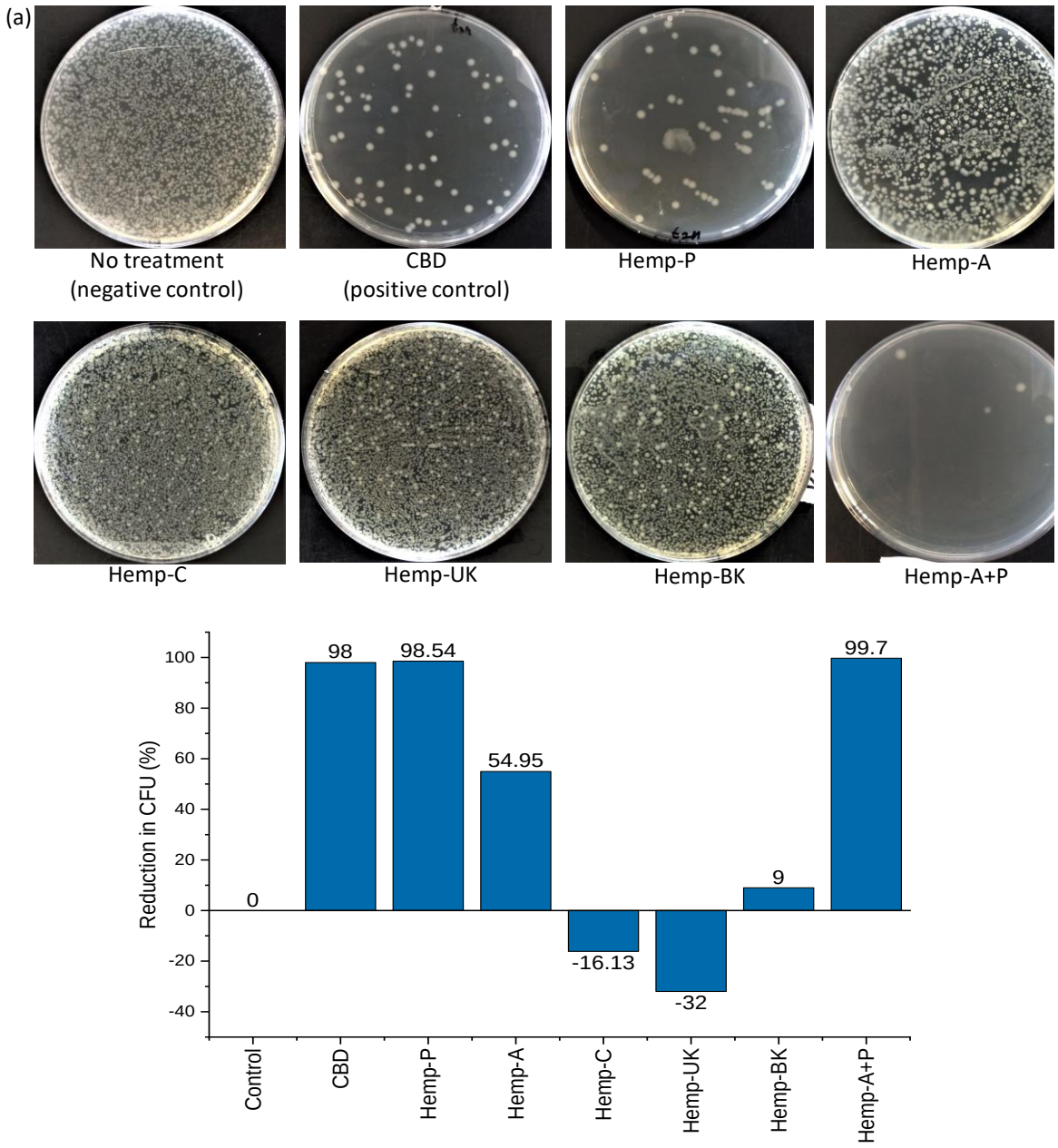

Figure 5-13. Colony forming assay for antibacterial activity of hemp extractives treated paper and hemp-P extractives treated hemp-A nanocellulose film.

5.5 Conclusion

5.5.1 Part I: Barrier coating

Hemp hurd lignin containing nanocellulose fibers were obtained from differently treated (autydrolyzed, 4% carbonated, unbleached and bleached kraft processed) pulp fibers using Masuko grinder. Eucalyptus hardwood nanocellulose fibers were also obtained using similar processes to compare the barrier properties. The morphological, crystallinity and chemical characterization of CNF films was carried out using SEM, XRD, EDX and ToF-SIMS analytical techniques. Water barrier properties of lignin containing CNF films from hemp and HW were measured in terms of water contact angle, water vapor transmission rate and water absorption. The barrier properties were found to be dependent not only on the lignin content and lignin distribution but also on the CNF film density and porous structure. Lignin containing CNF films and coated paper showed much higher WCA (80°-102°) than bleached CNF films. Similar results were observed for LCNF coated papers. WVP was found to be more dependent on density of films than lignin content.

5.5.2 Part II: Antimicrobial coating

The hemp extractives obtained from hemp hurd powder and processed hemp pulp showed the presence of many active compounds. Only hemp hurd powder evidently had the CBD. The antimicrobial tests with hemp CNF films and coated paper did not show any antimicrobial activity. However, paper disks treated with extractives from hemp-P and hemp-A showed significant reductions in bacterial growth conformed by disk diffusion as well as a colony forming assay. Finally, the hemp-A CNF were treated with the extractives obtained from hemp-p and found to be 99.7% effective for antibacterial activity against *E. coli*. This work has paved the way for combining the barrier and antimicrobial properties in lignin containing nanocellulose fibers obtained from hemp hurds.

CHAPTER 6. Summary and Future Directions

This chapter provides a brief summary and gives major highlights to the readers in each chapter. In addition, the limitations with current work and future direction in my understanding to continue the current work is included.

6.1 Chapter 1

6.1.1 Summary

The need and motivation for this dissertation has been laid out in this chapter. The different types of nanocellulose were discussed. The characterizations of different types of nanocellulose in terms of size, chemical, structural and morphological parameters were described and correlated with their application potentials. Namely, cellulose nanofibers (CNF), cellulose nanocrystals (CNC) and lignin containing cellulose nanofibers (LCNF) were discussed. The highlights of the scope of nanocellulose-based materials applications specifically for barrier coatings were discussed. After a detailed literature survey, it was concluded that nanocellulose materials have great potential in the field of oxygen barrier properties when used as films and coatings for paper packaging. However, these films and coatings are highly sensitive to water and low barriers to oil and grease. In the past, reduction in water sensitivity of nanocellulose has been studied by doing extensive chemical modifications and using materials such as fluorocarbons, silicates etc., which vanish the objective of producing sustainable and biodegradable coatings. The potential of cellulose nanocrystals for antimicrobial properties was also discussed. It was concluded that there is great scope for exploring nanocellulose materials and functionalizing them to obtain better barrier and antimicrobial coatings and films for food packaging.

6.2 CHAPTER 2

6.2.1 Summary

This chapter focused on exploring the potential of cellulose nanocrystals for gas, oil and water barrier coatings with more sustainable and less chemical-intensive modifications for food pcakging. The CNC were selected over CNF based on their crystalline structure. Considering the higher crystallinity of CNC materials, we believe a CNC coating should have more intact and dense structure to avoid permeability of water and oil. The sustainable approach of making CNC-composites with functionalized bio-based and sustainable materials was used to reduce the water sensitivity of CNC coatings. The selection of functionalized additive materials (soy protein(S), MMT clay, kaolin clay (K) and alkyne-ketene-dimer (AKD)) was carried out based on specific function to impart into the CNC-composite coating. The CNC-composite coatings were coated on three different type of papers: linerboard, whiteboard and linerkraft. The rheological characterization of CNC-composite coating with soy protein, MMT and AKD showed much lower viscosity compared to the CNC-only suspension at the same solid concentration (10wt.%). The morphological characterization of coated surface with CNC-composite provided the most compact and dense structure with the least defects observed. On the other hand, CNC-only coating was found to be fractured in a regular fashion throughout the paper due to its brittleness. The FTIR spectra of CNC-composite showed the significant reduction in the hydroxyl group intensity due to more hydrophobic moieties from protein present on the top surface. Due to the following changes in the morphology and chemistry of the CNC-composite coating surface, a significant reduction in water absorption, gas permeability and improvement in oil resistance was observed. A very high oil resistance with CNC-composite coating was obtained with a kit reading of 6, which is a good number for applications such as burger wraps, pizza boxes etc.

6.2.2 Future Direction

A detailed study on chemical profilometry of CNC-composite coatings was not carried out. It was hypothesized that AKD and hydrophobic moieties should phase out of the bulk of coated paper due to hydrophobic interactions. However, results were in the favor of the hypothesis by showing lower -OH groups on the surface and lowering water sensitivity. A detailed chemical profile of coating thickness could help better explain barrier properties. Another limitation found with CNC-composite coatings was brittleness of coatings. The brittleness of CNC-composite coating was much lower than the CNC-only coatings, which were confirmed by stiffness tests and tensile tests. Nevertheless, to make a more flexible barrier coatings using CNC, the use of suitable plasticizer can be considered in future. Comparing the results of barrier properties of modified CNC coatings with commercially available coatings, we see there is still a huge potential for improvement in water vapor and gas barrier properties.

6.3 CHAPTER 3.

6.3.1 Summary

In this chapter we studied the potential of combining CNC-composite coatings (CNC*) developed in chapter 1 with CNF in a multilayer coating system to obtain all-rounder barrier coating against gas, water and oil. A versatile laboratory bench-top rod coating method was used to obtain the two two layer coating system of CNC* and CNF. The oxygen, air water and oil barrier properties were improved by multitude. The air resistance (>10,000 Gurley seconds) and oil resistance (Kit reading = 11) properties were found to be comparable to the commercially available petroleum-based materials and fluorocarbons. The surface tension of CNF/CNC* coated paper (CNF as bottom layer and CNC* as top layer facing atmosphere) measured using diiodomethane and water was found to be reduced to 30 mJ/m^2 comparing surface tension (γ_{sv}) of CNF and CNC

as 61 and 67 mJ/m^2 respectively. These results can be correlated to the chemical and morphological characterized coated surface. The FTIR spectra and SEM images confirmed the formation of stagnant double layer coatings of CNF and CNC* over paper. In SEM images it was found that a very uniform and compact double layer of CNF/CNC* was formed. The ToF-SIMS spectra of CNF/CNC* coated surface confirmed the presence of more hydrophobic moieties ($C_4H_8^+$, C_4H_8N, $C_8H_6N^+$, $C_9H_8N^+$) from protein and fewer CNC particles exposed to the top surface. This can be the most probable reason for reduction in the surface energy of the CNF/CNC* coated surface.

6.3.2 Future Direction

One of the major limitations that still exist with these CNF and CNC multilayer coatings is their low water barrier properties. Though a significant reduction in surface energy was observed with CNF/CNC* (30 mj/m^2) coatings which is equivalent to the surface energy of polyethylene, polypropylene and polypropylene films, bulk water sensitivity of the coating was still high. The major limitation of the currently developed coatings was their instability due to their brittle nature. Again, future work can be directed towards improving stability and lowering the brittleness of the films. The stability of the coatings can be improved either by using a relatively hydrophobic topmost layer or covalently bonding the hydrophobic moieties of soy protein or any other suitable alternative on the surface.

6.4 CHAPTER 4.

6.4.1 Summary

A versatile approach to synthesize an antimicrobial coating using CNC and chitosan was used. The chitosan and CNC were used to complement the antimicrobial and hydrophilic properties respectively to be used for tissue paper and hygiene product application. The

deacetylated chitosan having amine groups was deliberately brought to a pH lower than its pKa (>6.3) and then mixed with CNC suspension at a chitosan to CNC ratio of 80:20. The ratio of the chitosan and CNC was opted such that total charge of the composite would remain positive for antimicrobial activity. The obtained suspension of CNC in the chitosan matrix was spray coated over tissue paper and dried using a chromalox 2110 dryer system with zero load at 110 °C. To activate the surface groups of coated surfaces of tissue paper, the surface was treated with oxygen plasma. The SEM images of Chitosan-CNC composite showed a unique morphology: the rigid, narrow, and needle like CNC particles were observed to be protruding out of the chitosan matrix. The CNC particles instead of getting trapped inside the chitosan matrix were observed mostly on the surface of the composite. The following morphology and architecture of the CNC and chitosan composite were confirmed using ToF-SIMS and Auger microscopy. The water contact angle of chitosan-CNC composite was found to be reduced to 41° compared to contact angle of chitosan (~90°). The water absorption of the composite treated tissue paper was observed to be almost equal to the untreated tissue paper. The antibacterial activity of chitosan-CNC composite treated tissue paper against *E.coli* was carried out using colony forming assay. A 99% reduction in *E.coli* colony forming units (CFU) was observed after treatment.

6.4.2 Future Direction

This study was terminated after observing the significant reduction in the growth of gram-negative bacteria (*E. coli)*. However, no antimicrobial activity test was carried out against other family of pathogens such as gram-positive bacteria and fungi. The developed chitosan CNC composite coating should be tested against gram-positive bacteria and fungi too. During the tests the phase separation between chitosan and CNC was observed after a prolonged resting of samples in beaker. To obtain the required morphology of the final composite over tissue paper, a proper

mixing of composite was necessary just before spray coating. Though almost no difference in water absorption was observed for chitosan-CNC treated tissue paper, the absorption rate was

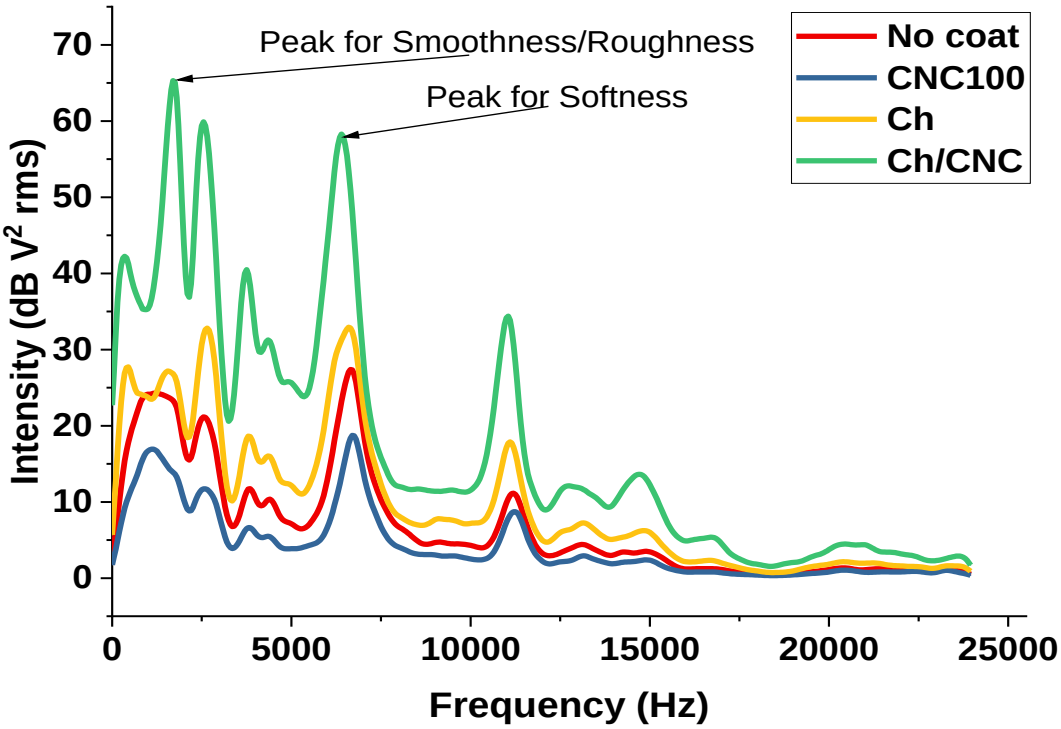

Figure 6-1. Softness of chitosan, CNC and composite treated tissue paper

reduced. Also, the softness of chitosan and CNC composite treated paper was reduced (Figure 6.1) potentially due to significant increase in strength. In the future, the study of improvement in water absorption rate and softness of these antimicrobial tissue papers can receive more focus.

6.5 CHAPTER 5.

6.5.1 Summary

In this chapter, we aimed to explore the potential of lignin containing CNF obtained from hemp hurds waste for barrier and antimicrobial coating. The project was divided into two major focus. The first objective was focused on obtain the CNF from hemp hurds and evaluating their barrier properties. The second objective was focused on studying hemp fibers and extractives for their antimicrobial activity. The defibration of hemp hurds was carried out using low severity to

high severity treatments including autohydrolysis, mild alkaline (4% carbonate) treatment, (Na_2S and NaOH) kraft process and bleached kraft. The low severity treatments, autohydrolysis and carbonate allowed to retain most of the native lignin and active compounds in the fibers. For comparison of hemp with hardwood, the *Eucalyptus* chips were also treated in similar fashion. Among lignin containing fibers the mildly treated fibers (autohydrolyzed and carbonate) were observed to get fibrillated easily compared to the kraft treated fibers. A similar trend was observed for hardwood fibers. However, the bleached fibers consumed much lower energy compared to the lignin containing fibers, which can be related to the higher swellability of bleached nanocellulose. Further, the lignin particles were observed as the globular particles over the CNF surfaces. The distribution of lignin over the CNF film surfaces showed a gradual decrease for carbonate < kraft < bleached CNF for both hemp and *Eucalyptus.* Alternatively, the surface lignin on autohydrolyzed hemp CNF was much lower than carbonate treated fibers. As expected the crystallinity of Eucalyptus CNF films was found to increase with a decrease in lignin content for carbonate < kraft < bleach pretreatments. However, no change in crystallinity among hemp CNF was observed except for autohydrlyzed fibers. The reason for the following was unknown.

The water barrier properties of CNF films and coated paper were evaluated in terms of water contact angle, water absorption and water vapor permeability. For the first time, a water contact angle of 104 ° was reported for the lignin containing CNF. The water contact angles of films and coated paper were largely affected by the surface lignin content. Alternatively, no big difference in the contact angles of carbonate and kraft CNF films and coated paper were observed, which can be explained on the basis that after a certain limit of surface lignin a plateau is reached for surface energy. The water absorption was also observed as lower for lignin containing CNF, however, this could entirely be related to lignin distribution. The water absorption was observed

as more like a bulk phenomenon and found to be dependent on the bulk density of CNF films rather than just on lignin content. A similar trend of correlation of density with water vapor permeability was also observed. However, the air resistance was found be more correlated to the hydrogen bonding between fibers. A decreased amount of lignin was correlated to more hydrogen bonding between fibers, resulting in better air resistance for bleached CNF.

For the second objective, the extractives obtained from differently processed hemp fibers were characterized using gas chromatography and mass spectrometry (GC-MS). Extractives only from untreated hemp-hurd powder showed traces of cannabidiol (CBD). The extractives from other treated fibers did not show any presence of CBD. Extractives from autohydrolyzed hemp fibers were acquainted with many fatty acids and active compounds. However, no significant amount of active compounds were observed in other treated fibers. The antimicrobial activity of hemp extractives and hemp CNF films were analyzed using a disk diffusion assay and a colony forming assay. The paper discs treated with extractives from hemp hurd powder and autohydrolyzed hemp fibers showed a significant reduction in bacterial growth and were observed reducing the bacterial colony forming units by 98% and 55% respectively.

6.5.2 Future Direction

This is a preliminary study on lignin containing hemp nanocellulose being used as barrier and antimicrobial coatings and films. Most of the barrier properties were understood and explained based on the lignin content and distribution. However, it was hard to correlate some of the properties with lignin content. The chemical characterization of differently processed lignin was not carried out, which could provide a better understanding of chemical and structural properties of lignin containing films. *Detailed analysis of any chemical modification in lignin after any differently processed fibers is suggested.*

The extractives from autohydrolyzed fibers also presented a significant inhibition in bacterial growth. However, no traces of CBD were observed in hemp autohydrolyzed extractives. Any further study can be focused on examining the antimicrobial activity of each individually active component from hemp hurds. In the current study it appeared that, it's not only CBD that acts as an antimicrobial agent as other antimicrobially active agents are also present in hemp hurds.

REFERENCES

1. Gustini, L. *et al.* Sustainable coatings from bio-based, enzymatically synthesized polyesters with enhanced functionalities. *Polym. Chem.* **7**, 6586–6597 (2016).
2. Martin Koepenick. Nanotechnology Supports Grade Evolution. *Pulp and paper Canada* (2002).
3. Moon, R. & Frihart, C. Nanotechnology applications in the forest products industry. *For. Prod. J.* 4–10 (2006).
4. Haggith, M. *et al. The State of the Global Paper Industry 2018*. (2018).
5. FAO. *The outlook for pulp and paper to 1995. Paper products, and industrial update', Food and Agricultural Organization of the United Nations*. (1996).
6. *Paper Packaging Market - Segmented by Product Type (2018 - 2023)*. (2018).
7. Miller, J. Nanocellulose: State of the Industry, December, 2015. *TAPPI Nano* 10 (2015).
8. Turbak, A.F.; Snyder, F.W.; Sandberg, K. R. Microfibrillated cellulose, a new cellulose product: properties, uses, and commercial potential. *J. Appl. Polym. Sci* **37**, 815–827 (1983).
9. Hamad, W. On the Development and Applications of Cellulosic Nanofibrillar and Nanocrystalline Materials. *Can. J. Chem. Eng.* **84**, 513–519 (2006).
10. Nasir, M., Hashim, R., Sulaiman, O. & Asim, M. Nanocellulose : Preparation methods and applications. in *Cellulose-Reinforced Nanofibre Composites* 261–276 (Elsevier Ltd, 2017). doi:http://dx.doi.org/10.1016/B978-0-08-100957-4.00011-5
11. Guo, R. *et al.* Collagen-cellulose nanocrystal scaffolds containing curcumin-loaded microspheres on infected full-thickness burns repair. *J. Tissue Eng. Regen. Med.* **11**, 3544–3555 (2017).

12. Alkhatib, Y. *et al.* Controlled extended octenidine release from a bacterial nanocellulose/Poloxamer hybrid system. *Eur. J. Pharm. Biopharm.* **112**, 164–176 (2017).

13. Khalid, A., Khan, R., Ul-Islam, M., Khan, T. & Wahid, F. Bacterial cellulose-zinc oxide nanocomposites as a novel dressing system for burn wounds. *Carbohydr. Polym.* **164**, 214–221 (2017).

14. Halib, N. *et al.* Potential applications of nanocellulose-containing materials in the biomedical field. *Materials (Basel).* **10**, 1–31 (2017).

15. Abraham, E. *et al.* Highly Modified Cellulose Nanocrystals and Formation of Epoxy-Nanocrystalline Cellulose (CNC) Nanocomposites. *ACS Appl. Mater. Interfaces* **8**, 28086–28095 (2016).

16. Aitomäki, Y. & Oksman, K. Reinforcing efficiency of nanocellulose in polymers. *React. Funct. Polym.* **85**, 151–156 (2014).

17. Miao, C. & Hamad, W. Y. Cellulose reinforced polymer composites and nanocomposites: A critical review. *Cellulose* **20**, 2221–2262 (2013).

18. Mondal, S. Preparation, properties and applications of nanocellulosic materials. *Carbohydr. Polym.* **163**, 301–316 (2017).

19. Puceković, N., Hooimeijer, A. & Lozo, B. Cellulose nanocrystals coating – A novel paper coating for use in the graphic industry Authors Abstract : Keywords : **26**, 21–26 (2015).

20. Kumar, V., Elfving, A., Koivula, H., Bousfield, D. & Toivakka, M. Roll-to-Roll Processed Cellulose Nanofiber Coatings. *Ind. Eng. Chem. Res.* **55**, 3603–3613 (2016).

21. Quellmalz, A. & Mihranyan, A. Citric Acid Cross-Linked Nanocellulose-Based Paper for Size-Exclusion Nanofiltration. *ACS Biomater. Sci. Eng.* **1**, 271–276 (2015).

22. Azeredo, H. M. C., Rosa, M. F. & Mattoso, L. H. C. Nanocellulose in bio-based food

packaging applications. *Ind. Crops Prod.* **97**, 664–671 (2017).

23. Hubbe, M. A. *et al.* Nanocellulose in Thin Films, Coatings, and Plies for Packaging Applications: A Review. *BioResources* **12**, 2143–2233 (2017).
24. Herrera, M. A., Mathew, A. P. & Oksman, K. Barrier and mechanical properties of plasticized and cross-linked nanocellulose coatings for paper packaging applications. *Cellulose* **24**, 3969–3980 (2017).
25. Ataide, J. A. *et al.* Bacterial Nanocellulose Loaded with Bromelain: Assessment of Antimicrobial, Antioxidant and Physical-Chemical Properties. *Sci. Rep.* **7**, 2–10 (2017).
26. Salah, S. M. Application of Nano-Cellulose in Textile. *J. Text. Sci. Eng.* **03**, (2013).
27. DP, C. & BH, P. Synthesis, Characterization and Application of Nano Cellulose for Enhanced Performance of Textiles. *J. Text. Sci. Eng.* **06**, (2016).
28. Habibi, Y. Chemical Modification of Nanocelluloses. in *Biopolymer Nanocomposites: Processing,Properties and Applications* (eds. Dufresne, A., Thomas, S. & Pothan, L. A.) 367–390 (John Wiley & Sons, Inc., 2013).
29. Li, F., Mascheroni, E. & Luciano Piergiovanni. The Potential of NanoCellulose in the Packaging Field: A Review By. *Packag. Technol. Sci.* **28**, 475–508 (2015).
30. Mohammad Tajul Islam, Mohammad Mahbubul Alam, M. Z. Review on modification of nanocellulose for application in composites. *Int. J. Innov. Res. Sci.* **2**, 5444–5451 (2014).
31. Peter A. Signoretti. *The Future of Functional and Barrier Coatings for Paper and Board to 2022*. (2017).
32. Schaider, L. A. *et al.* Fluorinated Compounds in U.S. Fast Food Packaging. *Environ. Sci. Technol. Lett.* **4**, 105–111 (2017).
33. Andre, C. M., Hausman, J.-F. & Guerriero, G. Cannabis sativa: The Plant of the Thousand

and One Molecules. *Front. Plant Sci.* **7**, 1–17 (2016).

34. Herrick, F.W., Casebier, R.L., Hamilton, J.K. & Sandberg, K. R. Microfibrillated cellulose: Morphology and accessibility. in *Applied Polymer Symposium* 797-813. (Journal of Applied Polymer Science).

35. Pääkko, M. *et al.* Enzymatic hydrolysis combined with mechanical shearing and high-pressure homogenization for nanoscale cellulose fibrils and strong gels. *Biomacromolecules* **8**, 1934–1941 (2007).

36. Siró, I. & Plackett, D. Microfibrillated cellulose and new nanocomposite materials : a review. *Cellulose* **17**, 459–494 (2010).

37. Eichhorn, S. J. *et al. Review: Current international research into cellulose nanofibres and nanocomposites*. *Journal of Materials Science* **45**, (2010).

38. Saito, T., Kimura, S., Nishiyama, Y. & Isogai, A. Cellulose nanofibers prepared by TEMPO-mediated oxidation of native cellulose. *Biomacromolecules* **8**, 2485–2491 (2007).

39. Lavoine, N., Desloges, I., Dufresne, A. & Bras, J. Microfibrillated cellulose – Its barrier properties and applications in cellulosic materials : A review materials : A review. *Carbohydr. Polym.* **90**, 735–764 (2017).

40. Nechyporchuk, O., Belgacem, M. N. & Pignon, F. Current Progress in Rheology of Cellulose Nanofibril Suspensions. *Biomacromolecules* **17**, 2311–2320 (2016).

41. He, M., Yang, G., Chen, J., Ji, X. & Wang, Q. Production and Characterization of Cellulose Nanofibrils from Different Chemical and Mechanical Pulps. *J. Wood Chem. Technol. ISSN* **32**, 149–158 (2018).

42. Siddiqui, N., Mills, R. H., Gardner, D. J. & Bousfield, D. Production and Characterization

of Cellulose Nanofibers from Wood Pulp. *J. ofAdhesion Sci. Technol. 25* **25**, 709–721 (2011).

43. Jonoobi, M., Khazaeian, A., Tahir, P. M., Azry, S. S. & Oksman, K. Characteristics of cellulose nanofibers isolated from rubberwood and empty fruit bunches of oil palm using chemo-mechanical process. *Cellulose* **18**, 1085–1095 (2011).

44. Jonoobi, M., Harun, J., Shakeri, A., Misra, M. & Oksman, K. Chemical composition, crystallinity, and thermal degradation of bleached and unbleached kenaf bast. *Bioresources* **4**, 626–639 (2009).

45. Wang, B., Sain, M. & Oksman, K. Study of structural morphology of hemp fiber from the micro to the nanoscale. *Appl. Compos. Mater.* **14**, 89–103 (2007).

46. Chen, W. *et al.* Individualization of cellulose nanofibers from wood using high-intensity ultrasonication combined with chemical pretreatments. *Carbohydr. Polym.* **83**, 1804–1811 (2011).

47. Castro, C. *et al.* Bacterial cellulose produced by a new acid-resistant strain of Gluconacetobacter genus. *Carbohydr. Polym.* **89**, 1033–1037 (2012).

48. Hassan, M. L., Mathew, A. P., Hassan, E. A., El-Wakil, N. A. & Oksman, K. Nanofibers from bagasse and rice straw: Process optimization and properties. *Wood Sci. Technol.* **46**, 193–205 (2012).

49. Zuluaga, R. *et al.* Cellulose microfibrils from banana rachis: Effect of alkaline treatments on structural and morphological features. *Carbohydr. Polym.* **76**, 51–59 (2009).

50. Jonoobi, M. *et al.* Characteristics of nanofibers extracted from kenaf core. *BioResources* **5**, 2556–2566 (2010).

51. Cao, X., Ding, B., Yu, J. & Al-Deyab, S. S. Cellulose nanowhiskers extracted from

TEMPO-oxidized jute fibers. *Carbohydr. Polym.* **90**, 1075–1080 (2012).

52. Morais, J. P. S. *et al.* Extraction and characterization of nanocellulose structures from raw cotton linter. *Carbohydr. Polym.* **91**, 229–235 (2013).

53. Lu, P. & Hsieh, Y. Preparation and properties of cellulose nanocrystals : Rods , spheres , and network. *Carbohydr. Polym.* **82**, 329–336 (2010).

54. Tonoli, G. H. D. *et al.* Cellulose micro/nanofibres from Eucalyptus kraft pulp: Preparation and properties. *Carbohydr. Polym.* **89**, 80–88 (2012).

55. Zaini, L. H., Jonoobi, M., Tahir, P. M. & Karimi, S. Isolation and Characterization of Cellulose Whiskers from Kenaf (<i>Hibiscus cannabinus</i> L.) Bast Fibers. *J. Biomater. Nanobiotechnol.* **04**, 37–44 (2013).

56. Beck-candanedo, S., Roman, M. & Gray, D. G. Effect of Reaction Conditions on the Properties and Behavior of Wood Cellulose Nanocrystal Suspensions. *Biomacromolecules* **6**, 1048–1054 (2005).

57. Dong, X. U. E. M. I. N. Effect of microcrystallite preparation conditions on the formation of colloid crystals of cellulose. *Cellulose* **5**, 19–32 (1998).

58. Delgado-Aguilar, M., Tarrés, Q., Pèlach, M. À., Mutjé, P. & Fullana-I-Palmer, P. Are Cellulose Nanofibers a Solution for a More Circular Economy of Paper Products? *Environ. Sci. Technol.* **49**, 12206–12213 (2015).

59. J, A., M, W., S, K. & T., O. Flow properties of microcrystystalline cellulose suspension prepared by acid treatment of native cellulose. *Colloids Surfaces A Physicochem. Eng. Asp.* **142**, 75–82 (1998).

60. Lee, S. Y. *et al.* Nanocellulose reinforced PVA composite films: Effects of acid treatment

and filler loading. *Fibers Polym.* **10**, 77–82 (2009).

61. Zhang, P. P. *et al.* Effects of acid treatments on bamboo cellulose nanocrystals. *Asia-Pac. J. Chem. Eng* **9**, 686–695 (2014).

62. Taniguchi, T. & Okamura, K. New Films Produced from Microfibrillated Natural Fibres. *Polym. Int.* **47**, 291–294 (1998).

63. Ahmed, M., Azizi, S., Alloin, F., Sanchez, J. & Dufresne, A. Cellulose nanocrystals reinforced poly (oxyethylene). *Polymer (Guildf).* **45**, 4149–4157 (2004).

64. Ahola, S., Österberg, M. & Laine, J. Cellulose nanofibrils — adsorption with poly (amideamine) epichlorohydrin studied by QCM-D and application as a paper strength additive. *Cellulose* **15**, 303–314 (2008).

65. Henriksson, M., Berglund, L. A., Isaksson, P. & Lindstrom, T. Cellulose Nanopaper Structures of High Toughness. *Biomacromolecules* **9**, 1579–1585 (2008).

66. Syverud, K. & Stenius, Æ. P. Strength and barrier properties of MFC films. 75–85 (2009). doi:10.1007/s10570-008-9244-2

67. Aulin, C., G??llstedt, M. & Lindstr??m, T. Oxygen and oil barrier properties of microfibrillated cellulose films and coatings. *Cellulose* **17**, 559–574 (2010).

68. Yano, H. *et al.* Optically transparent composites reinforced with networks of bacterial nanofibers. *Adv. Mater.* **17**, 153–155 (2005).

69. Nogi, M., Iwamoto, S., Nakagaito, A. N. & Yano, H. Optically Transparent Nanofiber Paper. *Adv. Mater.* **21**, 1595–1598 (2009).

70. Okahisa, Y., Yoshida, A., Miyaguchi, S. & Yano, H. Optically transparent wood-cellulose nanocomposite as a base substrate for flexible organic light-emitting diode displays. *Compos. Sci. Technol.* **69**, 1958–1961 (2009).

71. Kettunen, M. *et al.* Photoswitchable superabsorbency based on nanocellulose aerogels. *Adv. Funct. Mater.* **21**, 510–517 (2011).

72. Korhonen, J. T., Kettunen, M., Ras, R. H. A. & Ikkala, O. Hydrophobic nanocellulose aerogels as floating, sustainable, reusable, and recyclable oil absorbents. *ACS Appl. Mater. Interfaces* **3**, 1813–1816 (2011).

73. Beck, S., Bouchard, J. & Berry, R. Controlling the reflection wavelength of iridescent solid films of nanocrystalline cellulose. *Biomacromolecules* **12**, 167–172 (2011).

74. Rastogi, V. & Samyn, P. Bio-Based Coatings for Paper Applications. *Coatings* **5**, 887–930 (2015).

75. Aulin, C., Gällstedt, M. & Lindström, T. Oxygen and oil barrier properties of microfibrillated cellulose films and coatings. *Cellulose* **17**, 559–574 (2010).

76. Aulin, C. & Ström, G. Multilayered alkyd resin/nanocellulose coatings for use in renewable packaging solutions with a high level of moisture resistance. *Ind. Eng. Chem. Res.* **52**, 2582–2589 (2013).

77. Rastogi, V. K., Samyn, P. & Resources, N. Bio-Based Coatings for Paper Applications. 887–930 (2015). doi:10.3390/coatings5040887

78. Zhang, H. *et al.* A robust superhydrophobic TiO2NPs coated cellulose sponge for highly efficient oil-water separation. *Nat. Sci. Reports* **7**, 3–10 (2017).

79. Ansari, F., Ding, Y., Berglund, L. A. & Dauskardt, R. H. Toward Sustainable Multifunctional Coatings Containing Nanocellulose in a Hybrid Glass Matrix. *ACS Nano* **12**, 5495–5503 (2018).

80. Teisala, H., Tuominen, M. & Kuusipalo, J. Superhydrophobic Coatings on Cellulose-Based Materials: Fabrication, Properties, and Applications. *Adv. Mater. Interfaces* **1**, 1–20

(2014).

81. Tang, Q., Pan, D., Sun, Y., Cao, J. & Guo, Y. Preparation, Characterization and Antimicrobial Activity of Sodium Alginate Nanobiocomposite Films Incorporated with E-Polylysine and Cellulose Nanocrystals. *J. Food Process. Preserv.* **41**, (2017).

82. Jebali, A. *et al.* Antimicrobial activity of nanocellulose conjugated with allicin and lysozyme. *Cellulose* **20**, 2897–2907 (2013).

83. Tang, J. *et al.* Polyrhodanine Coated Cellulose Nanocrystals: A Sustainable Antimicrobial Agent. *ACS Sustain. Chem. Eng.* **3**, 1801–1809 (2015).

84. Sundaram, J., Pant, J., Goudie, M. J., Mani, S. & Handa, H. Antimicrobial and Physicochemical Characterization of Biodegradable, Nitric Oxide-Releasing Nanocellulose-Chitosan Packaging Membranes. *J. Agric. Food Chem.* **64**, 5260–5266 (2016).

85. Iglesias, M. C. Lignin-containing cellulose nanofibrils (LCNF): processing and characterization. (Auburn University, 2018).

86. Wang, X., Jia, Y., Liu, Z. & Miao, J. Influence of the lignin content on the properties of poly(lactic acid)/lignin-containing cellulose nanofibrils composite films. *Polymers (Basel).* **10**, (2018).

87. Peng, Y., Nair, S. S., Chen, H., Yan, N. & Cao, J. Effects of Lignin Content on Mechanical and Thermal Properties of Polypropylene Composites Reinforced with Micro Particles of Spray Dried Cellulose Nanofibrils. *ACS Sustain. Chem. Eng.* **6**, 11078–11086 (2018).

88. Lê, H. Q., Dimic-Misic, K., Johansson, L.-S., Maloney, T. & Sixta, H. Effect of lignin on the morphology and rheological properties of nanofibrillated cellulose produced from γ-

valerolactone/water fractionation process. *Cellulose* **25**, 179–194 (2018).

89. Herrera, M. *et al.* Preparation and evaluation of high-lignin content cellulose nanofibrils from eucalyptus pulp. *Cellulose* **25**, 3121–3133 (2018).

90. Osong, S. H., Norgren, S. & Engstrand, P. Processing of wood-based microfibrillated cellulose and nanofibrillated cellulose, and applications relating to papermaking: a review. *Cellulose* **23**, 93–123 (2016).

91. Bian, H., Chen, L., Dai, H. & Zhu, J. Y. Integrated production of lignin containing cellulose nanocrystals (LCNC) and nanofibrils (LCNF) using an easily recyclable di-carboxylic acid. *Carbohydr. Polym.* **167**, 167–176 (2017).

92. Wei, L., Agarwal, U. P., Matuana, L., Sabo, R. C. & Stark, N. M. Performance of high lignin content cellulose nanocrystals in poly(lactic acid). *Polymer (Guildf).* **135**, 305–313 (2018).

93. Agarwal, U. P. *et al.* Production of high lignin-containing and lignin-free cellulose nanocrystals from wood. *Cellulose* **25**, 5791–5805 (2018).

94. Rojo, E. *et al.* Comprehensive elucidation of the effect of residual lignin on the physical, barrier, mechanical and surface properties of nanocellulose films. *Green Chem.* **17**, 1853–1866 (2015).

95. Hubbe, Ma. A. Prospects for Maintaining Strength of Paper and Paperboard Products While Using Less Forest Resources: A Review. *BioResources* **9**, 1–130 (2014).

96. Przybysz, P., Dubowik, M., Kucner, M. A., Przybysz, K. & Buzała, K. P. Contribution of hydrogen bonds to paper strength properties. *PLoS One* **11**, 1–10 (2016).

97. Leonard, M. Gas Barrier Coatings For Flexible Packaging. in *Aimcal Europe Web Coating Conference* (Aimcal Europe Web Coating Conference, 2012).

98. Siracusa, V. Food packaging permeability behaviour: A report. *Int. J. Polym. Sci.* **2012**, (2012).

99. Gajdoš, J., Galić, K., Kurtanjek, Ž. & Ciković, N. Gas permeability and DSC characteristics of polymers used in food packaging. *Polym. Test.* **20**, 49–57 (2000).

100. Kofinas, P., Cohen, R. E. & Halasa, A. F. Gas permeability of polyethylene/poly(ethylene-propylene) semicrystalline diblock copolymers. *Polymer (Guildf).* **35**, 1229–1235 (1994).

101. Pilar, F. L. The Flow of Gases Through High Polymer Films in Equilibrium with Sorbed Vapors. *J. Polym. Sci.* **XLV**, 205–215 (1960).

102. Bae, J. & Yang, Y. Thiol-ene/hyperbranched polymer hybrid thin films: Cure behavior and gas barrier properties. *J. Non. Cryst. Solids* **357**, 3103–3107 (2011).

103. Ferrer, A., Pal, L. & Hubbe, M. Nanocellulose in packaging: Advances in barrier layer technologies. *Industrial Crops and Products* **95**, (2017).

104. Wu, C. N., Saito, T., Fujisawa, S., Fukuzumi, H. & Isogai, A. Ultrastrong and high gas-barrier nanocellulose/clay-layered composites. *Biomacromolecules* **13**, 1927–1932 (2012).

105. Österberg, M. *et al.* A fast method to produce strong NFC films as a platform for barrier and functional materials. *ACS Appl. Mater. Interfaces* **5**, 4640–4647 (2013).

106. Sharma, S., Zhang, X., Nair, S. S. & Ragauskas, A. RSC Advances Thermally enhanced high performance cellulose nano fi bril barrier membranes. *RSC Adv.* **4**, 45136–45142 (2014).

107. Rodionova, G. & Lenes, M. Surface chemical modification of microfibrillated cellulose : improvement of barrier properties for packaging applications. 127–134 (2011). doi:10.1007/s10570-010-9474-y

108. Saxena, A., Elder, T. J. & Ragauskas, A. J. Moisture barrier properties of xylan composite films. *Carbohydr. Polym.* **84**, 1371–1377 (2011).

109. Luís, A. *et al.* Improvement of polyvinyl alcohol properties by adding nanocrystalline cellulose isolated from banana pseudostems. *Carbohydr. Polym.* **112**, 165–172 (2014).

110. Belbekhouche, S. *et al.* Water sorption behavior and gas barrier properties of cellulose whiskers and microfibrils films. *Carbohydr. Polym.* **83**, 1740–1748 (2011).

111. Hirschfelder, J. O., Byron Bird, R. & Spotz, E. L. The transport properties for non-polar gases. *J. Chem. Phys.* **16**, 968–981 (1948).

112. Alkhadra, M. A. *et al.* Quantifying the Fracture Behavior of Brittle and Ductile Thin Films of Semiconducting Polymers. *Chem. Mater.* **29**, 10139–10149 (2017).

113. Kim, J. H., Kim, Y. G., Lee, H. K. & Kim, D. K. Characterization of Mechanical Properties of Brittle Coating Systems by Various Indentation Techniques. *Key Eng. Mater.* **352**, 53–58 (2007).

114. Kisonen, V. *et al.* Composite films of nanofibrillated cellulose and O-acetyl galactoglucomannan (GGM) coated with succinic esters of GGM showing potential as barrier material in food packaging. *J. Mater. Sci.* **50**, 3189–3199 (2015).

115. Nair, S. S., Zhu, J., Deng, Y. & Ragauskas, A. J. High performance green barriers based on nanocellulose. *Sustain. Chem. Process.* **2**, 1–7 (2014).

116. Raynaud, S. Development of new barrier materials using microfibrillated cellulose To cite this version : HAL Id : tel-01796806 Développement de nouveaux matériaux barrières utilisant des microfibrilles de cellulose. (Université Grenoble Alpes, 2018).

117. Matikainen, L. Nanocellulose as barrier coating deposited by a laboratory rod coater. *Aalto University* (Aalto University, 2017).

118. Choi, C. H. & Kim, C. J. Large slip of aqueous liquid flow over a nanoengineered superhydrophobic surface. *Phys. Rev. Lett.* **96**, 1–4 (2006).

119. Chinga-Carrasco, G. & Syverud, K. On the structure and oxygen transmission rate of biodegradable cellulose nanobarriers. *Nanoscale Res. Lett.* **7**, 192 (2012).

120. Yang, Q., Saito, T. & Isogai, A. Facile fabrication of transparent cellulose films with high water repellency and gas barrier properties. *Cellulose* **19**, 1913–1921 (2012).

121. Follain, N. *et al.* Water transport properties of bio-nanocomposites reinforced by Luffa cylindrica cellulose nanocrystals. *J. Memb. Sci.* **427**, 218–229 (2013).

122. Shimizu, M., Saito, T. & Isogai, A. Water-resistant and high oxygen-barrier nanocellulose films with interfibrillar cross-linkages formed through multivalent metal ions. *J. Memb. Sci.* **500**, 1–7 (2016).

123. Song, Z., Xiao, H. & Zhao, Y. Hydrophobic-modified nano-cellulose fiber/PLA biodegradable composites for lowering water vapor transmission rate (WVTR) of paper. *Carbohydr. Polym.* **111**, 442–448 (2014).

124. Khan, R. A. *et al.* Production and properties of nanocellulose-reinforced methylcellulose-based biodegradable films. *J. Agric. Food Chem.* **58**, 7878–7885 (2010).

125. Aulin, C. *et al.* Nanoscale cellulose films with different crystallinities and mesostructures - Their surface properties and interaction with water. *Langmuir* **25**, 7675–7685 (2009).

126. Sacui, I. A. *et al.* Comparison of the properties of cellulose nanocrystals and cellulose nanofibrils isolated from bacteria, tunicate, and wood processed using acid, enzymatic, mechanical, and oxidative methods. *ACS Appl. Mater. Interfaces* **6**, 6127–6138 (2014).

127. Spence, K. L., Venditti, R. A., Rojas, O. J., Habibi, Y. & Pawlak, J. J. The effect of chemical composition on microfibrillar cellulose films from wood pulps: Water

interactions and physical properties for packaging applications. *Cellulose* **17**, 835–848 (2010).

128. Minelli, M. *et al.* Investigation of mass transport properties of microfibrillated cellulose (MFC) films. *J. Memb. Sci.* **358**, 67–75 (2010).

129. Rodionova, G., Hoff, B., Lenes, M., Eriksen, Ø. & Gregersen, Ø. Gas-phase esterification of microfibrillated cellulose (MFC) films. *Cellulose* **20**, 1167–1174 (2013).

130. Fukuzumi, H., Saito, T., Iwata, T., Kumamoto, Y. & Isogai, A. Transparent and High Gas Barrier Films of Cellulose Nanofibers Prepared by TEMPO-Mediated Oxidation Transparent and High Gas Barrier Films of Cellulose Nanofibers Prepared by TEMPO-Mediated Oxidation. 162–165 (2009). doi:10.1021/bm801065u

131. Pereda, M., Dufresne, A., Aranguren, M. I. & Marcovich, N. E. Polyelectrolyte films based on chitosan/olive oil and reinforced with cellulose nanocrystals. *Carbohydr. Polym.* **101**, 1018–1026 (2014).

132. Visanko, M. *et al.* Butylamino-functionalized cellulose nanocrystal films: Barrier properties and mechanical strength. *RSC Adv.* **5**, 15140–15146 (2015).

133. Lindström, T. Aspects on nanofibrillated cellulose (NFC) processing, rheology and NFC-film properties. *Curr. Opin. Colloid Interface Sci.* **29**, 68–75 (2017).

134. Iwamoto, S., Abe, K. & Yano, H. The Effect of Hemicelluloses on Wood Pulp Nanofibrillation and Nanofiber Network Characteristics The Effect of Hemicelluloses on Wood Pulp Nanofibrillation and Nanofiber Network Characteristics. *Scan. Electron Microsc.* 1022–1026 (2008). doi:10.1021/bm701157n

135. Plackett, D. *et al.* Physical properties and morphology of films prepared from microfibrillated cellulose and microfibrillated cellulose in combination with amylopectin.

J. Appl. Polym. Sci. **117**, 3601–3609 (2010).

136. Spence, K. L., Venditti, R. A., Rojas, O. J., Habibi, Y. & Pawlak, J. J. A comparative study of energy consumption and physical properties of microfibrillated cellulose produced by different processing methods. *Cellulose* **18**, 1097–1111 (2011).

137. Dufresne, A., Cavaille, J.-Y. & Vignon, M. R. Mechanical behavior of sheets prepared from sugar beet cellulose microfibrils. *J. Appl. Polym. Sci.* **64**, 1185–1194 (1997).

138. Qing, Y. *et al.* A comparative study of cellulose nanofibrils disintegrated via multiple processing approaches. *Carbohydr. Polym.* **97**, 226–234 (2013).

139. Siró, I., Plackett, D., Hedenqvist, M., Ankerfors, M. & Lindström, T. Highly transparent films from carboxymethylated microfibrillated cellulose: The effect of multiple homogenization steps on key properties. *J. Appl. Polym. Sci.* **119**, 2652–2660 (2011).

140. Asadi, A., Miller, M., Moon, R. J. & Kalaitzidou, K. Improving the interfacial and mechanical properties of short glass fiber/epoxy composites by coating the glass fibers with cellulose nanocrystals. *Express Polym. Lett.* **10**, 587–597 (2016).

141. Kaboorani, A., Auclair, N., Riedl, B. & Landry, V. Mechanical properties of UV-cured cellulose nanocrystal (CNC) nanocomposite coating for wood furniture. *Prog. Org. Coatings* **104**, 91–96 (2017).

142. Varanasi, S. & Batchelor, W. J. Rapid preparation of cellulose nanofibre sheet. *Cellulose* **20**, 211–215 (2013).

143. Sehaqui, H., Liu, A., Zhou, Q. & Berglund, L. A. Fast preparation procedure for large, flat cellulose and cellulose/inorganic nanopaper structures. *Biomacromolecules* **11**, 2195–2198 (2010).

144. Baez, C., Considine, J. & Rowlands, R. Influence of drying restraint on physical and

mechanical properties of nanofibrillated cellulose films. *Cellulose* **21**, 347–356 (2014).

145. Benítez, A. J. & Walther, A. Cellulose nanofibril nanopapers and bioinspired nanocomposites: A review to understand the mechanical property space. *J. Mater. Chem. A* **5**, 16003–16024 (2017).

146. GILL, U. Mechanical Properties of Cellulose Nanocrystal Thin Films. (McMaster University –, 2017).

147. Nishino, T., Takano, K. & Nakamae, K. Elastic modulus of the crystalline regions of cellulose polymorphs. *J. Polym. Sci. Part B Polym. Phys.* **33**, 1647–1651 (1995).

148. Moon, R. J., Martini, A., Nairn, J., Simonsen, J. & Youngblood, J. *Cellulose nanomaterials review: Structure, properties and nanocomposites*. *Chemical Society Reviews* **40**, (2011).

149. Azizi, S. & Mohamad, R. Mechanical and barrier properties of kappa-carrageenan/cellulose nanocrystals bio-nanocomposite films. in *IOP Conference Series: Materials Science and Engineering* **368**, (2018).

150. Martins, I. M. G. *et al.* New biocomposites based on thermoplastic starch and bacterial cellulose. *Compos. Sci. Technol.* **69**, 2163–2168 (2009).

151. Pereda, M., Amica, G., Rácz, I. & Marcovich, N. E. Structure and properties of nanocomposite films based on sodium caseinate and nanocellulose fibers. *J. Food Eng.* **103**, 76–83 (2011).

152. Rafieian, F. & Simonsen, J. Fabrication and characterization of carboxylated cellulose nanocrystals reinforced glutenin nanocomposite. *Cellulose* **21**, 4167–4180 (2014).

153. Santos, T. M. *et al.* Fish gelatin films as affected by cellulose whiskers and sonication. *Food Hydrocoll.* **41**, 113–118 (2014).

154. Anglès, M. N. & Dufresne, A. Plasticized Starch/Tunicin Whiskers Nanocomposites. 1. Structural Analysis. *Macromolecules* **33**, 8344–8353 (2000).

155. López-Rubio, A. *et al.* Enhanced film forming and film properties of amylopectin using micro-fibrillated cellulose. *Carbohydr. Polym.* **68**, 718–727 (2007).

156. Mikkonen, K. S. *et al.* Composite films from spruce galactoglucomannans with microfibrillated spruce wood cellulose. *Cellulose* **18**, 713–726 (2011).

157. Abdul Khalil, H. P. S. *et al.* A review on chitosan-cellulose blends and nanocellulose reinforced chitosan biocomposites: Properties and their applications. *Carbohydr. Polym.* **150**, 216–226 (2016).

158. Zhao, S.-W., Guo, C.-R., Hu, Y.-Z., Guo, Y.-R. & Pan, Q.-J. The preparation and antibacterial activity of cellulose/ZnO composite: a review. *Open Chem-y Gruyter* **16**, 9–20 (2018).

159. Bideau, B., Bras, J., Saini, S., Daneault, C. & Loranger, E. Mechanical and antibacterial properties of a nanocellulose-polypyrrole multilayer composite. *Mater. Sci. Eng. C* **69**, 977–984 (2016).

160. Liyaskina, E. *et al.* Nanomaterials from bacterial cellulose for antimicrobial wound dressing. in *International Symposium Physics, Engineering and Technologies for Bio-Medicine* **784**, (IOP Publishing, 2017).

161. Nguyen, H. L. *et al.* Mussel-inspired anisotropic nanocellulose and silver nanoparticle composite with improved mechanical properties, electrical conductivity and antibacterial activity. *Polymers (Basel).* **8**, 1–13 (2016).

162. Angelova, T., Rangelova, N., Dineva, H., Georgieva, N. & Müller, R. Synthesis, Characterization and antibacterial assessment of sio2-hydroxypropylmethyl cellulose

hybrid materials with embedded silver nanoparticles. *Biotechnol. Biotechnol. Equip.* **28**, 747–752 (2014).

163. Barud, H. S. *et al.* Antimicrobial bacterial cellulose-silver nanoparticles composite membranes. *J. Nanomater.* **2011**, (2011).

164. Jafary, R., Khajeh Mehrizi, M., Hekmatimoghaddam, S. hossein & Jebali, A. Antibacterial property of cellulose fabric finished by allicin-conjugated nanocellulose. *J. Text. Inst.* **106**, 683–689 (2015).

165. Zhang, P., Chen, L., Zhang, Q. & Hong, F. F. Using in situ dynamic cultures to rapidly biofabricate fabric-reinforced composites of chitosan/bacterial nanocellulose for antibacterial wound dressings. *Front. Microbiol.* **7**, 1–15 (2016).

166. Saini, S. *et al.* Nisin anchored cellulose nanofibers for long term antimicrobial active food packaging. *Rsc Adv.* **6**, 12437–12445 (2016).

167. Andresen, M. *et al.* Nonleaching antimicrobial films prepared from surface-modified microfibrillated cellulose. *Biomacromolecules* **8**, 2149–2155 (2007).

168. Dobre, L. M. *et al.* Modelling of sorbic acid diffusion through bacterial cellulose-based antimicrobial films. *Chem. Pap.* **66**, 144–151 (2012).

169. Lago, M. A. *et al.* Preparation and Characterization of Antimicrobial Films Based on Chitosan for Active Food Packaging Applications. *Food Bioprocess Technol.* **7**, 2932–2941 (2014).

170. Dehnad, D., Emam-Djomeh, Z., Mirzaei, H., Jafari, S. M. & Dadashi, S. Optimization of physical and mechanical properties for chitosan- nanocellulose biocomposites. *Carbohydr. Polym.* **105**, 222–228 (2014).

171. Amini, E., Azadfallah, M., Layeghi, M. & Talaei-Hassanloui, R. Silver-nanoparticle-

impregnated cellulose nanofiber coating for packaging paper. *Cellulose* **23**, 557–570 (2016).

172. Beyth, N., Houri-haddad, Y., Domb, A., Khan, W. & Hazan, R. Alternative Antimicrobial Approach : Nano-Antimicrobial Materials. **2015**, 16 (2015).

173. Pelgrift, R. Y. & Friedman, A. J. Nanotechnology as a therapeutic tool to combat microbial resistance. *Adv. Drug Deliv. Rev.* **65**, 1803–1815 (2013).

174. Huh, A. J. & Kwon, Y. J. 'Nanoantibiotics': A new paradigm for treating infectious diseases using nanomaterials in the antibiotics resistant era. *J. Control. Release* **156**, 128–145 (2011).

175. Blecher, K., Nasir, A. & Friedman, A. The growing role of nanotechnology in combating infectious disease. *Virulence* **2**, 395–401 (2011).

176. Some, S. *et al.* Biosynthesis of silver nanoparticles and their versatile antimicrobial properties. *Mater. Res. Express* **6**, 012001 (2018).

177. Palanikumar, L., Ramasamy, S. N. & Balachandran, C. Size-dependent antimicrobial response of zinc oxide nanoparticles. *IET Nanobiotechnology* **8**, 111–117 (2014).

178. Ren, G. *et al.* Characterisation of copper oxide nanoparticles for antimicrobial applications. *Int. J. Antimicrob. Agents* **33**, 587–590 (2009).

179. Gherardi, F., Roveri, M., Goidanich, S. & Toniolo, L. Photocatalytic nanocomposites for the protection of European architectural heritage. *Materials (Basel).* **11**, 1–15 (2018).

180. MANESS, P.-C. *et al.* Bactericidal Activity of Photocatalytic TiO2 Reaction: toward an Understanding of Its Killing Mechanism. *Appl. Environ. Microbiol.* **65**, 4094–4098 (1999).

181. Chung, Y. C., Wang, H. L., Chen, Y. M. & Li, S. L. Effect of abiotic factors on the

antibacterial activity of chitosan against waterborne pathogens. *Bioresour. Technol.* **88**, 179–184 (2003).

182. Tavaria, F. K., Costa, E. M., Gens, E. J., Malcata, F. X. & Pintado, M. E. Influence of abiotic factors on the antimicrobial activity of chitosan. *J. Dermatol.* **40**, 1014–1019 (2013).

183. Ibrahim, M. *et al.* Deciphering the role of Burkholderia cenocepacia membrane proteins in antimicrobial properties of chitosan. *Arch. Microbiol.* **196**, 9–16 (2014).

184. Abdulkhani, A., Hosseinzadeh, J., Ashori, A. & Esmaeeli, H. Evaluation of the Antibacterial Activity of Cellulose Nanofibers/Polylactic Acid Composites Coated With Ethanolic Extract of Propolis. *Polym. Compos.* 13–19 (2017). doi:10.1002/pc.23554

185. Foong, C. Y., Hamzah, M. S. A., Razak, S. I. A., Saidin, S. & Nayan, N. H. M. Influence of Poly(lactic acid) Layer on the Physical and Antibacterial Properties of Dry Bacterial Cellulose Sheet for Potential Acute Wound Healing Materials. *Fibers Polym.* **19**, 263–271 (2018).

186. Lavoine, N., Desloges, I. & Bras, J. Microfibrillated cellulose coatings as new release systems for active packaging. *Carbohydr. Polym.* **103**, 528–537 (2014).

187. Lavoine, N., Tabary, N., Desloges, I., Martel, B. & Bras, J. Controlled release of chlorhexidine digluconate using β-cyclodextrin and microfibrillated cellulose. *Colloids Surfaces B Biointerfaces* **121**, 196–205 (2014).

188. Lavoine, N. *et al.* Elaboration of a new antibacterial bio-nano-material for food-packaging by synergistic action of cyclodextrin and microfibrillated cellulose. *Innov. Food Sci. Emerg. Technol.* **26**, 330–340 (2014).

189. Lavoine, N., Desloges, I., Manship, B. & Bras, J. Antibacterial paperboard packaging

using microfibrillated cellulose. *J. Food Sci. Technol.* **52**, 5590–5600 (2015).

190. Lavoine, N., Desloges, I., Sillard, C. & Bras, J. Controlled release and long-term antibacterial activity of chlorhexidine digluconate through the nanoporous network of microfibrillated cellulose. *Cellulose* **21**, 4429–4442 (2014).

191. Tsai, T. T. *et al.* Antibacterial cellulose paper made with silver-coated gold nanoparticles. *Sci. Rep.* **7**, 1–10 (2017).

192. Pasquale, J. A. & President, S. V. An in-depth look at reverse roll coating. *New era converting machinery, Inc.* Available at: https://www.aimcal.org/uploads/4/6/6/9/46695933/pasquale_pres.pdf.

193. Wu, L. *et al.* Dip-Coating Process Engineering and Performance Optimization for Three-State Electrochromic Devices. *Nanoscale Res. Lett.* **12**, (2017).

194. Kapur, N. *et al.* A Review of Gravure Coating Systems. *Convert. e-Print* **1**, 56–60 (2011).

195. Tripathi, P. Stabilization of Curtain Coater at High Speeds. (Western Michigan University, 2005).

196. Kugge, C. Consolidation and Structure of Paper Coating and Fibre Systems. (Institute for Surface Chemistry, YKI and KTH, Valhallavagen, 2003).

197. Nazari-Nasrabad, B. NEW APPLICATIONS FOR CELLULOSE NANOFIBERS: RHEOLOGICAL CHALLENGES. (The University of Maine, 2015). doi:ProQuest 10096039 Published

198. Hamada, H., Beckvermit, J. & Bousfield, D. W. Nanofibrillated Cellulose with Fine Clay as a Coating Agent to Improve Print Quality. in *PaperCon 2010 Conference* 1–27 (TAPPI, 2010). doi:http://imisrise.tappi.org/TAPPI/Products/10/PAP/10PAP39.aspx

199. Hamada, H., and Bousfield, D. W. Nano-fibrillated cellulose as a coating agent to improve

print quality of synthetic fiber sheets. in *TAPPI 11th Advanced Coating Fundamentals Symposium, October* 11–13 (TAPPI PRESS, 2010).

200. Hamada, H., Tahara, K., Bousfield, D. W. The effects of nanofibrillated cellulose as a coating agent for screen printing. in *TAPPI Advanced Coating Fundamentals Symposium*, (TAPPI PRESS, 2012).

201. Luu, W. T., Bousfield, D. W., Kettle, J. Application of nanofibrillated cellulose as a paper surface treatment for inkjet printing. in *TAPPI Paper Conference and Trade Show* (2011).

202. BALAN, T., GUEZENNEC, C., NICU, R., CIOLACU, F. & BOBU, E. IMPROVING BARRIER AND STRENGTH PROPERTIES OF PAPER BY MULTI-LAYER COATING WITH BIO-BASED ADDITIVES. *Cellul. Chem. Technol.* **49**, 607–615 (2015).

203. Afra, E., Mohammadnejad, S. & Saraeyan, A. Progress in Organic Coatings Cellulose nanofibils as coating material and its effects on paper properties. *Prog. Org. Coatings* **101**, 455–460 (2016).

204. Mousavi, S. M. M., Afra, E., Tajvidi, M. & Bousfield, D. W. Cellulose nanofiber / carboxymethyl cellulose blends as an efficient coating to improve the structure and barrier properties of paperboard. *Cellulose* **24**, 3001–3014 (2017).

205. Li, L., Yunzhi, C. & Zhengjian, Z. Preparation of the Microfibrillated Cellulose and Its Application in the Food Packaging Paper. *Appl. Mech. Mater.* **469**, 87–90 (2014).

206. Lavoine, N., Desloges, I., Khelifi, B. & Bras, J. Impact of different coating processes of microfibrillated cellulose on the mechanical and barrier properties of paper. *J. Mater. Sci.* **49**, 2879–2893 (2014).

207. Boissard, Y. MFC for paper surface treatment. (Luleå University of Technology, 2017).

208. Richmond, F. Cellulose Nanofibers Use in Coated Paper. *Electronic Theses and Dissertations* **2242**, (The University of Maine, 2014).

209. Kinnunen-raudaskoski, Hjelt, T., Kentta, E. & ForsstrÖm, U. Thin coatings for paper by foam coating. *Tappi J.* **13**, (2014).

210. Beneventi, D. *et al.* Highly Porous Paper Loading with Micro fi brillated Cellulose by Spray Coating on Wet Substrates. *Ind. Eng. Chem. Res.* **53**, 10982−10989 (2014).

211. Quested, T. E., Parry, A. D., Easteal, S. & Swannell, R. N E W S A N D VI E W S Food and drink waste from households in the UK. 460–467 (2011). doi:10.1111/j.1467-3010.2011.01924.x

212. Wikström, B. F. & Williams, H. Potential Environmental Gains from Reducing Food Losses Through Development of New Packaging – A Life-Cycle Model. 403–411 (2010). doi:10.1002/pts

213. Syverud, G. C. Æ. K. Computer-assisted quantification of the multi-scale structure of films made of nanofibrillated cellulose. 841–851 (2010). doi:10.1007/s11051-009-9710-2

214. Eichhorn, S. J. Cellulose nanowhiskers : promising materials for advanced applications. 303–315 (2011). doi:10.1039/c0sm00142b

215. Elazzouzi-hafraoui, S. *et al.* The Shape and Size Distribution of Crystalline Nanoparticles Prepared by Acid Hydrolysis of Native Cellulose. 57–65 (2008).

216. Kjellgren, H., Paper, N., Ab, S. & Engström, G. Paper and paper coating performance chemicals Influence of base paper on the barrier properties of chitosan-coated papers. **21**, 685–689 (2006).

217. Liu, X., Pang, J., Zhang, X., Wu, Y. & Sun, R. Regenerated cellulose film with enhanced tensile strength prepared with ionic liquid 1-ethyl-3-methylimidazolium acetate

(EMIMAc). *Cellulose* **20**, 1391–1399 (2013).

218. Mathew, A. P., Thielemans, W. & Dufresne, A. Mechanical Properties of Nanocomposites from Sorbitol Plasticized Starch and Tunicin Whiskers. (2008). doi:10.1002/app

219. Saxena, A., Elder, T. J. & Ragauskas, A. J. Moisture barrier properties of xylan composite films. *Carbohydr. Polym.* **84**, 1371–1377 (2011).

220. Luís, A. *et al.* Improvement of polyvinyl alcohol properties by adding nanocrystalline cellulose isolated from banana pseudostems. *Carbohydr. Polym.* **112**, 165–172 (2014).

221. Belbekhouche, S. *et al.* Water sorption behavior and gas barrier properties of cellulose whiskers and microfibrils films. *Carbohydr. Polym.* **83**, 1740–1748 (2011).

222. Lu, P. & Hsieh, Y. Lo. Preparation and properties of cellulose nanocrystals: Rods, spheres, and network. *Carbohydr. Polym.* **82**, 329–336 (2010).

223. Christiab Aulin, Erdem Karabulut, A. T. Transparent Nanocellulosic Multilayer Thin Films on olylactic Acid with Tunable Gas Barrier Properties. *Acs* **5**, 7352–7359 (2013).

224. Sharma, S., Zhang, X., Nair, S. S. & Ragauskas, A. RSC Advances Thermally enhanced high performance cellulose nano fi bril barrier membranes. *RSC Adv.* **4**, 45136–45142 (2014).

225. Yu, H. & Yao, J. RSC Advances Fully biodegradable food packaging materials based on functionalized cellulose nanocrystals /. *RSC Adv.* **4**, 59792–59802 (2014).

226. Bardet, R. *et al.* Substitution of nanoclay in high gas barrier films of cellulose nanofibrils with cellulose nanocrystals and thermal treatment. *Cellulose* **22**, 1227–1241 (2015).

227. Khan, A. *et al.* Mechanical and barrier properties of nanocrystalline cellulose reinforced chitosan based nanocomposite films. *Carbohydr. Polym.* **90**, 1601–1608 (2012).

228. Yang, H., Tejado, A., Alam, N. & Antal, M. Films Prepared from Electrosterically

Stabilized Nanocrystalline Cellulose. (2012). doi:10.1021/la2049663

229. Groen, J. & Ahlroos, J. Influence of Base Paper Filler Content and Pre-calendering on Metered Film Press Coating - Part I : A Coating Process Study. in *TAPPI 1998 Coating and papermakers conference proceedings* 899 (TAPPI PRESS, 1998).

230. Pal, L., Joyce, M. K., Fleming, P. D., Cretté, S. A. & Ruffner, C. High barrier sustainable co-polymerized coatings. *J. Coatings Technol. Res.* **5**, 479–489 (2008).

231. Katti, K. & Katti, D. Effect Of Clay-Water Interactions On Swelling In Montmorillonite Clay. 1–9 (2001). doi:https://www.researchgate.net/publication/242072574_Effect_Of_Clay-Water_Interactions_On_Swelling_In_Montmorillonite_Clay

232. Hubbe, M. A. Puzzling Aspects of the Hydrophobic Sizing of Paper and its Inter-Fiber Bonding Ability. *BioResources* **9**, 5782–5783 (2014).

233. Mohtaschemi, M. *et al.* Rheological characterization of fibrillated cellulose suspensions via bucket vane viscometer. *Cellulose* **21**, 1305–1312 (2014).

234. Salo, T., Dimic-misic, K., Gane, P. & Paltakari, J. Application of pigmented coating colours containing MFC / NFC : Coating properties and link to rheology. **30**, (2015).

235. Hubbe, M. A. *et al.* Rheology of nanocellulose-rich aqueous suspensions: A review. *BioResources* **12**, 9556–9661 (2017).

236. Pei, A., Zhou, Q. & Berglund, L. A. Functionalized cellulose nanocrystals as biobased nucleation agents in poly (L -lactide) (PLLA) – Crystallization and mechanical property effects. *Compos. Sci. Technol.* **70**, 815–821 (2010).

237. Ciannamea, E. M., Stefani, P. M. & Ruseckaite, R. A. Food Hydrocolloids Physical and mechanical properties of compression molded and solution casting soybean protein

concentrate based fi lms. *Food Hydrocoll.* **38**, 193–204 (2014).

238. Zhang, S. *et al.* Soy protein isolate-based films reinforced by surface modified cellulose nanocrystal. *Ind. Crops Prod.* **80**, 207–213 (2016).

239. Saikia, B. J. & Parthasarathy, G. Fourier Transform Infrared Spectroscopic Characterization of Kaolinite from Assam and Meghalaya, Northeastern India. *J. Mod. Phys.* **2010**, 206–210 (2010).

240. Tyagi, B., Chudasama, C. D. & Jasra, R. V. Determination of structural modification in acid activated montmorillonite clay by FT-IR spectroscopy. **64**, 273–278 (2006).

241. Bildik, A. E., Hubbe, M. A. & Gürboy, K. B. Alkyl ketene dimer (AKD) sizing of paper under simplified treatment conditions. *Tappi J.* **15**, 545–552 (2016).

242. Barry, V., Winquist, A. & Steenland, K. Perfluorooctanoic acid (PFOA) exposures and incident cancers among adults living near a chemical plant. *Environ. Health Perspect.* **121**, 1313–1318 (2013).

243. Stein, C. R., Savitz, D. A. & Dougan, M. Serum levels of perfluorooctanoic acid and perfluorooctane sulfonate and pregnancy outcome. *Am. J. Epidemiol.* **170**, 837–846 (2009).

244. Fei, C., McLaughlin, J. K., Tarone, R. E. & Olsen, J. Perfluorinated chemicals and fetal growth: A study within the Danish national birth cohort. *Environ. Health Perspect.* **115**, 1677–1682 (2007).

245. Begley, T. H., Hsu, W., Noonan, G. & Diachenko, G. Migration of fluorochemical paper additives from food-contact paper into foods and food simulants. *Food Addit. Contam. - Part A Chem. Anal. Control. Expo. Risk Assess.* **25**, 384–390 (2008).

246. *Indirect Food Additives: Paper and Paperboard Components Final Rule*. *US Food and*

Drug Administration **81**, (2016).

247. Tyagi, P., Hubbe, M. A., Lucia, L. & Pal, L. High performance nanocellulose-based composite coatings for oil and grease resistance. *Cellulose* **25**, 3377–3391 (2018).

248. Hubbe, M. A. *et al.* Nanocellulose in thin films, coatings, and plies for packaging applications: A review. *BioResources* **12**, 2143–2233 (2017).

249. Lavoine, N., Desloges, I., Dufresne, A. & Bras, J. Microfibrillated cellulose - Its barrier properties and applications in cellulosic materials: A review. *Carbohydr. Polym.* **90**, 735–764 (2012).

250. Savadekar, N. R., Karande, V. S., Vigneshwaran, N., Bharimalla, A. K. & Mhaske, S. T. Preparation of nano cellulose fibers and its application in kappa-carrageenan based film. *Int. J. Biol. Macromol.* **51**, 1008–1013 (2012).

251. Naderi, A. *et al.* Phosphorylated nanofibrillated cellulose : production and properties. *Nord. Pulp Pap. Res. J.* **31**, (2016).

252. Liimatainen, H. *et al.* High-strength nanocellulose-talc hybrid barrier films. *ACS Appl. Mater. Interfaces* **5**, 13412–13418 (2013).

253. Dai, L. *et al.* Properties of hydroxypropyl guar/TEMPO-oxidized cellulose nanofibrils composite films. *Cellulose* **22**, 3117–3126 (2015).

254. Trifol, J. *et al.* Hybrid poly(lactic acid)/nanocellulose/nanoclay composites with synergistically enhanced barrier properties and improved thermomechanical resistance. *Polym. Int.* **65**, 988–995 (2016).

255. Cozzolino, C. A., Campanella, G., Türe, H., Olsson, R. T. & Farris, S. Microfibrillated cellulose and borax as mechanical, O2-barrier, and surface-modulating agents of pullulan biocomposite coatings on BOPP. *Carbohydr. Polym.* **143**, 179–187 (2016).

256. Rezayati Charani, P., Dehghani-Firouzabadi, M., Afra, E. & Shakeri, A. Rheological characterization of high concentrated MFC gel from kenaf unbleached pulp. *Cellulose* **20**, 727–740 (2013).

257. El-Wakil, N. A., Hassan, E. A., Abou-Zeid, R. E. & Dufresne, A. Development of wheat gluten/nanocellulose/titanium dioxide nanocomposites for active food packaging. *Carbohydr. Polym.* **124**, 337–346 (2015).

258. Kumar, V. *et al.* Comparison of nano- and microfibrillated cellulose films. *Cellulose* 3443–3456 (2014). doi:10.1007/s10570-014-0357-5

259. Kumar, V., Koppolu, V. R., Bousfield, D. & Toivakka, M. Substrate role in coating of microfibrillated cellulose suspensions. *Cellulose* **24**, 1247–1260 (2017).

260. Miettinen, A., Chinga-Carrasco, G. & Kataja, M. Three-dimensional microstructural properties of nanofibrillated cellulose films. *Int. J. Mol. Sci.* **15**, 6423–6440 (2014).

261. Belbekhouche, S. *et al.* Water sorption behavior and gas barrier properties of cellulose whiskers and microfibrils films. *Carbohyd. Polym.* **83**, 1740–1748 (2011).

262. Saxena, A., Elder, T. J., Kenvin, J. & Ragauskas, A. J. High Oxygen Nanocomposite Barrier Films Based on Xylan and Nanocrystalline Cellulose. *Nano-Micro Lett.* **2**, 235–241 (2010).

263. Costa, S. S., Druzian, J. I., Machado, B. A. S., De Souza, C. O. & Guimaraes, A. G. Bi-functional biobased packing of the cassava starch, glycerol, licuri nanocellulose and red propolis. *PLoS One* **9**, (2014).

264. Hansen, N. M. L., Blomfeldt, T. O. J., Hedenqvist, M. S. & Plackett, D. V. Properties of plasticized composite films prepared from nanofibrillated cellulose and birch wood xylan. *Cellulose* **19**, 2015–2031 (2012).

265. Sun, X. S. *et al.* Morphology and phase separation of hydrophobic clusters of soy globular protein polymers. *Macromol. Biosci.* **8**, 295–303 (2008).

266. Börjesson, M. & Westman, G. Crystalline Nanocellulose — Preparation , Modification , and Properties. in *Cellulose - Fundamental Aspects and Current Trends* 159–191 (Cellulose Matheus Poletto, IntechOpen, 2015). doi:http://dx.doi.org/10.5772/61899 191

267. Hefnawy, H. T. M. & Ramadan, M. F. Physicochemical characteristics of soy protein isolate and fenugreek gum dispersed systems. *J. Food Sci. Technol.* **48**, 371–377 (2011).

268. Shin, J. Y., Jones, N., Fleming, P. D., Joyce, M. K. & Bloembergen, S. Dynamic Water Retention Properties of Biobased Latex Containing Coating Colors. in *TAPPI PaperCon* 1–20 (2013).

269. Huhtamäki, T., Tian, X., Korhonen, J. T. & Ras, R. H. A. Surface-wetting characterization using contact-angle measurements. *Nat. Protoc.* **13**, 1521–1538 (2018).

270. Pajari, Heikki & Rautkoski, Hille & Moilanen, P. Replacement of synthetic binders with nanofibrillated cellulose in board coating: Pilot scale studies. in *TAPPI International Conference on Nanotechnology for Renewable Materials* 409–425 (2012).

271. Song, J. & Rojas, O. J. Approaching super-hydrophobicity from cellulosic materials: A Review. *Pap. Chem. Nord. Pulp Pap. Res. J.* **28**, (2013).

272. De Gennes, P. G. Wetting: Statics and dynamics. *Rev. Mod. Phys.* **57**, 827–863 (1985).

273. Mertaniemi, H., Laukkanen, A., Teirfolk, J. E., Ikkala, O. & Ras, R. H. A. Functionalized porous microparticles of nanofibrillated cellulose for biomimetic hierarchically structured superhydrophobic surfaces. *RSC Adv.* **2**, 2882–2886 (2012).

274. Dankovich, T. A. & Gray, D. G. Contact Angle Measurements on Smooth Nanocrystalline Cellulose (I) Thin Films. *J. Adhes. Sci. Technol.* **25**, 699–708 (2011).

275. Jiang, L., Tang, Z., Clinton, R. M., Breedveld, V. & Hess, D. W. Two-Step Process To Create 'Roll-Off' Superamphiphobic Paper Surfaces. *ACS Appl. Mater. Interfaces* **9**, 9195–9203 (2017).

276. Wulandari, W. T., Rochliadi, A. & Arcana, I. M. Nanocellulose prepared by acid hydrolysis of isolated cellulose from sugarcane bagasse. *IOP Conf. Ser. Mater. Sci. Eng.* **107**, (2016).

277. Wang, L., Li, J., Zhang, S. & Shi, J. Preparation and characterization of all-biomass soy protein isolate-based films enhanced by epoxy castor oil acid sodium and hydroxypropyl cellulose. *Materials (Basel).* **9**, (2016).

278. Adikary, S. U., Ashokcline, M. & Nirojan, K. Characterization of Montmorillonite Clay from Naturally Occurring Clay Deposits in Murunkan Area. *Int. Res. Conf. KDU* 163–169 (2015).

279. Garusinghe, U. M., Swambabu Varanasi, Raghuwanshi S., V., Garnier, G. & Warren Batchelor. Nanocellulose-Montmorillonite Composites of Low Water Vapour Permeability. *Colloids Surfaces A Physicochem. Eng. Asp.* (2018). doi:https://doi.org/10.1016/j.colsurfa.2018.01.010

280. Strnad, S., Šauperl, O., Fras, L. & Jazbec, A. Hitozan - Vsestransko uporaben biopolimer. *Tekstilec* **50**, 243–261 (2007).

281. Zemljic, L. F., Valh, J. V. & Kreže, T. Preparation of antimicrobial paper sheets using chitosan. *Cellul. Chem. Technol.* **51**, 75–81 (2017).

282. Mead, P. S. *et al.* Food-related illness and death in the United States. *Emerg. Infect. Dis.* **5**, 607–625 (1999).

283. NEILL, MA; TARR, PI; CLAUSEN, CR; CHRISTIE, DL; HICKMAN, R. Hemolytic

Uremic Syndrome Epidemiology: A Population-Based Study in King County, Washington, 1971 to 1980. *Pediatrics* **80**, 37–40 (1987).

284. Richard L. Siegler, Ryan D. Christofferson, Mark K. Milligan, A. T. P. A 20-Year Population-Based Study of Postdiarrheal Hemolytic Uremic Syndrome in Utah. *Pediatrics* **94**, 35–40 (1994).

285. Wolfson, L. J. *et al.* Estimating the costs of achieving the WHO – UNICEF Global Immunization Vision and Strategy , 2006 – 2015. *Bull. World Health Organ.* **86**, 27–39 (2008).

286. Ehreth, J. The Global value of vaccination. *Vaccine* **21**, 596–600 (2003).

287. Richard, B. *Antibacterial toilet tissue*. (2003).

288. Hafdani, F. N. & Sadeghinia, N. A Review on Application of Chitosan as a Natural Antimicrobial. *World Acad. Sci. Eng. Technol.* **5**, 225–229 (2011).

289. Goy, R. C., Britto, D. De & Assis, O. B. G. A Review of the Antimicrobial Activity of Chitosan. *Polímeros Ciência e Tecnol.* **19**, 241–247 (2009).

290. Dutta, J., Tripathi, S. & Dutta, P. K. *Progress in antimicrobial activities of chitin, chitosan and its oligosaccharides: A systematic study needs for food applications*. *Food Science and Technology International* **18**, (2012).

291. Tsai, G. J., Zhang, S. L. & Shieh, P. L. Antimicrobial activity of a low-molecular-weight chitosan obtained from cellulase digestion of chitosan. *J. Food Prot.* **67**, 396–398 (2004).

292. Chen, C. S., Liau, W. Y. & Tsai, G. J. Antibacterial effects of N-sulfonated and N-sulfobenzoyl chitosan and application to oyster preservation. *J. Food Prot.* **61**, 1124–1128 (1998).

293. Cuero, R. G., Osuji, G. & Washington, A. A. N-Carboxymethylchitosan Inhibition of

Aflatoxin Production: Role of Zinc. *Biotechnol. Lett.* **13**, 441–444 (1991).

294. Roller, S. & Covill, N. The antifungal properties of chitosan in laboratory media and apple juice. *Int. J. Food Microbiol.* **47**, 67–77 (1999).

295. Badawy, M. E. I., Rabea, E. I., Taktak, N. E. M. & El-Nouby, M. A. M. The Antibacterial Activity of Chitosan Products Blended with Monoterpenes and Their Biofilms against Plant Pathogenic Bacteria. *Scientifica (Cairo).* **2016**, (2016).

296. Nechita, P., Bobu, E., Parfene, G., M, D. R. & T., B. Antimicrobial coatings based on chitosan derivatives and quareternary ammonium salts for packaging paper application. *Cellul. Chem. Technol.* **49**, 625–632 (2015).

297. Bobu, E. *et al.* Antimicrobial Properties of Coatings Based on Chitosan Conservation. *Cellul. Chem. Technol.* **50**, 689–699 (2016).

298. Bordenave, N., Grelier, S. & Coma, V. Hydrophobization and antimicrobial activity of chitosan and paper-based packaging material. *Biomacromolecules* **11**, 88–96 (2010).

299. Duan, J. *et al.* The preparation of a novel environmentally friendly green antimicrobial packaging film. *Appl. Mech. Mater.* **151**, 665–667 (2012).

300. Salam, A., Lucia, L. A. & Jameel, H. Chitosan-Based Reagents Endow Recycled Paper Fibers with Remarkable Physical and Antimicrobial Properties. *Ind. Eng. Chem. Res.* **55**, 7282–7286 (2016).

301. Cuero, R. G., Osuji, G. & Washington, A. A. N-Carboxymethylchitosan Inhibition of Aflatoxin Production: Role of Zinc. *Biotechnol. Lett.* **13**, 441–444 (1991).

302. El-Samahy, M. A., Mohamed, S. A. A., Abdel Rehim, M. H. & Mohram, M. E. Synthesis of hybrid paper sheets with enhanced air barrier and antimicrobial properties for food packaging. *Carbohydr. Polym.* **168**, 212–219 (2017).

303. Duan, J. *et al.* The preparation of a novel environmentally friendly green antimicrobial packaging film. *Appl. Mech. Mater.* **151**, 665–667 (2012).

304. ZEMLJIC, L. F., VALH, J. V. & KREŽE, T. Preparation of antimicrobial paper sheets using chitosan. *Cellul. Chem. Technol.* **51**, 75–81 (2017).

305. El-Sakhawy1, M. *et al.* Improving the antimicrobial activity of baggase packaging paper using organophosphorous dimers. *Int. J. Technol.* **6**, 932–942 (2016).

306. Roe, D., Karandikar, B., Bonn-Savage, N., Gibbins, B. & Roullet, J. baptiste. Antimicrobial surface functionalization of plastic catheters by silver nanoparticles. *J. Antimicrob. Chemother.* **61**, 869–876 (2008).

307. Lellouche, J., Friedman, A., Lahmi, R., Gedanken, A. & Banin, E. Antibiofilm surface functionalization of catheters by magnesium fluoride nanoparticles. *Int. J. Nanomedicine* **7**, 1175–1188 (2012).

308. El Miri, N. *et al.* Bio-nanocomposite films based on cellulose nanocrystals filled polyvinyl alcohol/chitosan polymer blend. *J. Appl. Polym. Sci.* **132**, 1–13 (2015).

309. De Mesquita, J. P., Donnici, C. L., Teixeira, I. F. & Pereira, F. V. Bio-based nanocomposites obtained through covalent linkage between chitosan and cellulose nanocrystals. *Carbohydr. Polym.* **90**, 210–217 (2012).

310. Deng, Z., Jung, J., Simonsen, J., Wang, Y. & Zhao, Y. Cellulose Nanocrystal Reinforced Chitosan Coatings for Improving the Storability of Postharvest Pears Under Both Ambient and Cold Storages. (2011). doi:10.1111/1750-3841.13601

311. El-Samahy, M. A., Mohamed, S. A. A., Abdel Rehim, M. H. & Mohram, M. E. Synthesis of hybrid paper sheets with enhanced air barrier and antimicrobial properties for food packaging. *Carbohydr. Polym.* **168**, 212–219 (2017).

312. Hong, D., Cao, G., Qu, J., Deng, Y. & Tang, J. Antibacterial activity of Cu2O and Ag co-modified rice grains-like ZnO nanocomposites. *J. Mater. Sci. Technol.* **34**, 2359–2367 (2018).

313. Sun, S. *et al.* Bioresource Technology Synergistic effects of chitosan – guanidine complexes on enhancing antimicrobial activity and wet-strength of paper. *Bioresour. Technol.* **101**, 5693–5700 (2010).

314. Eriksson, M., Torgnysdotter, A. & Wågberg, L. Surface Modification of Wood Fibers Using the Polyelectrolyte Multilayer Technique : Effects on Fiber Joint and Paper Strength Properties. 5279–5286 (2006). doi:10.1021/ie060226w

315. Enarsson, L.-E. & Wågberg, L. Kinetics of sequential adsorption of polyelectrolyte multi-layers on pulp fibres and their effect on paper strength. *Nord. Pulp Pap. Res. J.* **22**, 258–266 (2007).

316. Fatehi, P., Qian, L., Kititerakun, R., Rirksomboon, T. & Xiao, H. Complex formation of modified chitosan and carboxymethyl cellulose and its effect on paper properties, TAPPI JOURNAL June 2009. *Tappi J.* **8**, 29–35 (2009).

317. National Cheng Kung University. Standard Test Method for Determining the Antimicrobial Activity of Immobilized Antimicrobial Agents Under Dynamic Contact Conditions 1. 2–6 (2010). doi:10.1520/E2149-01.2

318. Biotechnology, A. G. *Testing an Antibiotic Using a Disk Diffusion Assay Introduction*.

319. Riva, G. H., Joaquín García-Estrada, B. V., Fernando, L.-D., E., H. M. & A., S. J. Cellulose - Chitosan Nanocomposites - Evaluation of Physical, Mechanical and Biological Properties. in *Cellulose-fundamental aspects and current trends* 229–250 (INTECH, 2015). doi:http://dx.doi.org/10.5772/61727

320. Alharbi, S. A. *et al.* Assessment of the bacterial contamination of hand air dryer in washrooms. *Saudi J. Biol. Sci.* **23**, 268–271 (2016).

321. Edmonds-wilson, S. L., Nurinova, N. I., Zapka, C. A., Fierer, N. & Wilson, M. Review of human hand microbiome research. *J. Dermatol. Sci.* **80**, 3–12 (2015).

322. Zapka, C. A. *et al.* Bacterial hand contamination and transfer after use of contaminated bulk-soap-refillable dispensers. *Appl. Environ. Microbiol.* **77**, 2898–2904 (2011).

323. Goy, R. C., Britto, D. De & Assis, O. B. G. A Review of the Antimicrobial Activity of Chitosan. *Ciência e Tecnol.* **19**, 241–247 (2009).

324. Dutta, P. K., Tripathi, S., Mehrotra, G. K. & Dutta, J. Perspectives for chitosan based antimicrobial films in food applications. *Food Chem.* **114**, 1173–1182 (2009).

325. Coma, V., Deschamps, A. & Martial-Gros, A. Bioactive Packaging Materials from Edible Chitosan Polymer - Antimicrobial Activity Assessment on Dairy-Related Contaminants. *J. Food Sci.* **68**, 2788–2792 (2003).

326. Karthikeyan, N., Vijayalakshmi, K. A. & Vignesh, K. Effect of glow discharge oxygen plasma treated surface and antimicrobial properties of viscose fabric. *Mater. Technol.* **31**, 166–175 (2016).

327. Boyce, J. M. Modern technologies for improving cleaning and disinfection of environmental surfaces in hospitals. *Antimicrob. Resist. Infect. Control* **5**, 1–10 (2016).

328. O'Connor, N., Cahill, O., Daniels, S., Galvin, S. & Humphreys, H. Cold atmospheric pressure plasma and decontamination. Can it contribute to preventing hospital-acquired infections? *J. Hosp. Infect.* **88**, 59–65 (2014).

329. Claro, T., Cahill, O. J., O'Connor, N., Daniels, S. & Humphreys, H. Cold-air atmospheric pressure plasma against clostridium difficile spores: A potential alternative for the

decontamination of hospital inanimate surfaces. *Infect. Control Hosp. Epidemiol.* **36**, 742–744 (2015).

330. Bristow, A. The swelling of paper during the sorption of aqueous liquids. *Sven. Papperstidning* **74**, 645-652. (1971).

331. Schuchardtl, D. R. & Berg, J. C. LIQUID TRANSPORT IN COMPOSITE CELLULOSE - SUPERABSORBENT FIBER NETWORKS. **23**, 342–357 (1991).

332. González, I. *et al.* Nanofibrillated Cellulose as paper additive in Eucalptus pulp. BioResources. *BioResources* **7**, 5167–5180 (2012).

333. Papineau, A. M., Hoover, D. G., Knorr, D. & Farkas, D. F. Antimicrobial effect of water-soluble chitosans with high hydrostatic pressure. *Food Biotechnol.* **5**, 45–57 (1991).

334. Bajpai, S. K., Chand, N., Ahuja, S. & Roy, M. K. Curcumin/cellulose micro crystals/chitosan films: Water absorption behavior and in vitro cytotoxicity. *Int. J. Biol. Macromol.* **75**, 239–247 (2015).

335. Bajpai, S. K., Pathak, V., Soni, B. & Mohan, Y. M. CNWs loaded poly(SA) hydrogels: Effect of high concentration of CNWs on water uptake and mechanical properties. *Carbohydr. Polym.* **106**, 351–358 (2014).

336. FAROUK EL-HOSSEINY AND DWIGHT ANDERSON. Effect of fiber length and coarseness on the burst strength of paper. *Tappi J.* **82**, 202–203 (1999).

337. Bras, J., Viet, D., Bruzzese, C. & Dufresne, A. Correlation between stiffness of sheets prepared from cellulose whiskers and nanoparticles dimensions. *Carbohydr. Polym.* **84**, 211–215 (2011).

338. Pellati, F. *et al.* Cannabis sativa L . and Nonpsychoactive Cannabinoids : Their Chemistry and Role against Oxidative Stress , Inflammation , and Cancer. *Biomed Res. Int.* **2018**, 1–

15 (2018).

339. Darby, H. *et al.* 2017 Industrial Hemp Fiber Variety Trial. *University of Vermont Extension* (2018).

340. Miller, N. G. THE GENERA OF THE CANNABACEAE IN THE SOUTHEASTERN UNITED STATES. *J. Arnold Arbor.* **51**, 185–203 (1970).

341. Raman, V., Lata, H., Chandra, S., Khan, I. A. & ElSohly, M. A. Morpho-Anatomy of Marijuana (Cannabis sativa L.). in *Cannabis sativa L. - Botany and Biotechnology* 123–136 (Springer International Publishing, 2017). doi:10.1007/978-3-319-54564-6

342. Ouajai, S. & Shanks, R. A. Composition, structure and thermal degradation of hemp cellulose after chemical treatments. *Polym. Degrad. Stab.* **89**, 327–335 (2005).

343. Marsh, G. Next step for automotive materials. *Mater. Today* **6**, 36–43 (2003).

344. Li, X. *et al.* Influence of hemp plant eccentric growth on physical properties and chemical compounds of hemp hurd. *BioResources* **13**, 290–298 (2018).

345. Gutiérrez, A. & Del Río, J. C. Chemical characterization of pitch deposits produced in the manufacturing of high-quality paper pulps from hemp fibers. *Bioresour. Technol.* **96**, 1445–1450 (2005).

346. Kiprono, P. C., Kaberia, F., Joseph, M. & Karanja, J. N. The in vitro Anti-Fungal and Anti-Bacterial Activities of ß-Sitosterol from Senecio lyratus (Asteraceae). *Zeitschrift für Naturforsch.* **55**, 485–488 (2000).

347. Ibrahim, T. A. Chemical Composition and Biological Activity of Extracts from Salvia bicolor Desf. Growing in Egypt. *Molecules* **17**, 11315–11334 (2012).

348. Khan, B. A., Warner, P. & Wang, H. Antibacterial Properties of Hemp and Other Natural Fibre Plants: A Review. *Bio Resour.* **9**, 3642–3659 (2014).

349. Appendino, G. *et al.* Antibacterial cannabinoids from Cannabis sativa: A structure-activity study. *J. Nat. Prod.* **71**, 1427–1430 (2008).

350. Głodowska, M. & Łyszcz, M. Cannabis sativa L . and its antimicrobial properties – A review. in *Badania i Rozwój Młodych Naukowców w Polsce – Agronomia i ochrona roślin* 77–82 (201AD).

351. Khan, B. A., Wang, J., Warner, P. & Wang, H. Antibacterial properties of hemp hurd powder against E. coli. *J. Appl. Polym. Sci.* **132**, 1–6 (2015).

352. M., E. M. A., Almagboul, A. Z. I., Khogali, S. M. E. & Gergeir, U. M. A. Antimicrobial Activity of Cannabis sativa L . *J. Chinese Med.* **3**, 61–64 (2012).

353. Tandon, C. & Mathur, P. Review Article Antimicrobial Efficacy of Cannabis sativa L . (Bhang): A Comprehensive Review. **44**, 94–100 (2017).

354. Zhuang, Z. *et al.* Optimizing the extraction of antibacterial compounds from pineapple leaf fiber. *Open Life Sci.* **11**, 391–395 (2016).

355. Mathur, P., Singh, A., Srivastava, V. R., Singh, D. & Mishra, Y. Antimicrobial activity of indigenous wildly growing plants: Potential source of green antibiotics. *African J. Microbiol. Res.* **7**, 3807–3815 (2013).

356. Borhade, S. S. Chemical Composition and Characterization of Hemp (Cannabis sativa) Seed oil and essential fatty acids by HPLC Method. *Sch. Res. Libr. Arch. Appl. Sci. Res.* **5**, 5–8 (2013).

357. K, W., IU, H. & Ashraf M. Antimicrobial studies of the leaf of Cannabis sativa. *Pakistran J. Pharm. Sci.* **8**, 29–38 (1995).

358. Leizer, C., Ribnicky, D., Poulev, A., Dushenkov, S. & Raskin, I. The Composition of Hemp Seed Oil and Its Potential as an Important Source of Nutrition. *J. Nutraceuticals,*

Funct. Med. Foods **2**, 35–53 (2000).

359. MILANOVIĆ, 2012.pdf.

360. Kostic, M. M., Milanovic, J. Z., Baljak, M. V., Mihajlovski, K. & Kramar, A. D. Preparation and characterization of silver-loaded hemp fibers with antimicrobial activity. *Fibers Polym.* **15**, 57–64 (2014).

361. Racu, C., Cogeanu, A. M., Diaconescu, R. M. & Grigoriu, A. Antimicrobial treatments of hemp fibers grafted with β-cyclodextrin derivatives. *Text. Res. J.* **82**, 1317–1328 (2012).

362. Khan, B. A. Development of Antibacterial Hemp Hurd / Poly (Lactic Acid) Biocomposite for Food Packaging. (2017).

363. Bian, H. *et al.* Lignin-Containing Cellulose Nanofibril-Reinforced Polyvinyl Alcohol Hydrogels. *ACS Sustain. Chem. Eng.* **6**, 4821–4828 (2018).

364. Ferrer, A. *et al.* Effect of residual lignin and heteropolysaccharides in nanofibrillar cellulose and nanopaper from wood fibers. *Cellulose* **19**, 2179–2193 (2012).

365. Yasuda, S., Fukushima, K. & Kakehi, A. Formation and chemical structures of acid-soluble lignin I: Sulfuric acid treatment time and acid-soluble lignin content of hardwood. *J. Wood Sci.* **47**, 69–72 (2001).

366. de Carvalho, D. M. & Colodette, J. L. Comparative study of acid hydrolysis of lignin and polysaccharides in biomasses. *BioResources* **12**, 6907–6923 (2017).

367. Xiao, C., Anderson, C. T., Scheller, H. & Berkeley, L. Roles of pectin in biomass yield and processing for biofuels. *Front. Plant Sci.* **4**, 67 (1–7) (2013).

368. Saito, K., Kato, T., Tsuji, Y. & Fukushima, K. Identifying the characteristic secondary ions of lignin polymer using ToF-SIMS. *Biomacromolecules* **6**, 678–683 (2005).

369. Daicho, K., Saito, T., Fujisawa, S. & Isogai, A. The Crystallinity of Nanocellulose:

Dispersion-Induced Disordering of the Grain Boundary in Biologically Structured Cellulose. *ACS Appl. Nano Mater.* **1**, 5774–5785 (2018).

370. Herrera, N., Salaberria, A. M., Mathew, A. P. & Oksman, K. Plasticized polylactic acid nanocomposite films with cellulose and chitin nanocrystals prepared using extrusion and compression molding with two cooling rates: Effects on mechanical, thermal and optical properties. *Compos. Part A Appl. Sci. Manuf.* **83**, 89–97 (2016).

371. Field, B. I. & Arndt, R. R. Cannabinoid compounds in South African Cannabis sativa L. *J. Pharm. Pharmacol.* **32**, 21–24 (1980).

372. Gandolfi, S., Ottolina, G., Riva, S., Fantoni, G. P. & Patel, I. Complete Chemical Analysis of Carmagnola Hemp Hurds and Structural Features of Its Components. *BioResources* **8**, 2641–2656 (2013).

APPENDIX

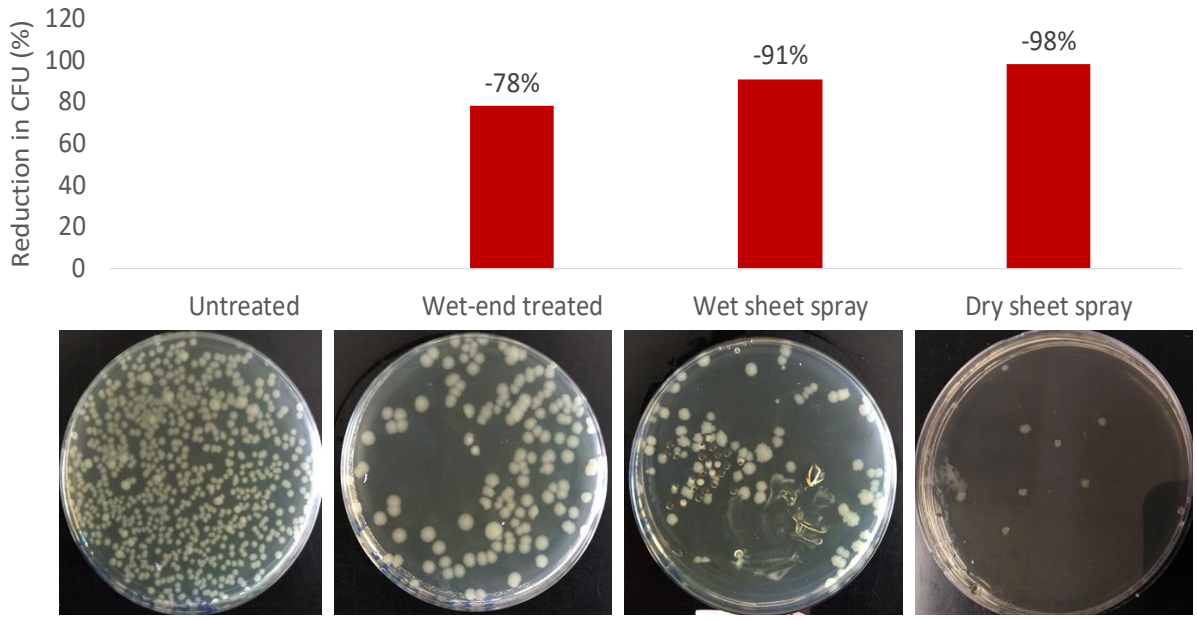

Figure A-1. Bacterial growth after 2-hour contact with ChCNC treated tissue paper (treated at different stages)

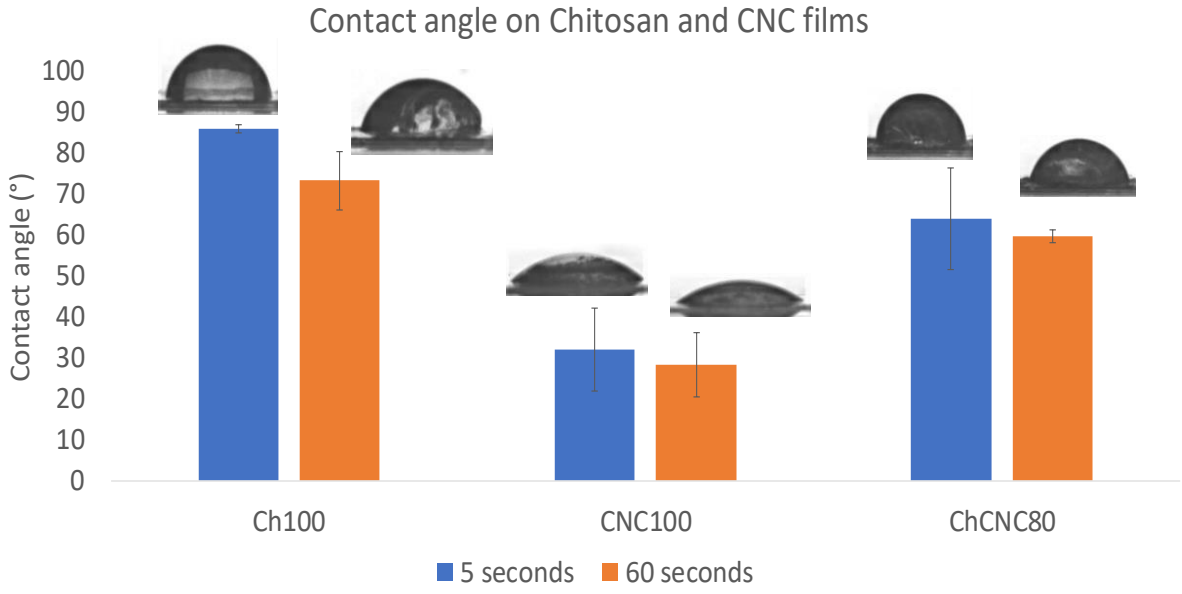

Figure A-2. Repetition of Contact angle on Chitosan and CNC films

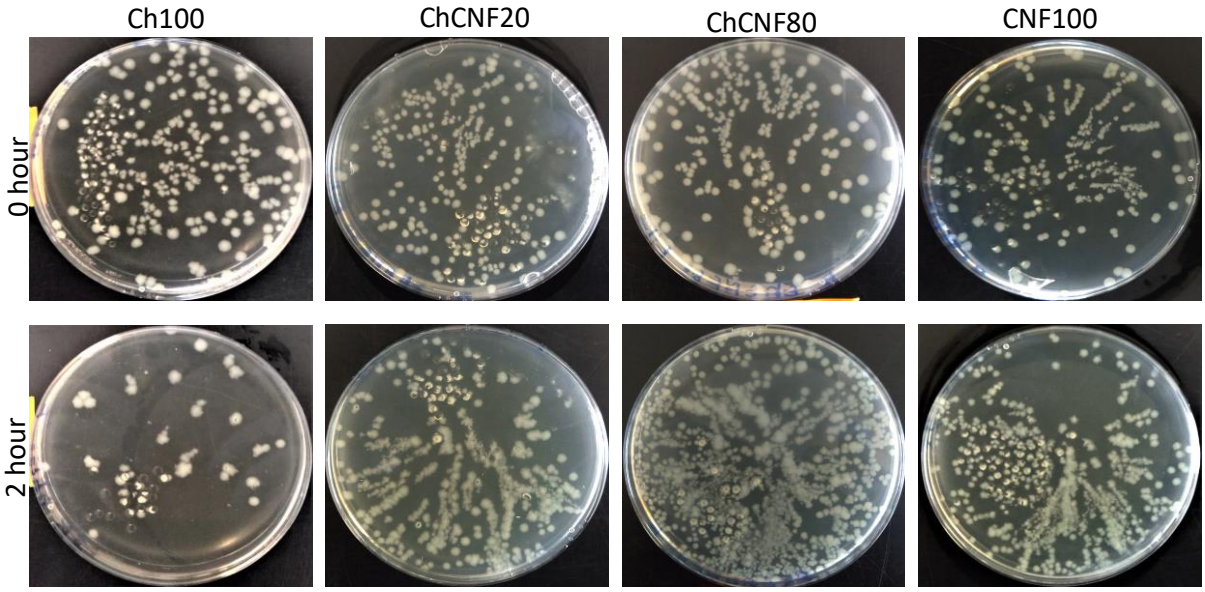

Figure A-3. Antimicrobial activity of Chitosan and CNF films

Table A.1 Pulping/Defibration conditions of different hemp hurds and HW chips

Process	Water/ Solid Ratio	Pulping Chemicals
Hemp-A	8	None
Hemp-C	8	4% sodium carbonate as Na_2O
Hemp-UK	8	12% active alkali 25% sufidity ($NaOH+Na_2S$) as Na_2O
Hardwood-C	4	4% sodium carbonate as Na_2O
Hardwood-UK	4	12% active alkali 25% sufidity ($NaOH+Na_2S$) as Na_2O

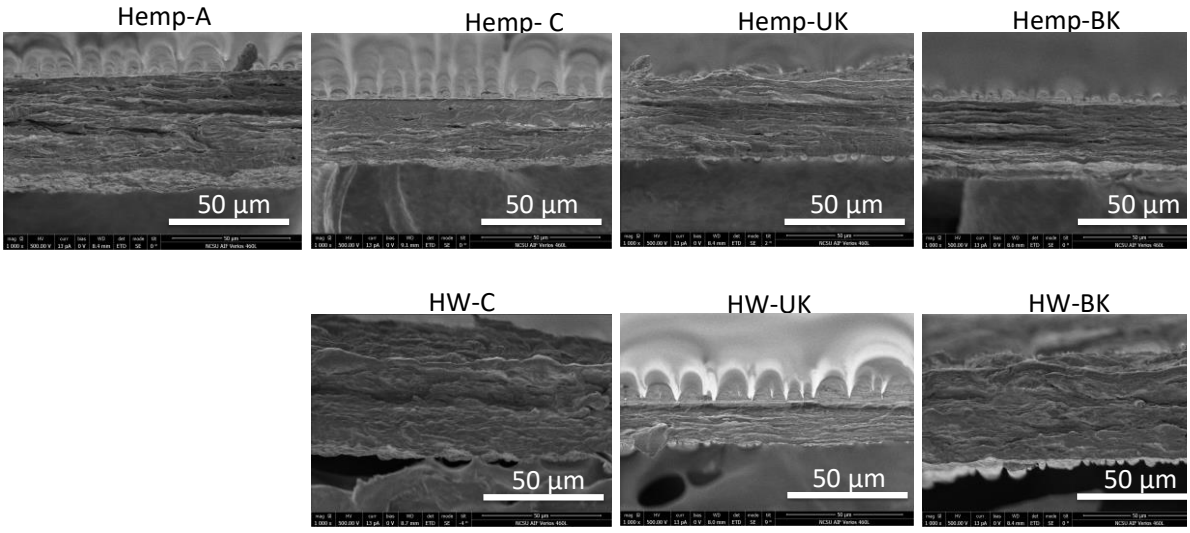

Figure A-4. Cross-section of Hemp and HW nanocellulose films

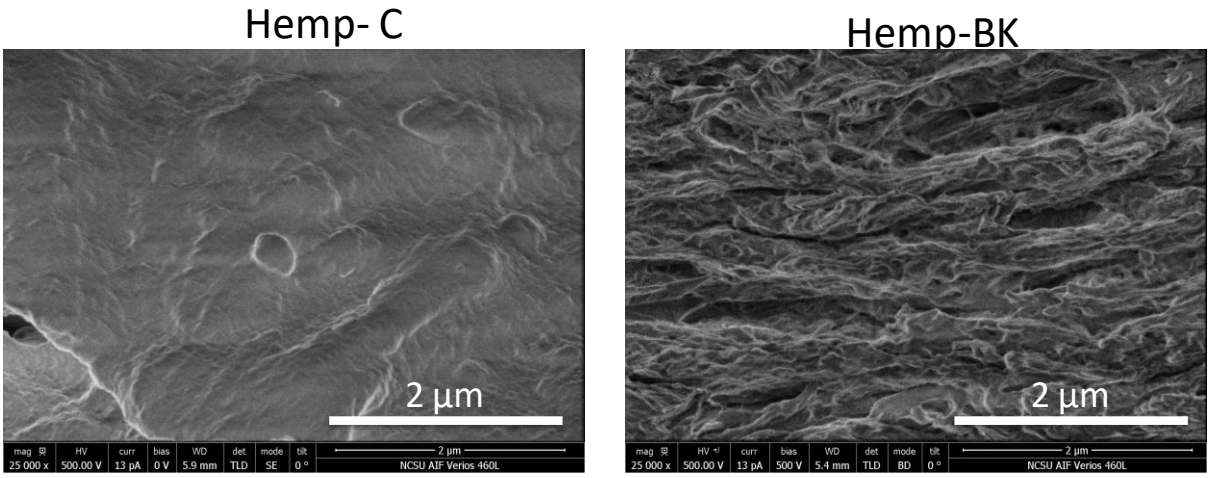

Figure A-5. High magnification imgaes of cross-section view of Hemp-C and and Hemp-BK LCNF films

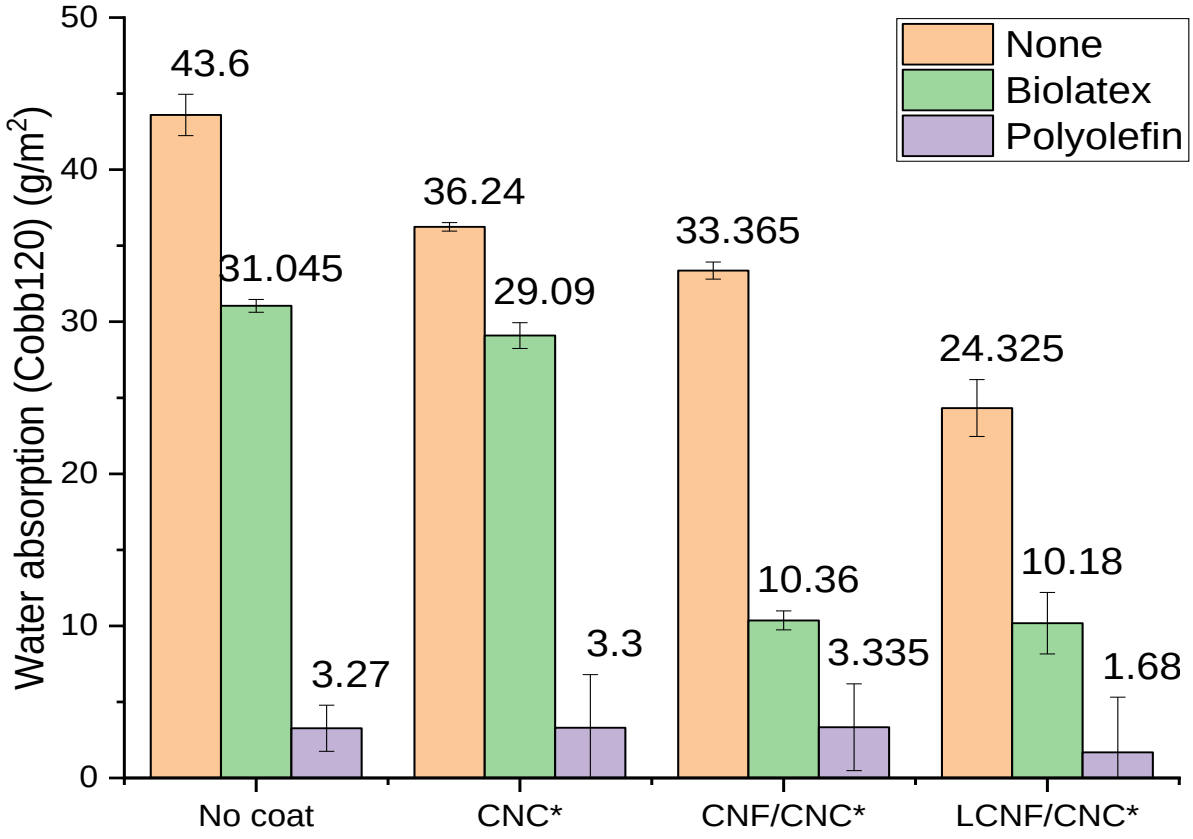

Figure A-6. Water absorption of biolatex and polyolefin overcoated on CNC*,CNF/CNC* and LCNF/CNC* coated WB papers